IAEA-TECDOC-1406

Primary coolant pipe rupture event in liquid metal cooled reactors

Proceedings of a technical meeting held in Kalpakkam, India, 13–17 January 2003

IAEA
International Atomic Energy Agency

August 2004

IAEA-TECDOC-1406

Primary coolant pipe rupture event in liquid metal cooled reactors

Proceedings of a technical meeting held in Kalpakkam, India, 13–17 January 2003

IAEA
International Atomic Energy Agency

August 2004

The originating Section of this publication in the IAEA was:

Nuclear Power Technology Development Section
International Atomic Energy Agency
Wagramer Strasse 5
P.O. Box 100
A-1400 Vienna, Austria

PRIMARY COOLANT PIPE RUPTURE EVENT IN LIQUID METAL COOLED REACTORS
IAEA, VIENNA, 2004
IAEA-TECDOC-1406
ISBN 92–0–109104–4
ISSN 1011–4289

© IAEA, 2004

Printed by the IAEA in Austria
August 2004

FOREWORD

The fast reactor, which can generate electricity and breed additional fissile material for future fuel stocks is a resource that will be needed when economic uranium supplies for the advanced light water reactors or other thermal-spectrum options diminish.

Further, the fast-fission fuel cycle in which material is recycled offers the flexibility needed to contribute decisively towards solving the problem of growing 'spent' fuel inventories by greatly reducing the volume of high level waste that must be disposed of in geological repositories. This is a waste management option that is currently being investigated.

Mainly due to economic and political reasons, fast reactor development has slowed down. However, some Member States (China, India, Japan, the Republic of Korea, and the Russian Federation) continue the development of this technology. Moreover, recent international initiatives (INPRO, Generation IV International Forum) have clearly reaffirmed the importance of fast neutron spectrum systems in ensuring that innovative reactors and fuel cycles will meet sustainability criteria with regard to both natural resources and radioactive waste management.

Through the Nuclear Energy Department's Technical Working Group on Fast Reactors (TWG-FR), the IAEA provides a forum for exchange of information on national programmes, collaborative assessments, knowledge preservation, and cooperative research in areas agreed by the Member States with fast reactor and partitioning and transmutation development programmes (e.g. accelerator driven systems (ADS)). Trends in innovative fast reactor and ADS designs and technology development are periodically summarized in status reports, symposia and seminar proceedings prepared by the IAEA to provide all interested IAEA Member States with balanced and objective information.

The rupture of the primary coolant pipe in a liquid metal cooled fast reactor (both critical and sub-critical) is a topic of major concern for the design of such reactors.

Based on expressed needs of some Member States, and in response to a TWG-FR recommendation, the IAEA has convened the Technical Meeting on Primary Coolant Pipe Rupture Event in Liquid Metal Cooled Reactors. The technical meeting, hosted by the Indira Gandhi Centre for Atomic Research (IGCAR), Kalpakkam, India, was held 13–17 January 2003.

The IAEA would like to express its appreciation to all the participants, authors of papers, chairpersons, and to the hosts at IGCAR.

The IAEA officer responsible for this publication was A. Stanculescu of the Division of Nuclear Power.

EDITORIAL NOTE

The papers in these proceedings are reproduced as submitted to the Publishing Section and have not undergone rigorous editorial review by the IAEA.

The views expressed do not necessarily reflect those of the IAEA, the governments of the nominating Member States or the nominating organizations.

The use of particular designations of countries or territories does not imply any judgement by the publisher, the IAEA, as to the legal status of such countries or territories, of their authorities and institutions or of the delimitation of their boundaries.

The mention of names of specific companies or products (whether or not indicated as registered) does not imply any intention to infringe proprietary rights, nor should it be construed as an endorsement or recommendation on the part of the IAEA.

The authors are responsible for having obtained the necessary permission for the IAEA to reproduce, translate or use material from sources already protected by copyrights.

CONTENTS

1. INTRODUCTION 1

2. NATIONAL PRESENTATIONS 1

2.1. China 1
2.2. France 3
2.3. India 3
2.4. Japan 5
2.5. Republic of Korea 6

3. TECHNICAL SUMMARY 7

3.1. Safety philosophy 7
3.1.1. China 7
3.1.2. France 7
3.1.3. India 8
3.1.4. Japan 8
3.1.5. Republic of Korea 8

3.2. Structural integrity assessment 8
3.2.1. China 8
3.2.2. France 9
3.2.3. India 9
3.2.4. Japan 10
3.2.5. Republic of Korea 10

3.3. Thermal hydraulics 10
3.3.1. China 10
3.3.2. France 11
3.3.3. India 11
3.3.4. Republic of Korea 12

3.4. Innovative concepts 12
3.4.1. China 12
3.4.2. India 12

3.5. Resolved issues 13

3.6. Open issues 13

3.7. Conclusion 14

Safety philosophy of primary pipe rupture event in prototype fast breeder reactor 17
S.B. Bhoje

Philosophy of leak before break assessment for Japanese prototype FBR 25
T. Wakai, K. Aoto, M. Ichimiya, K. Ito

Main pipe rupture accident analysis for the Chinese experimental fast reactor 35
H. Yang, M. Xu

Rupture of LIPOSO in Superphenix 47
Ph. Dufour, J. Louvet, P. Lo Pinto

Theoretical and experimental assessment of structural integrity of primary pipe 57
P. Chellapandi, A. Biswas, S.C. Chetal, S.B. Bhoje

A simplified crack growth assessment procedure for PCP in FBR..... 73
T. Wakai, K. Aoto

Thermal hydraulic consequences of primary pipe rupture.....87
N. Kasinathan, K. Natesan, P. Selvaraj, P. Chelapandi, S.C. Chetal

Analysis of primary pipe break for the Korean advanced
liquid metal reactor (KALIMER)..... 105
H.Y. Jeong, W.P. Chang, Y.B. Lee, D. Hahn

Analysis of emergency situations caused by BN-800 primary circuit pressure
pipe depressurization..... 125
V.S. Gorbunov, V.A. Zamiatin, Yu.L. Kamanin, N.G. Kuzavkov, V.A. Sobolev

Improved primary pipe design concepts for future FBR..... 141
S.C. Chetal, P. Chellapandi

ABBREIVIATIONS 145

LIST OF PARTICIPANTS 149

SUMMARY

1. INTRODUCTION

In liquid-metal cooled fast reactors (LMFR) or in accelerator driven sub-critical systems (ADS) with LMFR like sub-critical cores, the primary coolant pipes (PCP) connect the primary coolant pumps to the grid plate. A rupture in one of these pipes could cause significant loss of coolant flow to the core with severe consequences. In loop type reactors, all primary pipelines are provided with double envelopes and inter-space coolant leak monitoring systems that permit leak detection before break. Thus, the PCP rupture event can be placed in the beyond design basis event (BDBE) category. Such an arrangement is difficult to incorporate for pool type reactors, and hence it could be argued that the PCP rupture event needs to be analysed in detail as a design basis event (DBE, category 4 event).

However, the primary coolant pipes are made of ductile austenitic stainless steel material and operate at temperatures of the cold pool and at comparatively low pressures. For such low stressed piping with negligible creep and embrittlement effects, it is of interest to discuss under what design provisions, for pool type reactors, the guillotine rupture of PCP could be placed in the BDBE category.

The topical Technical Meeting (TM) on Primary Coolant Pipe Rupture Event in Liquid Metal Cooled Reactors' (Indira Gandhi Centre for Atomic Research, Kalpakkam, India, 13–17 January 2003) was called to enable the specialists to present the philosophy and analyses applied on this topic in the various Member States for different LMFRs.

The scope of the technical meeting was to provide a global forum for information exchange on the philosophy applied in the various participating Member States and the analyses performed for different LMFRs with regard to the primary coolant pipe rupture event. More specifically, the objectives of the technical meeting were to review the safety philosophy for the PCP rupture event in pool type LMFR, to assess the structural reliability of the PCP and the probability of rupture under different conditions (with/without in-service inspection), to review the classification of the PCP rupture event in DBE/BDBE categories and discuss the applicable design safety limits, to assess the need for consequency analysis, like pipe whip effects, primary pump seizure and multiple pipe rupture, and, last but not least, to present the results of analyses of the event *per se* for flows and/or temperatures and improved design concepts for minimizing the consequences to the core.

The TM was attended by 25 participants from six Member States and one international organization.

2. NATIONAL PRESENTATIONS

A brief overview of the respective national fast reactor programmes was given by the representatives of the participating Member States, before addressing the specific objectives of the TM.

2.1. China

Fast reactor research and development activities are pursued by the China Institute of Atomic Energy (CIAE). CIAE has evolved out of the Institute of Modern Physics, Academia Sinica, founded in 1950. It is the birthplace of nuclear science and technology in China. CIAE has a

staff of 3 400, including 660 senior scientists and senior engineers, 43 supervisors of doctoral students, and 9 members of Chinese Academy of Sciences and Chinese Academy of Engineering. CIAE has eight departments and several research centres, and it can count on five eminent nuclear facilities, as well as on many small laboratories. Presently, CIAE is implementing four significant projects: the Chinese Experimental Fast Reactor (CEFR), the Chinese Advanced Research Reactor (CARR), the HI-13 Tandem accelerator upgrading project, and the radiochemistry laboratory.

With regard to nuclear energy, China has adopted a strategy based on pressurized water reactors, fast breeder reactors, and fusion reactors. Nuclear power will contribute to China's long term sustainable energy supply, and help meet the challenges of the 21st century. However, due to economic reasons and to allow for a solid experience base to be built, nuclear power technology development is presently pursued at a moderate pace. In mainland China, there are two nuclear power plants (NPPs) in operation with a total capacity of 2.1 GW(e). Four NPPs are under construction, and two NPPs are planned for the Tenth Five Year Plan (2001–2005). One or two additional NPPs are still under discussion. A new NPP, located is near the Lin Ao NPP in Guang Dong, was licensed in December 2002. As of 2001, nuclear power represents 1% of the total installed electric power in China. The share of nuclear power will attain 3% before 2005. In absolute terms, it is foreseen that the total nuclear power capacity will reach 8.5 GW(e) by the year 2005, and 14–15 GW(e) before 2010. With CEFR presently under construction, it is hoped that a prototype fast breeder reactor will be commissioned before 2020.

The conceptual design of the CEFR was started in 1990 and completed in 1993. The CEFR preliminary design was started in early 1995 and finished in August 1997. In the period 1995–1996, CIAE had technical design cooperation with a Russian liquid metal fast breeder reactor association whose members were Institute of Physics & Power Engineering, Experimental Designing Bureau of Machine Building, and Atomenergoproekt. The CEFR detailed design work started in early 1998, and now is almost finished (as of beginning 2003).

The CEFR is a sodium cooled, bottom supported 65 MW(th) experimental fast reactor fuelled with mixed uranium-plutonium oxide (the first core, however, will be loaded with uranium oxide fuel). Fuel cladding and reactor block structural materials are made of Cr-Ni austenitic stainless steel. It is a pool type reactor with two main pumps, and two loops for the primary and secondary circuit, respectively. The water-steam tertiary circuit has also two loops, with the superheated steam collected into one pipe that is connected with the turbine. CEFR's has a natural circuit decay heat removal system.

As of the beginning of 2003, 95% of the CEFR detailed design was finished, and 70% of the components had been ordered, of which 20% have been delivered to CIAE. The status and further planning of the construction works were as follows:

- Reactor building construction had reached the top, i.e. 57 m above ground;
- More than one hundred components and shielding doors had been installed;
- Systems installation works was to start in March 2003;
- Sodium procurement was to start later in 2003;
- Equipment and system tests was to start later in 2003;
- Reactor vessel sodium filling is scheduled for 30 May 2005;
- First criticality is scheduled for the end of 2005.

2.2. France

For many years, France was involved in an important sodium cooled fast breeder reactor R&D, which has seen the construction of Rapsodie (40 MW(th)), Phénix (350 MW(e)) and Superphénix (1200 MW(e)). Given the extensive experience available, R&D for the liquid metal cooled fast reactor option appears to be no longer necessary, and efforts are instead concentrated on a new R&D programme on gas cooled reactors. However, it is clearly recognized that the knowledge and experience gained from the liquid metal cooled fast reactor development must be preserved. Hence, knowledge preservation efforts in France are directed towards the creation of a database on R&D and reactor design, as well as on the operational experience of the French fast reactors. This database does not consist of a mere compilation of technical data and results, but it includes also the collection of interviews of senior engineers involved in the design and/or operation of Rapsodie, Phénix, or Superphénix. Another area where continuing efforts are necessary is sodium technology in support of Superphénix decommissioning.

Within the framework of the 30 December 1991 law concerning management of long lived radioactive waste, CEA is implementing an irradiation programme in Phénix. As outlined below, Phénix operation will resume in June 2003. It is planned to operate the reactor for another 6 irradiation cycles, corresponding to a period of approximately 5.5 years (at 2/3 nominal power). The main scope of this irradiation programme is basic data acquisition for material and innovative fuel testing, plutonium incineration, as well as minor actinides and long lived fission product incineration and transmutation.

CEA is also continuing validation work for the re-criticality risk analysis code SIMMER III. An important aspect of this research is the analysis of the molten and boiling mixed pool behaviour of taking into account the CABRI/Raft ball-trap experiments.

As already mentioned, Phénix was restarted in June 2003. The reactor was shut down in November 1998 for plant inspection, normal maintenance, and renovation works in view of its lifetime extension. The renovation works comprised buildings seismic reinforcement, sodium fires protection measures, installation of new emergency cooling circuits, and steam generator (SG) repair after the detection of a significant crack on one SG module. Inspection work comprised the ultra-sonic inspection of the welds of the core support conical skirt, and the visual inspection of the hanging structures of the vessel, and of the upper internal structures of the reactor block (above-core structures and subassembly heads).

2.3. India

As of 31 March 2002, the installed electric capacity increased to 105 GW(e). The power generation in the period April to December 2002 was 397.6 billion kW·h that is 3.7% higher than in the corresponding 2001 period. The plant load factor during April to December 2002 was 71.1% for thermal power, and 78.7% for nuclear, respectively. While thermal and nuclear power generation were higher by 6.3 and 0.6% respectively, hydro-power generation decreased by 9.6% for the same period.

The Indian nuclear electric capacity of 2.77 GW(e) consists of 2 BWRs of 160 MW(e) each and 12 PHWRs of various capacities up to 220 MW(e) each. The performance of the nuclear power stations was very good with an average capacity factor of 85% in the 2001–2002 period.

The following new nuclear projects are under way: Tarapur 3 and 4 (2×540 MW(e) PHWR), Kaiga 3 and 4 (2×220 MW(e) PHWR), Rajasthan 5 and 6 (2×220 MW(e) PHWR), and Kudankulam 1 and 2 (2×1000 MW(e) WWER).

The fast breeder test reactor (FBTR) achieved a higher power level of 17.4 MW(th) corresponding to higher linear power rating of 400 W/cm (compared to 13.4 MW(th) and 320 W/cm earlier). The reactor has logged 1228 days of cumulative operation generating 164 GW·h of energy and 2.17 million units of electricity. 101.5 GW·d/t_{HM} peak burnup has been reached without any fuel failure, and clearance for further operation has been obtained. A subassembly at peak burnup was discharged for examination after cooling. An earthquake of intensity 5.6 on the Richter scale occurred in the sea 80 km south of the FBTR and had no effect on the plant. In the FBTR biological shield cooling system some coils were found leaking which limited reactor power operation. A consultant company was hired to chemically seal the leaks and the system was put back into operation after satisfactory testing for leak tightness.

Works towards the detailed design, manufacturing technology development, and safety clearances for the 500 MW(e) prototype fast breeder reactor (PFBR) project were continued. The radial blanket was re-designed with two rows, and the middle of equilibrium cycle breeding ratio was estimated as 1.049. The analysis of core reactivity fluctuations during seismic event showed that Category 1 design safety limits are met. The scenario of collapse of the core support structure was analysed and suitable preventive design measures implemented. It was concluded that the leak before break criterion cannot be fulfilled for the primary inlet pipe, and the guillotine rupture was assumed for the analysis of this Category 4 event. Transient analyses of the main vessel cover gas system showed that main vessel buckling failure risk is not present. However, as a measure of defence in depth a pressure relief valve is provided. Seismic analyses were completed for the primary sodium pump, the intermediate heat exchanger (IHX), and the rectangular shaped reactor containment building (RCB). The manufacturing technology development of the main nuclear steam supply system (NSSS) components and materials of PFBR was completed. A 75° sector of the roof slab of 12.9 m diameter and 1.8 m height was manufactured, meeting the required specifications.

As of beginning 2003, the review of the PFBR Preliminary Safety Analysis Report (PSAR) by a two level safety committee is nearing completion. Documents required for the environmental clearance were completed, and a public hearing was held for the project on 27 July 2001, being the first time that such a hearing was held for a nuclear power plant in India. Consequent to the clearance from the Tamilnadu Pollution Control Board, the project has been appraised by the Ministry of Environment and Forests, and the formal clearance is expected. A final report was prepared on the investigation of mechanical consequences of a core disruptive accident (CDA) in PFBR based on simulated tests on scaled down models. This covered all the tests done since 1997, and it is concluded that the integrity of the main vessel and roof slab are maintained for an energy release of ~ 1200 MJ, while the structural integrity of the IHX and of the safety grade decay heat removal system is assured up to 200 MJ. Primary sodium release to the RCB under CDA is estimated as 350 kg.

Fast reactor related R&D was continued in reactor physics, engineering development, safety engineering, structural mechanics, thermal-hydraulics, metallurgy, non-destructive evaluation, chemistry and reprocessing. Important works include: obtaining calculation vs. experiment (C/E) factors from flux measurements PFBR radial shield models using leakage neutrons from a thermal reactor; structural mechanical testing of a sodium pipe model, a main vessel model,

a core support structure model and a full size T-joint; and stress corrosion crack detection and nitric acid corrosion tests on special steels developed in India. Neutron radiography of FBTR fuel at burnups of 25 GW·d/t_{HM} and 50 GW·d/t_{HM} was completed and showed no major changes in the fuel region. The examination of the fuel at 100 GW·d/t_{HM} is to start.

2.4. Japan

In Japan, there are two fast reactors, JOYO and MONJU.

The loop type experimental fast reactor JOYO (2 loops, no steam generator installed) achieved initial criticality in 1977. The reactor was operated from 1978 to 1982 with the 50 MW(th) (increased to 75 MW(th) after appropriate modification works) MK-I breeder core, and from 1982 on with the 100 MW(th) MK-II irradiation core. Currently, JOYO is being upgraded to the MK-III core that will have an increased irradiation capacity (both increase of the fast neutron flux and of the number of irradiation rigs). The status of these upgrading works is as follows: the modification of the cooling system was completed in September 2001, the core replacement was started in the summer of 2002, and the MK-III initial criticality was scheduled for the summer of 2003. The fast neutron flux will increase by 30% in the MK-III core as compared to the MK-II one, while the number of irradiation rigs will be increased by a factor of two. At the same time, the MK-III core will have higher plant availability due to the reduction of the periodic inspection periods and reduced fuel exchange time. Overall, the MK-III core will lead to an increase of JOYO's irradiation ability by a factor of four as compared to the MK-II core.

The 714 MW(th) (280MW(e)) loop type prototype fast reactor MONJU has three loops. Sodium outlet and inlet temperatures are 529°C and 397°C, respectively. At turbine inlet, the steam temperature is 483°C, and the steam pressure is 12.5 MPa. The primary and secondary coolant pipes are made out of an austenitic 304-type stainless steel. MONJU construction works were started in October 1985, and by March 1991 component installation was completed. MONJU achieved initial criticality in April 1994, and was connected to the grid in August 1995. In December 1995, with the reactor at 40% power, a sodium leak incident took place in the secondary coolant pipe. In the aftermath of the sodium leak incident, JNC, performed a thorough investigation of the cause of the incident. A comprehensive safety review of all aspects of the MONJU design and operation has been conducted. At present, work is concentrated on the countermeasures against sodium leakage. The safety licensing examination by the Japanese government has been completed in December 2002. After the agreement of the local government, the actual improvement work will start and will take approximately 18 months to be completed.

In 1999, JNC started a feasibility study for the early commercialisation of the fast reactor cycle system. The scope of the study is to assess the feasibility of the fast reactor cycle system to meet the following requirements: ensure safety, achieve high economic competitiveness, establish effective utilization of resources, reduce the environmental burden, and enhance non-proliferation characteristics. The feasibility study is checked and reviewed approximately every 5 years. Looking at 2015 as time horizon, the feasibility study is carried out with the goal of establishing the most attractive fast reactor cycle system. In July 1999, JNC and Japanese electric utilities jointly started the first phase of the study, with the participation of the Central Research Institute of Electric Power Industry (CRIEPI) and the Japan Atomic Energy Research Institute (JAERI). During this phase, a wide range of technical alternatives incorporating innovative technologies were reviewed and evaluated. Data and materials

required for clarifying the commercialisation strategy were collected and developed, and the most promising concepts for the fast reactor cycle were selected. The first phase of the study was completed in March 2001. The second phase of the study was started in April 2001. During the second phase, the overall consistency of the fast reactor cycle is being assessed, on the basis of some engineering-scale tests. The second phase is scheduled to last till March 2006. At the end of the second phase, the number of promising concepts selected in the first phase will be narrowed down, and the essential research and development areas will be identified.

2.5. Republic of Korea

In Korea, nuclear power plants generate about 39% of the total electricity, and the role of nuclear power plants in electricity generation is expected to become more important in the future years due to the country's poor natural resources. The significance of nuclear power will become even greater, considering its practical potential in coping with the greenhouse gas emission control. The increase of nuclear power capacity eventually raises the issues of efficient utilization of uranium resources and of spent fuel storage. Liquid metal cooled fast reactors (LMR) will eventually be the most promising nuclear power option, considering their enhanced safety based on inherent safety characteristics, their transuranics (TRU) reduction capability (thus contributing towards solving spent fuel storage problems), and their proliferation-resistant actinide recycling capability.

The Korea Atomic Energy Commission (KAEC) revised the National Nuclear Energy Promotion Plan in 1997 and approved the LMR Design Technology Development Project as a national long term R&D programme. The objective of the LMR Design Technology Development Project is to develop the design technologies necessary for the design of an economically competitive, inherently safe, environmentally friendly, and proliferation-resistant fast reactor concept. Based upon the KAEC decision, the Korea Atomic Energy Research Institute (KAERI) has been developing KALIMER (Korea Advanced LIquid MEtal Reactor), a pool-type liquid metal cooled reactor generating 392 MW of thermal power. The first three-year phase of the project was completed in March 2000. During this first phase, the basic computer codes and methodologies necessary for design and analyses have been developed, and an effort has been made to establish a self-consistent conceptual design of the system configuration, arrangement and key features satisfying the design requirements. Efforts have also been made to develop basic sodium technologies, such as measurement or detection techniques, as well as investigations on thermal-hydraulics and sodium fires. The conceptual design of KALIMER was finalized during phase 2 of the project that started in April 2000 and was completed in March 2002. During the second phase, computer code improvements and experiments for model validation were performed. These codes and methodologies were utilized to develop a conceptual design based on the preliminary conceptual design obtained in the first phase. Phase 3 covers the three-year period from 2002 to 2004. The focus in this phase is on the development of basic key technologies and the establishment of advanced concepts. Any innovative trends in the development of fast reactor design will be reviewed thoroughly and included in the KALIMER design if it improves the safety and efficiency. Supporting R&D will be carried out to further validate the design codes and methods.

As an effort to enhance the key LMR technologies, KAERI decided to join the I-NERI, a three-year collaboration program between Argonne National Laboratory (ANL) and KAERI. The objective of this collaboration is to identify and quantify the performance of innovative design features in metallic-fuelled, sodium cooled fast reactor designs. Korea also expects to

contribute to the development of Generation IV nuclear energy systems through the worldwide R&D collaboration within the framework of the Generation IV International Forum (GIF). Korea considers the sodium cooled fast reactor (SFR) and the very high temperature reactor (VHTR) to be the most interesting GEN-IV reactor concepts.

The detailed design of KALIMER and the feasibility of the construction are to be examined sometime during the mid 2010s.

3. TECHNICAL SUMMARY

The TM heard ten papers. There was ample time allocated to discussion, and the participants did engage in a very lively dialogue. From the overall deliberations, the following four main themes emerged: safety philosophy, structural integrity assessment, thermal hydraulics, and new concepts.

In the following sections, the countrywise assessment of these four themes is summarized. Following that, the discussions that evolved around the major technical issues addressed in the meeting are summarized. Issues on which an overall agreement was reached amongst the participants are discussed as 'resolved', while the others, on which there was no agreement, or where it was difficult to reach an unanimous position, are discussed as 'open' issues. Finally, indications on further Member States information exchange and collaborative R&D needs.

3.1. Safety philosophy

3.1.1. China

For CEFR, safety reviewers demand the designers to assess the consequences of the Double Ended Guillotine Rupture (DEGR), including the identification of the most critical location for the rupture. The designers' safety philosophy is to consider the leakage through a crack area equal to Dt/4 (D: pipe diameter, and t: pipe thickness) as the Design Basis Accident (DBA), and to classify the DEGR of the primary pipe as a Beyond Design Basis Accident (BDBA). However, in the analyses carried out for the DEGR, instantaneous primary coolant pipe (PCP) rupture has been assumed, and the most critical location obtained is the junction of the PCP to the grid plate. Temperature limits used to assess the consequences are such that mechanical characteristics of the cladding and the structure of the fuel assembly are guaranteed and there is no coolant boiling in the reactor core.

3.1.2. France

The safety approach for Superphénix was deterministic. However, for historical reasons, the safety approach followed by CEA later for the European fast reactor (EFR) was a semi-probabilistic one, named 'lines of defence' (LOD). The deterministic approach leads to establish a list of events for each category of operating conditions, and to study the consequences of each event in order to verify that these consequences are in the allowed domain associated to the category. The LIPOSO ('LIaison POmpe SOmmier') break is classified in the last design basis class (Category 4, hypothetical event). In order to consider this event as an envelope of any fast loss of core-flow, it is assumed that it occurs in the most penalizing reactor conditions, so the break is a DEGR in 1s. To these assumptions, a fuel cladding failure in the hottest core channel is added, in application of the 'single failure' criterion. The radiological safety target for Category 4 events is 0.15 Sv at the site boundary, and the proof that the reactor is in a safe state. These safety targets are translated into two

decoupling criteria: first, the sodium temperature has to be below the boiling point in all the channels, and, second, the number of cladding failures must be limited.

In the frame of the LOD approach, in-service inspection (ISI) is considered to be the first level (prevention) of the defence in depth philosophy. While ISI was not possible for Superphénix, the MIR device in EFR was designed to measure relative displacements at junctions by ultrasonic telemetry.

3.1.3. India

The DEGR of one of the four pipes in PFBR has been considered as DBE, under Category 4. The worst location is found to be the junction of the pipe with the spherical header. The rupture time is assumed to be very close to zero, which can be considered as instantaneous. Under this event, the Category 4 temperature limits are to be respected, which means that bulk sodium boiling must be avoided, which, in turn, is achieved by limiting the mean subassembly sodium hotspot below 940°C, and the cladding hotspot below 1200°C, thus ensuring a coolable geometry. The design basis criteria such as to maintain the coolable geometry of a fuel subassembly is the same as in other reactors. However, the design safety limits on temperature are higher compared to other reactors. Such a prescription has been made mainly due to the fact that the coolable core geometry must be maintained after the occurrence of the event. However, currently efforts are being made to categorize the DEGR event under BDBE.

3.1.4. Japan

MONJU is a loop type reactor. The primary pipe, which is below the level of the system sodium, is located in the guard vessel whose function is to ensure the adequate sodium level. The leak-before-break (LBB) principle has been demonstrated for this design. Hence, the DEGR is not considered as DBE.

3.1.5. Republic of Korea

For KALIMER, the DEGR of the primary pipe is considered to be an extremely unlikely event. Hence, it is not included in the bounding event category. However, the inherent safety characteristics of KALIMER in the event of DEGR have been demonstrated.

3.2. Structural integrity assessment

3.2.1. China

The following reasons support the claim of high structural reliability of CEFR's primary coolant pipes:

- Large thermal inertia due to large sodium inventory (260 t in vessel);
- Low pressure in the primary coolant pipes;
- Good primary coolant pipes material (09×18G9 stainless steel);
- Large negative reactivity coefficients.

In the CEFR design, the primary coolant pipes are located between the upper and the lower core support. Thus, in the event of a DEGR of a primary coolant pipe, the pressure shock will not damage the bottom of the vessel. The results of comprehensive accident analyses have shown that the integrity of the pressure boundary of the primary vessel is maintained.

3.2.2. France

The prevention of accidents and ensuring structural integrity depends in the first place on design, dimensioning and manufacturing, i.e.:

- Number of pipes and pumps: in the case of Superphénix, each of the four pumps is connected by two primary coolant pipes to the core grid plate in order to minimize the consequences of a pipe rupture;
- The design of the coolant pipe and grid plate connections: their design ensures flexibility in order to avoid stresses in case of differential thermal expansions, pump vibrations, and pump seizure;
- Design and dimensioning considering the appropriate seismic loads;
- Stringent design rules and quality controls for manufacturing and welding;
- Specific tests (e.g. pump seizure) and periodic inspections during reactor start-up and operation (e.g. for the EFR, by means of the MIR device, which enables the measurement by ultrasonic telemetry of relative displacements at junctions).

3.2.3. India

A very comprehensive presentation of the structural mechanics analysis was given, starting from layout optimisation, including dimensioning of pipes. The CASTEM 2000 code has been used for the stress analysis, including fracture mechanics. The French code RCC–MR–1993 is used for checking the design compliance, and the fracture assessment is done according to the French Guidelines A16. The analysis shows that primary stresses due to internal pressure (0.8 MPa) and seismic moments have a margin of about a factor 2, over and above the safety factors provided in the design codes. The vibration loads are found to be insignificant.

Thermal transients following one secondary pump trip impose thermal loading on the primary pipe. All other transients have insignificant effects to this component. Due to these, the cumulative creep-fatigue damage is found to be < 0.2. An analysis, to check whether the critical crack length can be detected by means of core outlet temperature increase, indicates that the temperature rise in the core is very small (< 0.2 K). Hence, core outlet temperature monitoring cannot indicate any leak rate resulting by a critical crack opening. Alternative means are required.

For the PFBR, systematic experimental works have been carried out for assessing the integrity of the primary coolant pipes. This includes fracture propagation tests on plates and circular rings. The crack propagation behaviour predicted by the fracture mechanics analysis according to the A16 procedure have proved to be satisfactory when compared with test data. Tests have been conducted on 1/5 scale models of pipes to estimate the ratcheting strain including ovality of bend under simulated pressure, seismic loadings, as well as deflections corresponding to thermal transient loads. The data required for the analysis have been generated. Finally, it is concluded that ratcheting is not possible in the pipes, even under extreme loading conditions. The finite element prediction of ovalities and strains has excellently matched the experiments. Fatigue tests on the model indicate that cracks were not initiated, even after applying more than 500 plant life load cycles.
In view of the above results obtained for PFBR, it is recommended that DEGR need not be considered as a DBE. Nevertheless, as no leak detection is possible, DEGR is considered as a Category 4 DBE.

3.2.4. Japan

JNC presented the outline of the structural integrity assessment, as performed during the safety licensing process of MONJU. A large number of possible failure modes were investigated for the primary coolant pipes in MONJU, but most of them could be eliminated. Generally speaking, fatigue failure is the most likely failure mode. Therefore, fatigue crack growth evaluation was carried out in the structural integrity assessment. It was demonstrated that the crack growth under design duty cycles was negligible. Even if the crack penetrated under the loading conditions beyond design duty cycles, it resulted in detectable cracks, and there were large margins between the penetrated crack size and the critical crack size. As a design-base-leak path area, the conservativeness of the Dt/4 approach was demonstrated. As far as MONJU is concerned, the successful demonstration of LBB leads to the elimination of the DEGR as DBE, and supports the respective analyses for future fast reactor designs.

JNC presented the outline of the simplified creep-fatigue crack growth assessment procedure that will be applied for the structural integrity assessment of future fast reactor components. Within the framework of validation efforts, some experimental works have been carried out, and the results of the theoretical analyses were compared with the experimental results. Preliminary results of this validation effort indicate that there is the need for some improvement, especially with regard to the creep crack growth analysis method. For the time being, this simplified procedure can be adopted only to simple structures (e.g. plates, tubes) subjected to an idealized load. However, for all practical purposes, and in order to carry out the actual structural integrity assessment, it is necessary to improve the applicability of this simplified procedure to all structures (e.g. nozzles, elbows) under all loading conditions. JNC would propose to extend the validation basis for this simplified procedure by sharing the experimental data to an international benchmark exercise of the various fracture mechanics analysis methodologies.

3.2.5. Republic of Korea

Presently, efforts are being directed on basic studies of the creep crack growth and failure mechanisms with the objective of developing a model for the application of the LBB criterion to the KALIMER design.

3.3. Thermal hydraulics

3.3.1. China

The OASIS code has been used for the thermal hydraulics analyses. A large number of events were analysed. The objective of these studies was to identify the worst-case scenario. Therefore, rupture position, rupture time, and break size spectra must be analysed. Currently, the detailed thermal hydraulics analysis for the primary coolant pipe break accident as a function of the break position is being performed. This study is based on conservative assumptions, as required for Category 4 DBE analyses. The main results of this analysis are the core inlet and outlet temperatures, the break flow rate, the IHX inlet and outlet temperatures, as well as the and clad temperature distribution. The results of the calculations show that the hotspot temperatures for the cladding and for the coolant are below the design safety limits (DSL). These temperatures are lower than the sodium boiling temperature. The regulator accepted the methods applied, as well as the results of the analysis.

3.3.2. France

In the event of the LIPOSO break, the reactor thermal hydraulics depends on the core size and on the number of primary coolant pipes. In the case of Superphénix, with 8 primary coolant pipes, a large core, and the pessimistic assumptions of DEGR, the LIPOSO break leads to a fast over-heating of the sodium in the core, which causes both reactivity and a power increase. With all uncertainties taken into account, the accident is first detected by the measurement of the core sodium outlet/inlet temperature increase (ΔT), which causes fast reactor shutdown 3.6 s after the break.

Extensive studies, including experimental programmes, were performed, leading to the conclusion that the Superphénix safety provisions were able, under the more pessimistic conditions, to cope with this type of accident. Nevertheless, one conclusion, taken into account in the EFR design, was that it would be desirable to have the LIPOSO detection based on the power to flow ratio (P/Q). This would ensure earlier detection, and hence increase the safety margins on sodium boiling. Summarizing the French view, the LIPOSO break accident has two aspects: a mechanical and a safety demonstration aspect. The mechanical aspect is a design question, and it is evident that each country is able to design the pipe connecting the pump with the grid plate in such a way as to ensure that the DEGR is not a credible scenario. All improvements in the design are certainly desirable, but they do not change the necessity to tackle the second aspect, i.e. the safety demonstration under the assumption of the DEGR. With regard to this, the safety demonstration must be made in all cases that the DEGR accident can be detected, and that the reactor operational characteristics remain within the safety limits adopted in the respective safety philosophy.

3.3.3. India

The required thermal hydraulic analysis has been carried out using the one dimensional plant dynamics analysis code DYANA-P. The analysis of the instantaneous sodium coolant pipe rupture requires using two different sets of equations in the primary circuit hydraulic model for the initial steady state and subsequent transient.

Reactor shutdown (scram) parameters based on power to flow ratio, reactivity, power, and central subassembly (SA) sodium outlet temperature, are effective in limiting the consequences within Category 4 design safety limits (DSL). Sensitivity analyses have been carried out for input parameters like location of pipe break, amount of scram reactivity, and the value of the core by-pass flow pressure drop coefficients. In the worst case scenario, when all the above three parameters are assumed pessimistically, core flow reduces to a minimum of 30%, the maximum cladding hotspot is found to be varying between 1284 to 1406 K, and the mean SA sodium hotspot to be varying between 1120 to 1209 K, depending on the first or last scram parameters being effective. It has also been demonstrated that power to flow ratio and central SA sodium outlet temperature scram parameters are effectively available for all power levels from 50 to 100%. At power levels less than 50%, the DSL are not exceeded even without any safety actions The important assumptions made in the one-dimensional modelling are grid plate as a single pressure plenum, and integral momentum balance for rather long flow segments. These assumptions have been substantiated through separate three-dimensional hydraulic analyses of the grid plate, and through pressure wave propagation in the primary circuit (especially in fuel SA), respectively. Experimental investigation on a 1:2.75 scaled model pump under severe cavitation has been carried out to substantiate the assumption of cavitating pumps to give the stated flow.

3.3.4. Republic of Korea

In some advanced pool type reactors, the consequences of a postulated break of the primary coolant pipe can be mitigated by the inherent safety functions. This is achieved through the reactivity feedbacks induced by the Doppler, as well as sodium, radial and axial expansion reactivity effects. The control rod driveline length increase, and the operation of gas expansion modules (GEM) are also important reactivity feedback mechanisms.

The break of a pipe reduces the core flow, which results in power-to-flow mismatch for some seconds after the pipe break occurred. However, the power is stabilized, even though the automatic reactor scram is not activated. The GEM play an important role in providing the dominant reactivity feedback in case of an important core flow reduction resulting in the decrease of the GEM level below the top of the active core. The results of the primary coolant pipe break event analyses performed for the Korea Advanced Liquid Metal Reactor (KALIMER), which adopts several advanced design features, prove both a coolant sub-cooling margin of more than 400 K, and a stable system response.

3.4. Innovative concepts

3.4.1. China

The mechanical design of, and the supporting arrangement for the primary coolant pipes have to be carried out so as to prevent and eliminate the assumption of DEGR. This design will have to be substantiated and certified by detailed mechanical analyses and experiments. A double walled primary coolant pipe design should allow leak monitoring in the inter-space, thus permitting the assumption of leak-before-break, and, at the same time, strengthen the mechanical characteristics of the primary coolant pipes.

3.4.2. India

Various design concepts, to minimise the loss of coolant to core in case of pipe rupture, to improve ISI and to eliminate DEGR from DBE were presented for discussion.

Designs with increased number of pipes with reduced diameters have shown apparent advantages. Apart from bringing down the loss of core flow, it is possible to go for seamless pipes with reduced thickness, by which the structural reliability can be improved significantly. However, a general feeling has been expressed that increased number of pipes may decrease the structural reliability due to the overall increase of the pipe lengths. The incorporation of a flow diode device to increase the friction drop for break flow may also help to increase the core flow.

There are also various in service inspection (ISI) possibilities, by incorporating double wall pipes filled with argon in inter-space, which can be monitored for a sodium leak. As an example, the approach followed in BN-600 was discussed. In this concept, the outer wall is not leak tight, and a tube is incorporated through which sodium can flow from the inter space to the relatively hotter sodium in the space between inner vessel and thermal baffle. During no-leak condition, the temperature of the sodium in the tube is at its immediate surrounding. Any sodium leak in the primary pipe can cause flow in the tube that decreases the temperature of the sodium in it. Thereby, the leak can be detected. However, detailed discussions on this concept with Russian specialists are necessary.

The outcome of the discussion among the participants was that, while the safety implications of incorporating an increased number of pipes require careful considerations of all aspects, the idea of improved ISI, particularly the concept used in BN-600, was welcomed by all.

Finally, a possibility to relegate the DEGR event into the BDBA area is to demonstrate the primary coolant pipe integrity by performing the structural reliability analysis, based on probabilistic methods in conjunction with deterministic studies, evaluating the consequences for the maximum leak through a design basis crack opening area, e.g. Dt/4, as applied for MONJU.

3.5. Resolved issues

This section summarizes the issues on which consensus was reached among the participants.

- Number of ruptured pipes: only single pipe rupture needs to be considered, which itself is considered to be pessimistic.

- Availability of a reliable scram parameter: all the participants consider the power to flow ratio to be a reliable scram parameter. This requires a sodium flow meter in the circuit, which will truly represent the core flow. All the participants are unanimous on the choice of a core by-pass flow meter at the pump discharge, as in EFR.

- Location of rupture for study of consequences: the analysis of the primary coolant pipe rupture event has to be carried out for the rupture occurring at various locations of the pipe, and the worst location, including the junction between the grid plate and the coolant pipe, should be identified for DEGR analysis.

- Analysis method: the participants agreed that one-dimensional analyses to obtain the consequences of the event are good enough. However, flow redistribution amongst the various core subassemblies should be assessed separately. For this, three-dimensional hydraulic analyses or experiments, as performed by India, are required.

- Computer codes validation: considering the complexity involved in the analytical simulation of the entire phenomenon, agreement was reached on the necessity to quantify the approximations involved in the one-dimensional simulation codes with the help of experimental data from mock-up experiments of increasing complexity. This becomes even more important for larger cores.

3.6. Open issues

This section summarizes the status with regard to the contentious issues.

Categorization of the DEGR: there was consensus among the participants that the assumption of DEGR is very pessimistic, due to the fact that the structural reliability of the primary coolant pipe is very high, since it operates at low temperature and relatively low primary stresses. Moreover, the thermal stresses are moderate, and with the choice of highly ductile material, as well as adopting high quality design and manufacturing with high level of quality control. The participants agreed, therefore, that the DEGR is analysed within the framework of a ‘safety philosophy’, not because of any strong mechanistic reasons. The participants from China, India, Japan, and the Republic of Korea propose that DEGR should be categorized as

BDBA, and, provided the design ensures LBB characteristics, the design basis leakage area as Dt/4 should be considered as adequate.

- Time before primary coolant pipe rupture: coolant pipe rupture has been considered to be instantaneous in the DEGR event analyses performed in China, India, and the Republic of Korea. The analyses performed by the French colleagues considered 1 s time before rupture. The assumption made for the time before rupture highly influences the evolutions of the fuel temperatures, as well as of the cladding and coolant following the event. It is agreed that for highly ductile materials, the assumption must be made that crack propagation from critical length to DEGR should take a finite time. However, the choice of 1 s for this period in the French analysis seems to lack justification (it is surmised that this was the shortest time that could be used in the course of the numerical simulations during the 1970s). Therefore, the need for a comprehensive study in determining this parameter is recognized.

- Temperature limits: the analyses performed by the Chinese and Korean specialists have shown that the cladding temperatures are below the boiling point of sodium so that local and sub-cooled sodium boiling are avoided. This is most likely a consequence of the design characteristics of their reactor concepts (i.e. negative sodium expansion reactivity effect, long and small diameter pipelines, and higher flow from the other pumps unaffected by the DEGR). The results obtained by the French and Indian experts showed that only the bulk sodium temperature could be restricted below the boiling point. The argument put forward by the latter is that, since DEGR is a Category 4 event, maintenance of a coolable core geometry after the event is sufficient. Hence, avoiding bulk sodium boiling, and ensuring a coolable geometry in the fuel subassemblies is to be considered as adequate for the DEGR event. The participants concluded that a better resolution on this issue is required.

- Demonstration of leak detection and the LBB criterion: the LBB criterion has been applied for loop type reactors, and thus the DEGR event is eliminated. There was general agreement on the fracture mechanics methodology to be adopted for this purpose. However, LBB justification is not possible for the primary coolant pipes in pool type reactors, because of the on-line leak detection requirement. If this problem can be adequately resolved through improved design concepts, the LBB criterion and appropriate fracture mechanics methodology can then be adopted to eliminate the DEGR as a DBE also for pool type fast reactor designs.

- Innovative design concepts: while no final judgement on particular improved design concepts was possible, the participants agreed that emphasis should be put on the study of those innovative concepts that can facilitate leak detection, ISI, and limit core flow reduction in the DEGR. In this context, it is useful to consider the double wall concept adopted for Russian reactors (BN-600).

3.7. Conclusions

The technical meeting has attained its objectives of in-depth information exchange on the primary pump rupture topic.

The technical meeting identified R&D needs and opportunities for collaboration in the following areas:

- Code validation;
- Innovative concepts;
- Guidelines for safety analyses.

Based on the discussions during the technical meeting, international collaboration was noted several times as being of significant value to the Member States programmes. The IAEA's role as promoter and facilitator of information exchange and collaborative R&D was clearly acknowledged.

More specifically, the participants identified the following R&D needs:

- Analytical benchmark exercises focusing on the validation of computer codes used to assess the consequences of a primary coolant pipe rupture. The benchmark model would be a reference pool type LMFBR design. The objective includes studying the sensitivity of certain input parameters.

- Code validation efforts in the area of crack growth methodologies, including JNC's efforts (both analytical and experimental) to develop and validate a simplified creep-fatigue crack growth methodology.

- Develop innovative concepts with regard to in-service inspection and liquid metal fast breeder reactor primary coolant pipe leak detection.

- Develop guidelines for safety analysis of the primary coolant pipe-rupture event in liquid metal fast breeder reactor.

SAFETY PHILOSOPHY OF PRIMARY PIPE RUPTURE EVENT IN PROTOTYPE FAST BREEDER REACTOR

S.B. BHOJE
Indira Gandhi Centre for Atomic Research (IGCAR), Kalpakkam, India

Abstract

In this paper, the structural mechanics features of primary pipes of the 500 MWe Prototype Fast Breeder Reactor (PFBR), and theoretical and experimental structural mechanics analyses carried out to demonstrate high structural reliability of the primary pipes, are highlighted in the first part. Subsequently, for the defence in depth approach, Double Ended Guillotine Rupture (DEGR) of one of the four pipes is postulated as a design basis event. This has been investigated by thermal hydraulic analysis for estimating temperature rise in fuel cladding and coolant and thereby demonstrated that the temperature limits specified for the category 4 event are respected. This paper also indicates possible provisions that can be incorporated in the design to demonstrate that the DEGR can be eliminated from design basis events.

1. INTRODUCTION

PFBR is a 500 MWe capacity, sodium cooled, pool type fast reactor. The overall flow diagram is shown schematically in Fig. 1.

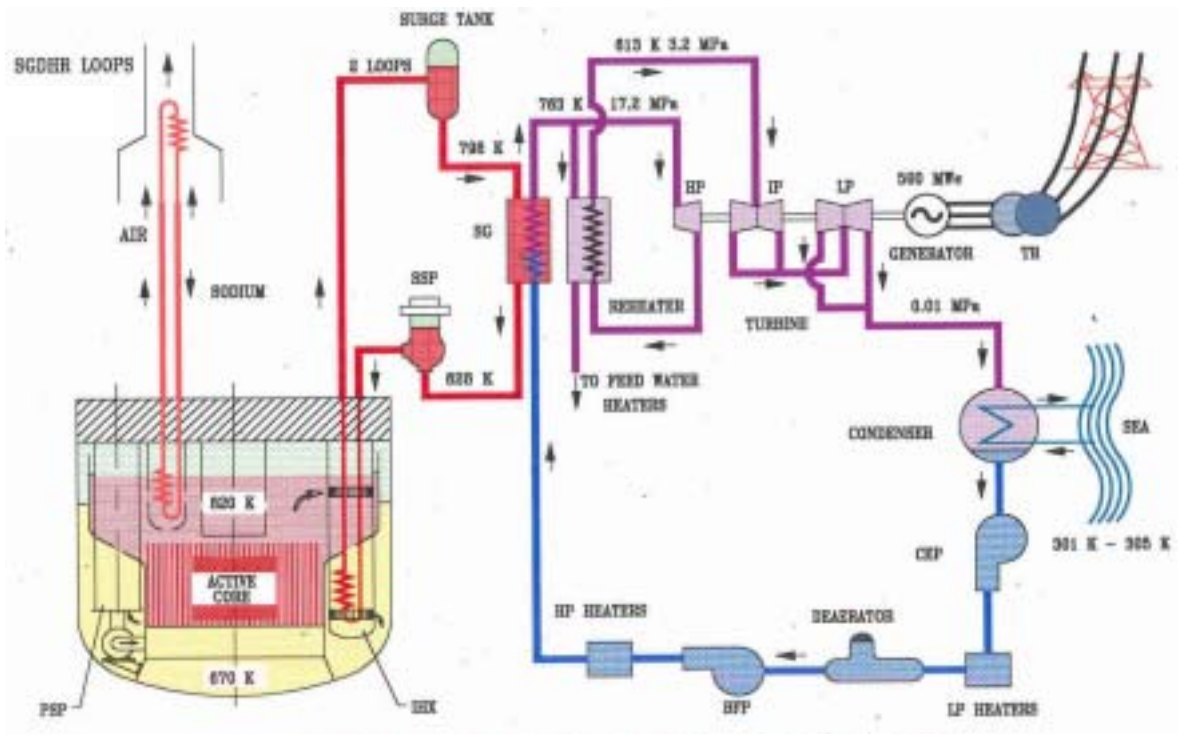

FIG. 1. PFBR flow sheet.

Nuclear heat generated in the 181 fuel sub-assembly (FSA) is transported to four intermediate heat exchangers (IHX) in which the heat is transferred from the primary to the secondary circuit, and in turn, is transferred to the steam generators (SG). Primary sodium is circulated by two primary sodium pumps (PSP). There are eight SGs in the secondary circuit. Steam

produced in SGs is supplied to a turbine through a steam–water system. The entire radioactive primary circuit is contained in the reactor assembly (RA). Figure 2 shows the Reactor Assembly (RA). It consists of the core, grid plate (GP), core support structure (CSS), inner vessel, main vessel (MV), primary sodium pump (PSP), IHX and the top shield (TS).

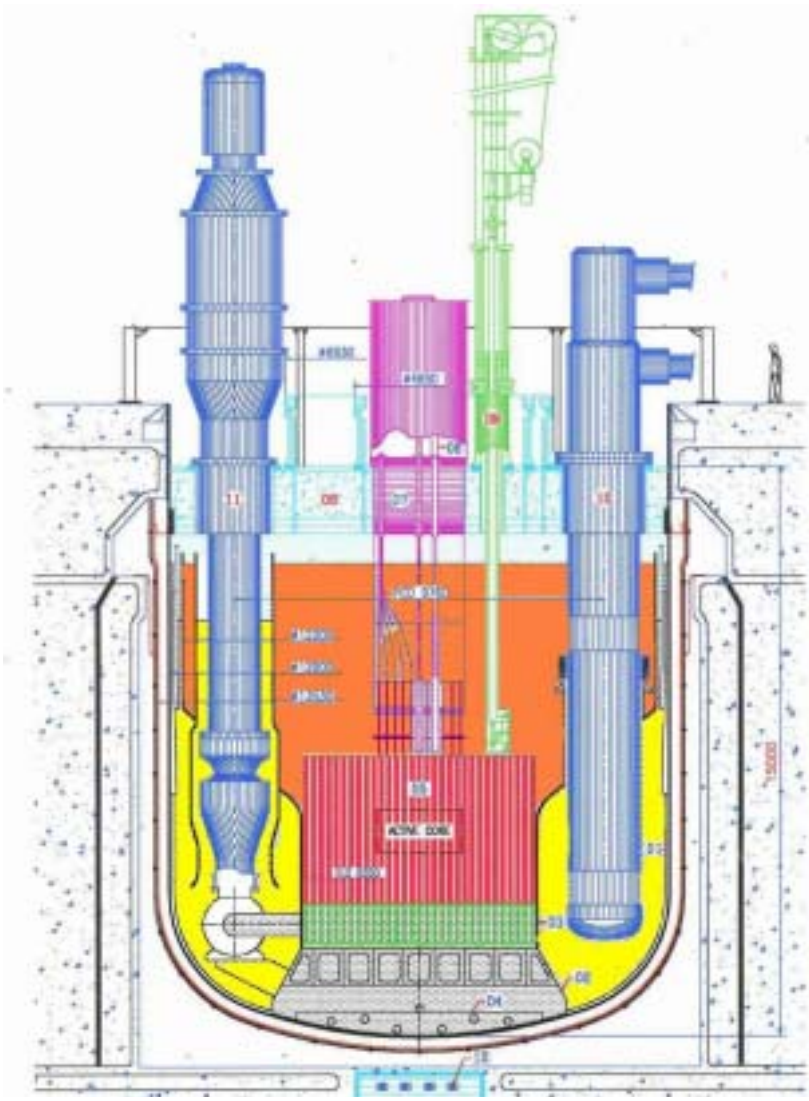

FIG. 2. Reactor assembly.

The sodium mass in the MV is ~ 1200 t. There are two sets of absorber rods, viz. nine control and safety rods (CSR), and three diverse safety rods (DSR). Each rod is independently driven by respective drives (CSRDM and DSRDM). The mechanisms are housed inside the control plug (CP) which, in turn, is supported on a small rotating plug (SRP), which is a part of TS.

Under normal operating condition, sodium at 670 K is drawn from the cold pool by PSP and is discharged through four pipes into the GP, which supports the Core Subassemblies (CSA) as well as distributes flow through them. The high temperature sodium (820 K) leaving the core impinges on the CP, which deflects the flow into the hot pool. Both hot and cold pools have a free sodium surface blanketed by argon. The flow of sodium through the IHX is driven

by a level difference (1.5 m of sodium) between the hot and cold pool free surfaces. The hot and cold pools are separated from each other by an inner vessel that is supported on the GP. Austenitic stainless steel of type 316 LN is the main structural material for the out-of-core components and modified 9Cr-1Mo (grade 91) is used for the SG. The PFBR is designed for a plant life of 40 y in compliance with design codes viz. RCC-MR (1993) and ASME (2001) and respects all the safety criteria formulated for PFBR (AERB, 1990).

This paper deals with the primary sodium pipes through which the primary sodium is fed to the core. Each PSP delivers sodium to a spherical header at the rate of 4.13 m^3/s at 75 mlc head. Subsequently, the sodium is fed to the grid plate through primary pipes. Each header is connected to two pipes, thus, there are 4 pipes in the primary circuit (Fig. 3).

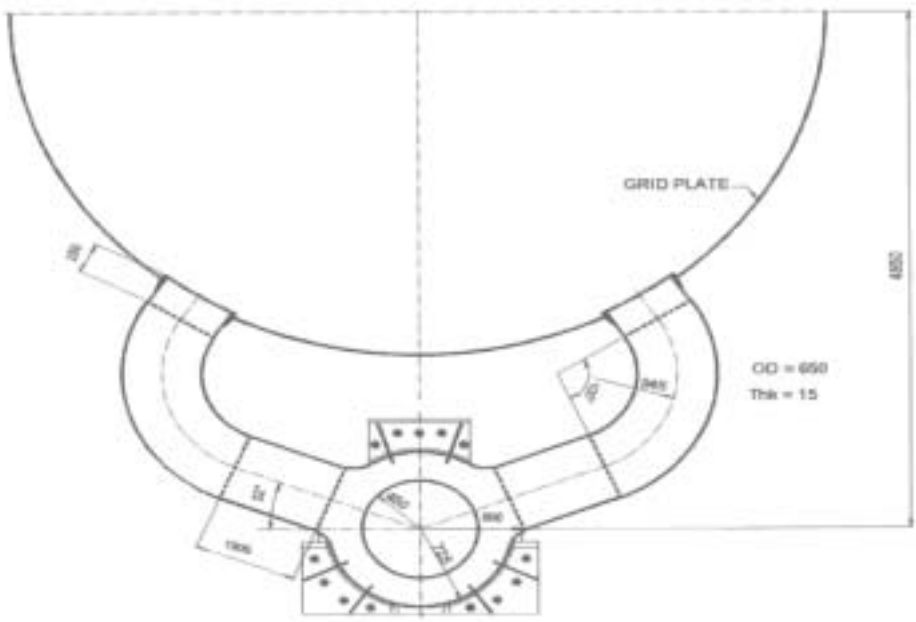

FIG. 3. Primary pipe details.

The failure of pipes, in form of large leaks or rupture can reduce the coolant flow to the core significantly, which is of great concern to reactor safety. Hence the structural integrity of the pipes should be very high. This has to be achieved by the selection of adequate materials, design, and manufacture, including quality control.

Structural integrity of the pipes has been demonstrated by detailed structural mechanics analyses, followed by experimental validations. Considering the safety philosophy of defence in depth, Double Ended Guillotine Rupture (DEGR) of one of the four pipes is postulated as a design basis event. This has been further investigated by thermal hydraulic analysis for estimating temperature rise in fuel, cladding and coolant and thereby demonstrated that the temperature limits specified for the Category 4 event are respected. In this paper, structural mechanics and thermal hydraulic analyses carried out on this subject are highlighted. Two companion papers provide more details of the investigations [1, 2].

2. STRUCTURAL MECHANICS ANALYSES

2.1. Structural mechanics features

The component is operating in a relatively comfortable environment. The neutron dose values are low (< 0.1 dpa) and hence irradiation effects are negligible. Sodium corrosion is negligible. The pipes operate at the cold pool temperature (670 K) where creep effects are insignificant. The operating pressure is 0.8 MPa. Steady state vibration and seismic load amplitudes are ~ 0.5 and 20 t respectively, which do not produce significant stresses. Thermal loadings are insignificant during normal operating conditions, since it is at isothermal temperature corresponding to the cold pool (670 K). Cold pool thermal transients, following secondary sodium and feed water pumps trips impose thermal loadings. However, they do not cause significant temperature differences on the pipe over and above the remaining part of the structure (< 50 K), and hence induced thermal stresses are moderate (~ 200 MPa). Flow induced as well as pump induced vibrations are negligible. Seismic stresses are also found to be negligible.

The material of construction is austenitic stainless steel SS 316 LN, which is highly ductile. The component is designed and constructed as per the class 1 rules of RCC-MR (1993). The pipe outer diameter of 630 mm is selected for proper flow distribution in the grid plate. By providing a sliding type arrangement for the spherical header, free movement of the pipe under thermal transients is ensured without sacrificing the rigidity requirements under seismic events.

2.2. Structural mechanics analysis: Theoretical

An optimum layout is arrived at, based on the requirement of flexibility to accommodate thermal expansion and the availability of space in the cold pool and compactness. The optimized layout consists of a short straight portion connected to a single curvature bend having a radius equal to 945 mm (1.5 times diameter). Stress analysis has been carried out for an internal pressure of 0.8 MPa and seismic loads imposed at the nozzle in the horizontal direction (peak value of 20 t under SSE). Analysis shows that the maximum P_m and (P_m+P_b) values are 76 and 80 Mpa, respectively, for the pipe wall thickness of 8 mm. These values are less than the primary stress limits of RCC-MR, 104 and 156 Mpa respectively. Considering the possible wall thinning during fabrication of the pipe bend, a plate thickness of 10 mm is used for the manufacture of the pipes, ensuring the minimum requirement of the wall thickness of 8 mm after fabrication.

Thermal stress analysis for the plant transients involving 10 different type of events, each with definite frequency of occurrence, due to pump trips and power failures, etc. shows that one secondary sodium pump trip is the most severe event that causes the maximum fatigue damage. The damages due to other transients are not significant. The cumulative creep-fatigue damage is ~ 0.2, which is less than the allowable value of 1. For the thermal transient analysis the spherical header is assumed to get stuck up during the initial reactor startup itself and remains under the stuck up condition throughout the plant life. Thus the computed creep-fatigue damage is on the conservative side. It is worth noting that the header stuck up condition results in lower primary stresses. Thermal transients obtained during a secondary pump trip followed by scram at 36 s are used. Figure 4 shows thermal and mechanical stress fields.

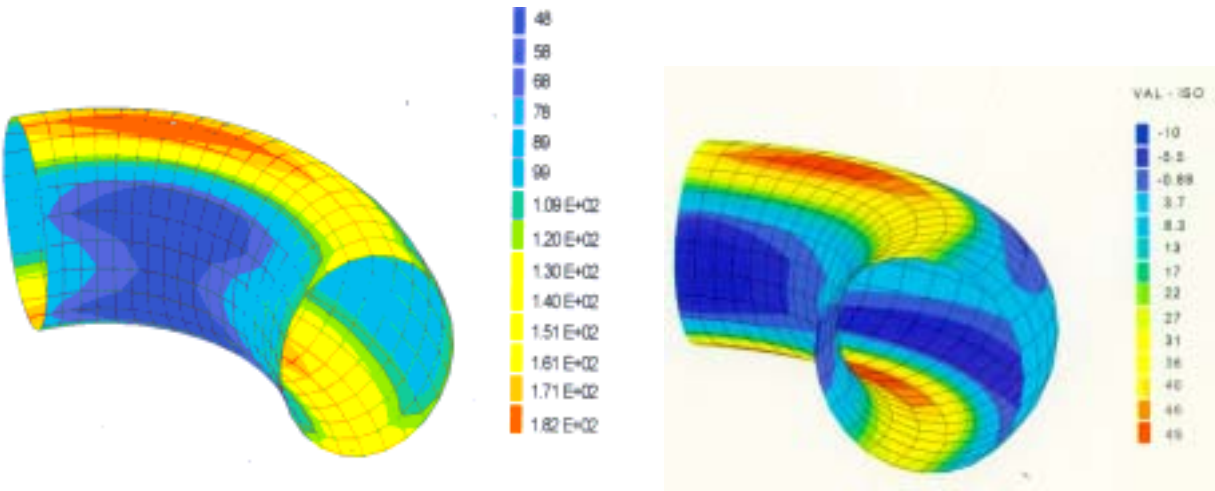

FIG. 4. Hoop stress contours under hot shock and SSE.

Fracture mechanics analysis has been carried out on the pipe, incorporating a surface crack like defect with depth (a) of 3.5 mm and length (2c) of 90 mm, indicating that the defect grows to a through wall crack (a = 15 mm) after application of 1270 load cycles as per French defect assessment procedure A16. This has a margin of 6 on the life and is judged to be adequate.

Figure 5 shows crack propagation behaviour.

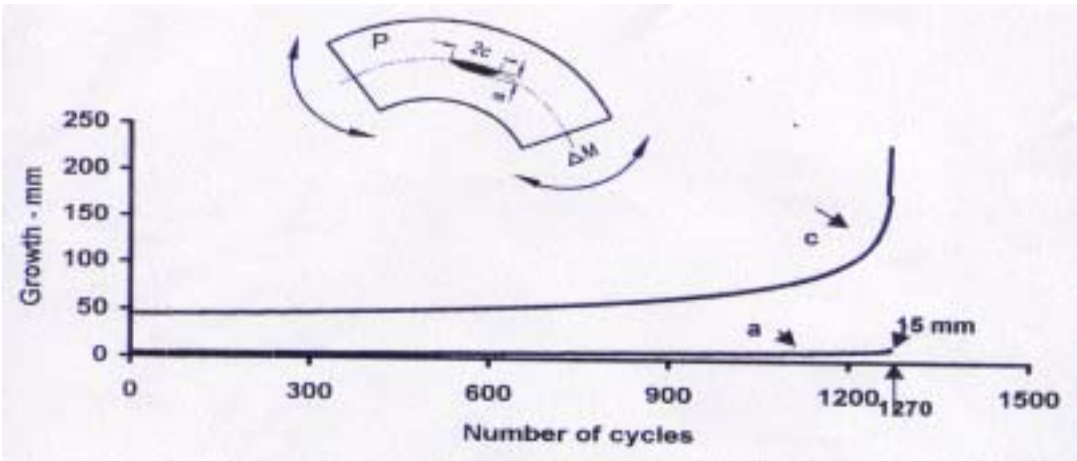

FIG. 5. Crack propagation at the crown.

2.3. Structural mechanics analysis: Experimental

The confidence on the structural reliability has been demonstrated by means of tests on 1/5th scaled down models (Fig. 6).

FIG. 6. Ratcheting tests on PSP model.

The tests focus on aspects, such as the validation of finite element prediction of strains at the critical locations, including ovalization under pressure and seismic loads, prediction of accumulated ratcheting strains under constant pressure, and cyclic secondary stresses imposed by axial displacement on the header (this simulates the cyclic thermal loadings), and identification of critical locations in the practical structures with welds. From these tests, it is confirmed that finite element prediction is satisfactory. Under a pressure of 1 MPa, ratcheting strains reached saturation at 1% on the crown, after about 200 load cycles of axial compression corresponding to 250 K temperature rise in the pipe. The conservative value of temperature rise in the pipe is 50 K. Hence, there is no possibility of ratcheting. A crack initiates at the junction of pipe at spherical header after about one million load cycles. So far two tests were completed. Further, six tests are planned to confirm various aspects. The availability of comfortable margins on the primary stress limits, as well as creep-fatigue damage limits over and above the safety factors that are incorporated in design code, and experimental validation of these results assure the structural integrity of the primary pipe under all the events.

3. SAFETY PHILOSOPHY

Since neither in-service inspection, nor leak detection is incorporated in the design, the lack of literature on this subject for FBR, following the traditional approach considered in water reactors which in fact operate at much higher pressures and as a defense-in-depth, a double ended guillotine rupture (DEGR) of one of the 4 pipes is postulated as a Category 4 Design Basis Event (DBE). With this assumption, thermal hydraulic analyses have been carried out to ensure that the temperature rise in the fuel, cladding and coolant are acceptable. The design safety limits for this event are: there should not be more than 50% melting of fuel in a pin, cladding hotspot should be less than 1473 K, and subassembly mean sodium hotspot should be less than the boiling point of sodium (to avoid bulk sodium boiling).

4. THERMAL HYDRAULIC INVESTIGATIONS

The analyses have been carried out in three steps. In the first step, evolutions of flow and temperature of the primary circuit and core respectively are obtained using the plant dynamics code DYANA-P. In the second step, the possibility of flow redistribution in the core under

pipe ruptured condition is analyzed. In the third step, the possibility of void formation in core is analyzed.

4.1. Pipe rupture event scenario

The scenario has been summarized in Fig. 7.

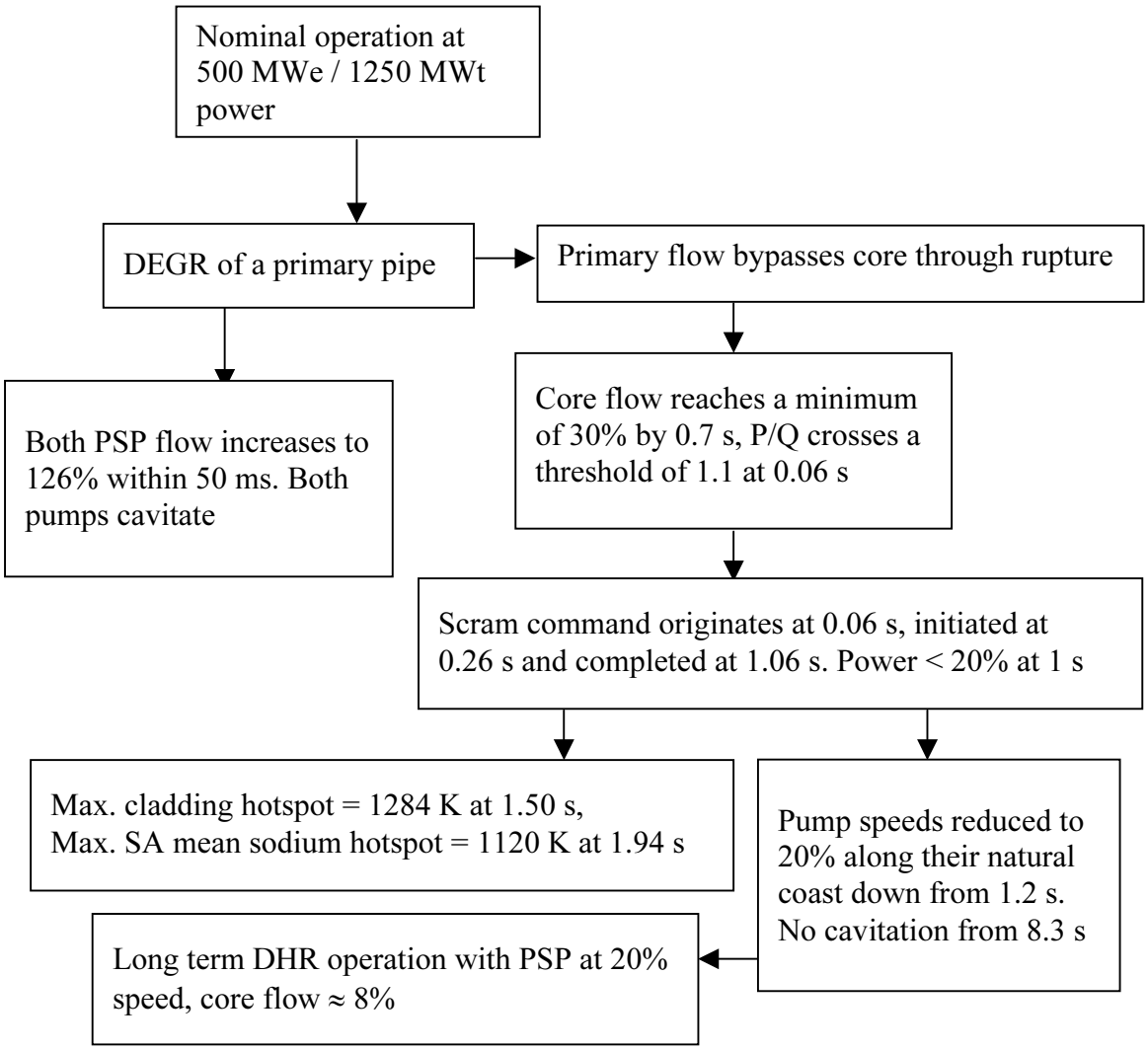

FIG. 7. Scenario following primary pipe rupture.

In DEGR of a primary pipe, the primary sodium flow bypasses core through the ruptured path back to the cold pool and the core flow decreases to a low value at a rapid rate and in turn causes sodium and cladding temperatures to rise. Any one of the scram parameters (for automatic emergency shutdown of the reactor), enabled by the Power to Flow Ratio (P/Q), Reactivity (ρ), Linear Power (Lin P), and Central SA Sodium Outlet Temperature (θ_{CSAM}) would shutdown the reactor. Other important consequences of this event are as follows. The resistance against which both pumps have to supply comes down sharply, which causes the pump flows to increase suddenly. Such sudden change of pump flow does not affect stand pipe flow immediately. Hence, a sudden increase in the pump flow causes reduction in the

stand pipe sodium level during the transient. This results in the reduction of available net positive suction head ($NPSH_A$) for the pump. Increase in the pump flow also results in an increase of the required net positive suction head ($NPSH_R$) of the pump. Thus, a situation of $NPSH_A$ becoming less than $NPSH_R$, leading to cavitation of the pump during this event.

4.2. Effects of analysis assumptions and pmp operability under cavitation

In evaluating the above results and concluding on the safety margins, two important model assumptions play key roles. They are (i) there is no circumferential redistribution of core flow amongst the various SA, and (ii) there is no vapour bubble formation in the SA due to flashing because of sudden reduction in pressure. These aspects have been investigated by separate analyses: (i) Three dimensional (3-D) hydraulic analysis of the flow pattern in the grid plate and (ii) pressure wave propagation analysis in the primary sodium circuit. It has been shown that there is no flow redistribution amongst various fuel SA and no chance of vapour bubble formation.

The pumps start cavitating within 0.05 s and their flows increase to 126% instantaneously. PSP speed reduction following scram causes $NPSH_R$ to fall and it becomes equal to $NPSH_A$ only at 3.4 s. $NPSH_R$ then follows $NPSH_A$ up to 8.3 s and then reduces below $NPSH_A$. There would be not cavitation in the pump beyond this time. Considering this predicted condition of the PSP, operating under cavitating conditions for a short duration following such an event, testing of a 1:2.75 scaled model pump under severe cavitation (80% head drop) condition has been carried out. The pump was operated for about 10 minutes. No flow fluctuation or vapour locking was observed. These investigations give a lot of confidence in the estimated parameters and safety margins demonstrated.

5. CONCLUSION

For the design conceived for PFBR, layout and thickness of the pipes are optimized to achieve better thermo-mechanical behaviour. Based on fatigue and fracture mechanics analysis, crack initiation life is found to be high (accumulated damage is < 0.2). Finite element modeling results are validated by experiments on $1/5^{th}$ scaled models. The experiments indicate that ratcheting failure mode is absent for the simulated pressure and cyclic loads. Cracks initiates after about one million load cycles. Thus structural reliability has been demonstrated with high confidence. Thermal hydraulic analysis of DEGR of one of the four pipes indicates that even though the core flow is reduced to 30% during the transient, specified temperature limits are respected. There is no significant flow redistribution among various subassemblies and formation of vapour in subassemblies. Efforts are being made to demonstrate that the failure probability of the pipe is less than 10^{-6} per reactor-year so that the DEGR can be eliminated from design basis events by means of providing additional inspections.

REFERENCES

[1] CHELLAPANDI, P., et al., “Theoretical and experimental assessment of structural integrity of primary pipe”, IAEA-TECDOC-1406, Vienna, (2004) 57–71.

[2] KASINATHAN, N., et al., “Thermal hydraulic consequences of primary pipe rupture”, IAEA-TECDOC-1406, Vienna, (2004) 91–107.

PHILOSOPHY OF LEAK BEFORE BREAK ASSESSMENT FOR JAPANESE PROTOTYPE FBR

T. WAKAI, K. AOTO, M. ICHIMIYA
Japan Nuclear Cycle Development Institute (JNC), O-arai Engineering Center, Japan

K. ITO
Japan Nuclear Cycle Development Institute (JNC), Monju Construction Office, Japan

Abstract

This paper outlines the concept of the leak before break (LBB) assessment applied to the primary coolant pipe of the Japanese prototype liquid metal cooled fast breeder reactor "MONJU". Reviewing possible failure modes for the primary coolant pipe made of an austenitic stainless steel, it could be concluded that the fatigue (creep-fatigue, for the hot leg piping) failure is most likely mode of pipe failure. Although through wall-penetration would not be expected to occur under design duty loading conditions, the maximum leak path area produced by fatigue crack growth was evaluated for the elbow of the reactor inlet down comer piping to consider a postulated sodium leak accident. In the estimation, an initial flaw was assumed at the beginning of service and fatigue crack growth from the initial flaw was simulated using a fracture mechanics technique up to a through-wall-penetration. The eventual crack length at through-wall-penetration was obtained under conditions beyond design duty cycles. Crack opening displacement for the penetrated crack in the pipe subjected to design duty internal pressure was also evaluated, which led to the postulated maximum leak path area. The sodium leak rate from a circular opening equivalent to the postulated maximum leak path area was evaluated and was much larger than detectable one by the leak detection system employed in MONJU. It was shown that there was much room between the detectable crack size and the size corresponding to the unstable fast fracture under design duty loading conditions and that LBB was ensured.

1. INTRODUCTION

MONJU is the Japanese prototype Liquid Metal cooled Fast Breeder Reactor (LMFBR). The principal characteristics are as follows:

Reactor type:	loop type (3 loops)
Thermal power:	714 MWt
Electrical power:	280 Mwe
Primary sodium temperature (reactor outlet/inlet):	529/397°C
Material of primary/secondary coolant pipe:	austenitic stainless steel (304SS)
Steam conditions (temperature/pressure):	483°C/127 kg/cm^{2}g (turbine inlet)

As MONJU employs the loop type design, it is one of the most essential issues in safety licensing to demonstrate the structural integrity of the primary coolant pipe.

The US Nuclear Regulatory Commission (NRC) expressed its point of view about the size of failure, through a classification by fluid energy for the class 2 pipes of Light Water Reactors (LWR) [1].

According to the US NRC point of view, a Double Ended Guillotine break (DEG) or an equivalent axial crack must be postulated for the High Energy Fluid System (HEFS) piping. In contrast, for the Moderate Energy Fluid System (MEFS) piping, a slit-like defect of D/2 in

length and t/2 in width (D and t are diameter and wall-thickness of the pipe, respectively) is postulated and it can be assumed that the fluid leaks through a circular opening of the area Dt/4. The MEFS is defined as that the maximum operating temperature is 100°C or less and the maximum operating pressure is 2MPa or less. Since all class 1 pipes of LWR are classified in HEFS piping, US NRC mentions only about class 2 pipes and does not classify the class 1 pipes for LWR. However, the classification can be applied for class 1 pipes for LMFBR.

In the classification, the temperature criterion is considered to be based on the relation between the maximum temperature and the boiling point of the fluid when the fluid is water.

When the fluid is sodium, the temperature criterion is not considered to be critical. Therefore, the primary coolant pipe in MONJU can be classified into MEFS piping and it is relevant to employ the point of view about the size of failure in the postulation of maximum leak path area. In this study, conservativeness of postulated leak path area, Dt/4 is discussed.

2. PROCEDURES

2.1. Failure mode investigation

The austenitic stainless steel 304SS, which is the structural material of the primary coolant pipe, is under stable environmental conditions, because the internal fluid is the coolant sodium under appropriate purity control and the external environment is nitrogen gas with the low content of oxygen and low humidity. The material is known for its compatibility with liquid sodium, high temperature strength and high ductility.

Hot leg piping must be used in the creep region, but the load-controlled stress in the primary coolant pipe is extremely low because of the low internal pressure. Under such a low internal pressure condition, creep rupture can not be expected to occur. The dominant loading is displacement-controlled thermal stress.

Several kinds of chemical tests, mechanical tests and non-destructive inspections were performed in production for the material of the primary coolant pipe. In manufacturing of piping system, pressure test and several kinds of non-destructive inspections were performed.

In addition, leakage of primary coolant is continuously monitored by sodium leak detectors as in-service inspection to confirm the integrity of the coolant boundary. These facts lead to the following judgments:

- Failure caused by corrosion is insignificant for stable environmental conditions;
- Ductile rupture, collapse or creep rupture caused by load-controlled stress is insignificant.
- Fatigue (creep-fatigue, for the hot leg piping) failure is the most likely mode of loss of pipe integrity;
- Fatigue failure, if it occurs, terminates as coolant leakage at the moment of crack penetration;
- Unstable fast fracturing is not expected to occur from such fatigue crack because of ductile and tough material and low internal pressure.

Therefore, the demonstration of the pipe integrity against fatigue failure for the primary coolant pipe is essential.

2.2. Structural integrity assessment

The flow diagram of the structural integrity assessment for primary coolant pipe is shown in Fig. 1.

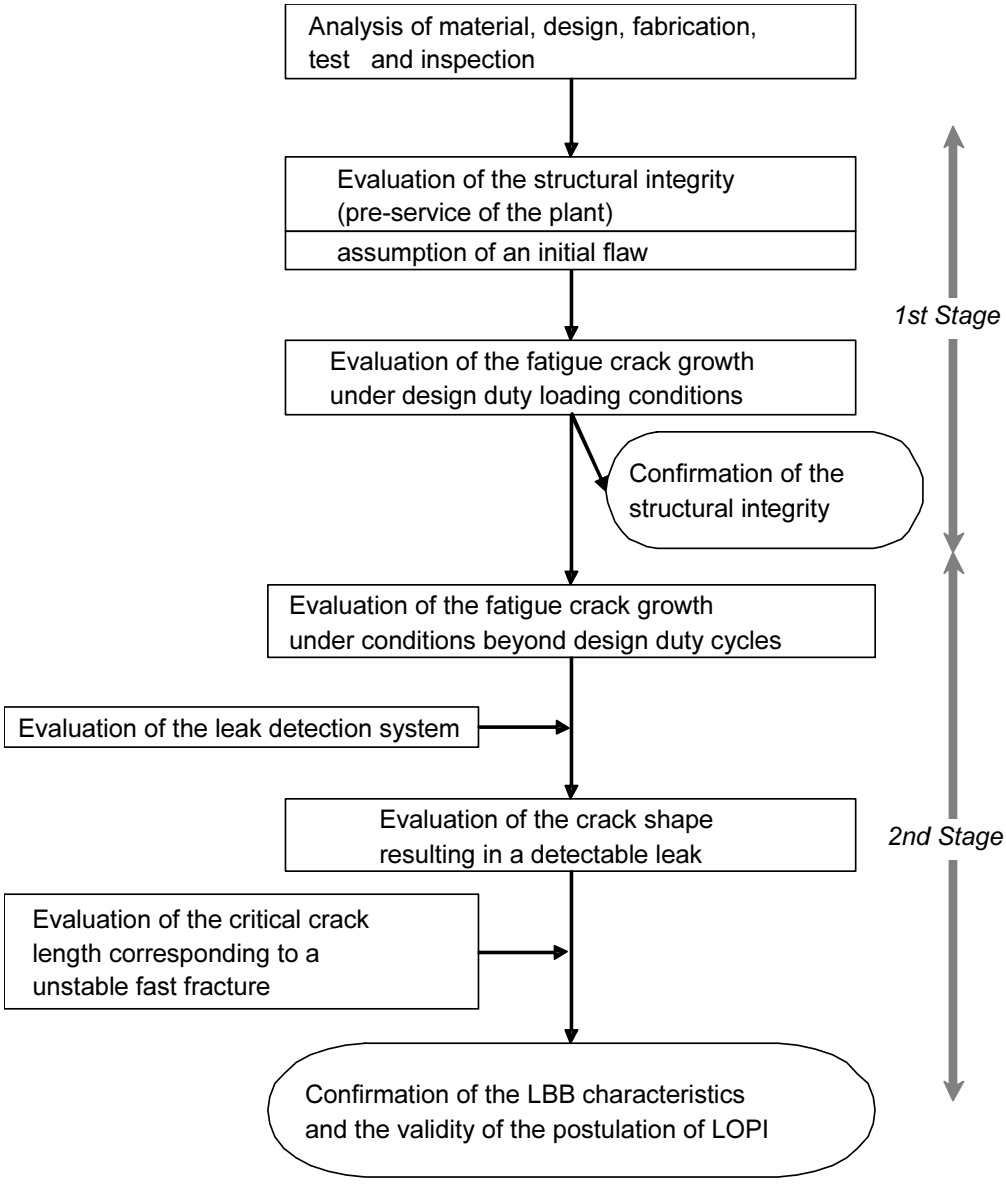

FIG. 1. Flow chart of pipe integrity assessment.

It consists of two major stages. The first stage is the demonstration of the pipe integrity during the plant service period. It is shown that even a small leakage of coolant will not occur, if a postulated initial flaw exists. The second stage is the demonstration of the LBB characteristics of a through-wall fatigue crack penetrating under load conditions beyond design duty cycles. The main tool for the structural integrity assessment is the fracture mechanics analysis program "FRAMSAP 5" developed to evaluate fatigue crack growth from a semi-elliptical surface flaw. This program was validated by fatigue crack growth tests [2].

Postulating an initial flaw on the inner surface of the crown of the elbow of the reactor inlet downcomer piping (diameter D = 609.6 mm), fatigue crack growth simulation under design duty loading condition was conducted as a most likely failure mode caused by the repetition of thermal expansion. The reason why this position was selected for the structural integrity assessment was that the stress on this part caused by thermal expansion was larger than that on any other part. Figure 2 shows the postulated initial flaw.

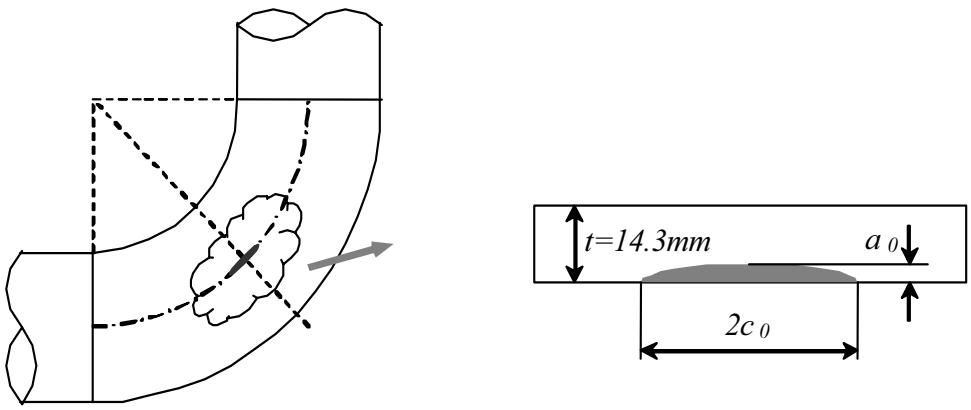

FIG. 2. Location, shape and dimension of the postulated initial flaw.

The flaw was a semi-elliptical crack of 25% in depth (3.6 mm) and 300% in length (42.9 mm) of the pipe thickness, respectively. The dimensions were determined considering detectable size in inspection before service referring some precedents (FFTF, CRBR).

The simulation gave small crack growth, approximately 0.3 mm in depth and 0.2 mm in length under design duty load conditions. It can be concluded that the fatigue crack growth from a postulated initial flaw is extremely small under design duty loading cycles and that the structural integrity of the pipes is assured during the plant service period.

2.3. Evaluation of maximum leak path area

2.3.1. Length of penetrated crack

As mentioned above, a crack will never penetrate the pipe thickness under design duty loading cycles. To consider a postulated sodium leak accident, the maximum leak path area produced by fatigue crack growth was evaluated for the elbow of the reactor inlet downcomer piping.

Postulating the same initial flaw at the same location as at that used in the structural integrity assessment, fatigue crack growth simulation was conducted up to a through-wall-penetration using “FRAMSAP 5”. The result is shown in Fig. 3.

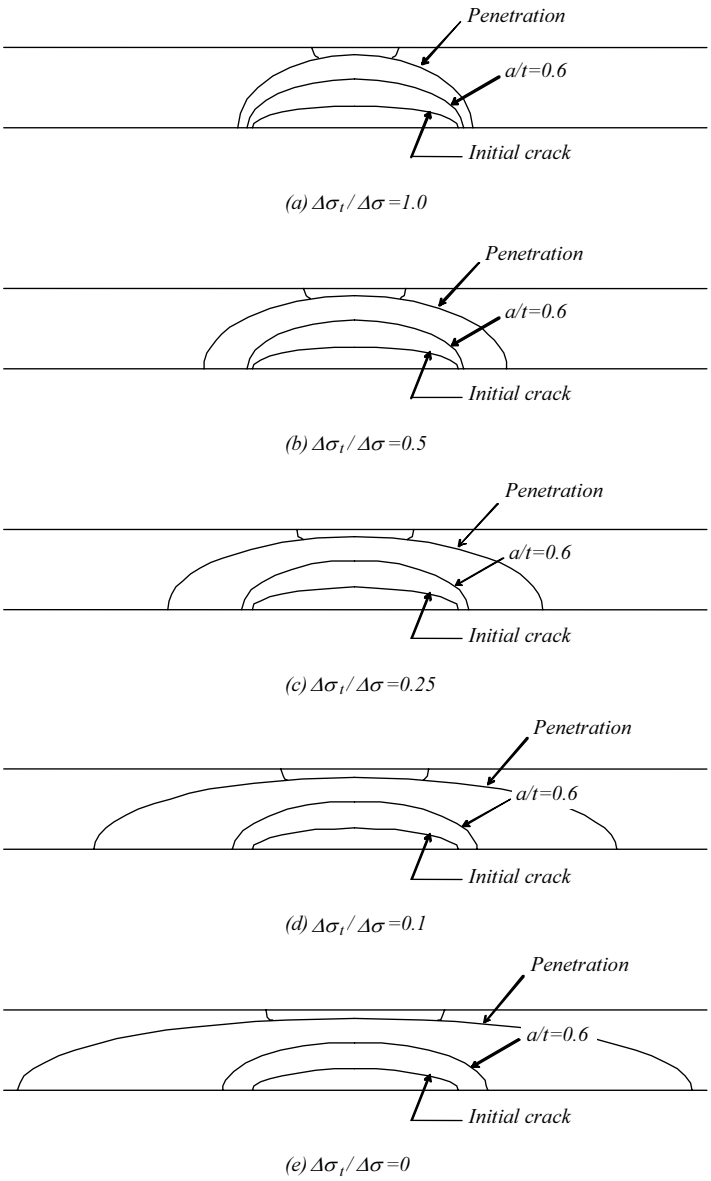

FIG. 3. Influence of stress field on crack configuration at a through-wall-penetration.

This figure shows that the eventual crack length at a through-wall-penetration becomes longer as the cyclic stress conditions varies from membrane stress field to bending one. Figure 4 shows the dependence of crack length at through-wall-penetration on the stress field.

As shown in this figure, the crack length at a through-wall-penetration is almost independent on the initial flaw configuration. The maximum crack length is achieved at a pure bending stress field and that is approximately 12 times of the pipe thickness, namely 180 mm for the elbow of the reactor inlet downcomer piping. It is expected that continuous sodium leak monitoring by detectors such as gas sampling leak detectors should detect leakage immediately and with certainty.

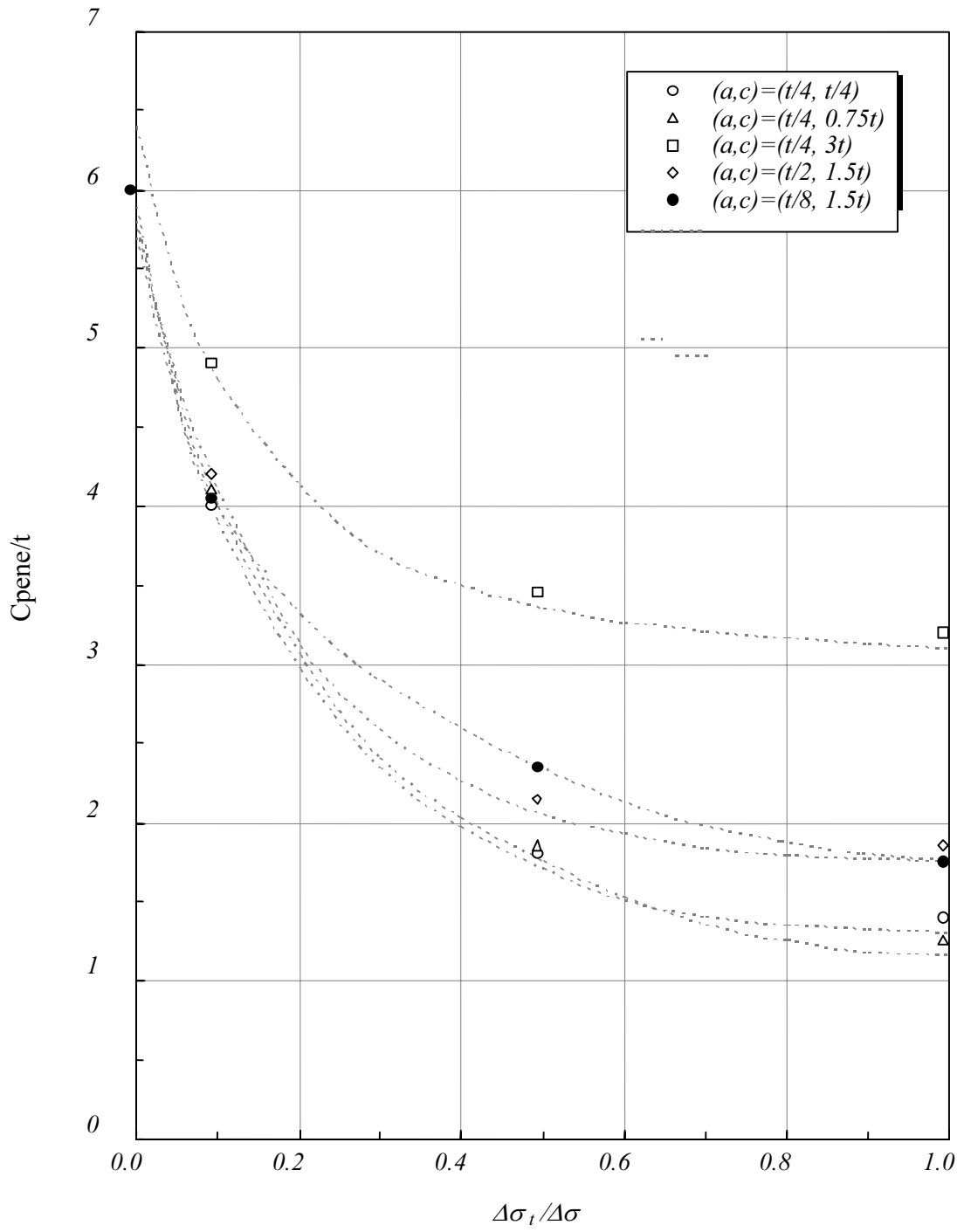

FIG. 4. Dependence of crack length at through-wall-penetration on the stress field.

As shown in this figure, the crack length at a through-wall-penetration is almost independent on the initial flaw configuration. The maximum crack length is achieved at a pure bending stress field and that is approximately 12 times of the pipe thickness, namely 180 mm for the elbow of the reactor inlet downcomer piping. It is expected that continuous sodium leak monitoring by detectors such as gas sampling leak detectors should detect leakage immediately and with certainty.

According to the Japanese Industrial Standard (JIS), for stainless steel pipes of a diameter lager than 3B and a wall-thickness smaller than Sch10S, or that of a diameter lager than 4B and a wall-thickness smaller than Sch20S, the following relation between D and t is retained:

$$D/t \geq 24 \tag{1}$$

Then

$$\ell \cong 12t \leq D/2 \tag{2}$$

Thus the postulation of a crack length of D/2 is considered to be conservative and to become more conservative as D/t becomes large except for the small diameter pipe. The diameter and the wall-thickness of the primary coolant pipe in the MONJU are shown in Fig. 5. This figure shows that the values of D/t satisfy eq.(1).

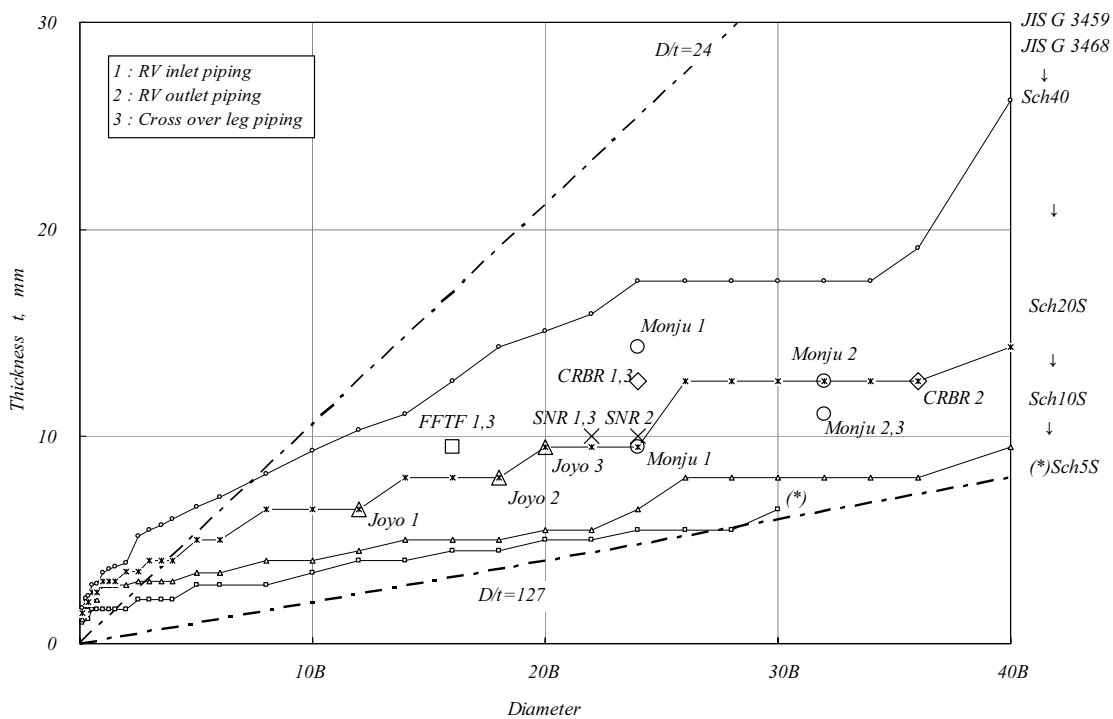

FIG. 5. Relationship between diameter and wall thickness of stainless steel pipes.

The internal pressure of the downcomer piping is approximately 1 MPa. The critical crack length corresponding to the unstable fast fracture under such a low internal pressure is also estimated to be larger than several times of the pipe diameter, based on modified Hahn's flow stress theory [3]. Therefore, it can be concluded that the eventual length of penetrated crack produced by fatigue is smaller than that corresponding to the unstable fast fracture and that the LBB of the pipes is ensured.

2.3.2. Crack opening displacement

The crack opening displacement is estimated for a penetrating crack of D/2 in length, contained in a cylindrical shell of D in diameter subjected to internal pressure as shown in Fig. 6(a). Approximating by using a plate model as shown in Fig. 6(b) and assuming $\sigma_f = 2M\sigma_\theta$ due to shape effect, the following equation is developed.

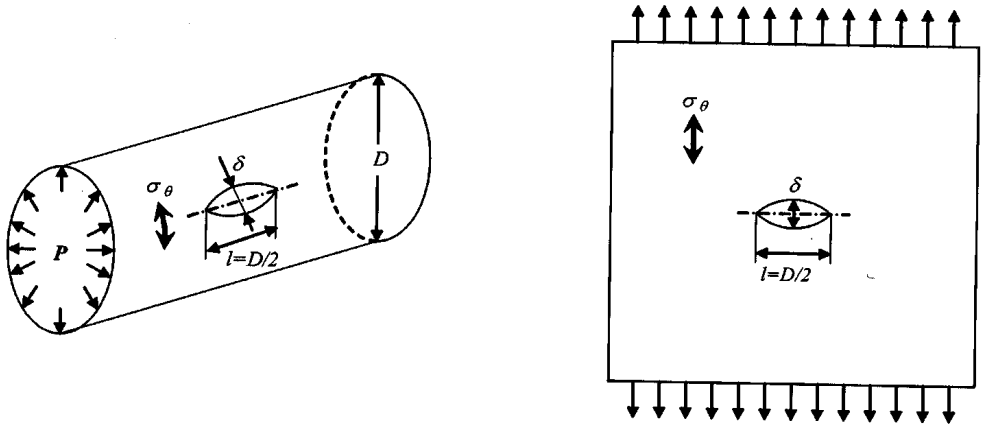

(a) Pipe with an axial through-wall crack *(b) Infinite plate with a through-wall crack*

FIG. 6. Approximation of central crack opening displacement.

$$\delta = \frac{2\ell\sigma_f}{E} = \frac{4\ell M\sigma_\theta}{E} = \frac{PM}{E}\left(\frac{D}{t}\right)^2 t \tag{3}$$

where ℓ=D/2, σ_θ=(PD)/(2t), E is Young's modulus and M is a parameter represented as follows.

$$M = 1.6 + 0.29\lambda \tag{4}$$

$$\lambda = \sqrt[4]{12(1-\nu^2)}\,\frac{\ell}{2}\Big/\sqrt{\frac{Dt}{2}}$$

where ℓ = D/2, is Poisson's ratio (= 0.300). In the case of ℓ = D/2,

$$\lambda = 0.643\sqrt{\frac{D}{t}} \tag{5}$$

As shown in Fig. 5, stainless steel pipes according to JIS retains following relation.

$$D/t \leq 127 \tag{6}$$

according to the MEFS conditions, assuming that the internal pressure is less than 2 MPa and that Young's modulus of 304SS is greater than 144 000 Mpa, because the maximum temperature is 650°C, the following equation is developed from eqs.(3) and (4).

$$\delta \leq 0.8t \tag{7}$$

The width δ_s is determined as follows for a slit which posses the same length and area as the crack of D/2 in length and 0.8t in central opening width.

$$\delta s \cong t/2 \tag{8}$$

Thus the width of t/2 is considered to be conservative when the penetrating crack is modelled on a slit.

In the primary coolant pipe in MONJU, it is expected that D/t is smaller than or equal to 120 to prevent buckling in evacuated conditions, when externally pressurized.

Based on above mentioned considerations, the leak path area of Dt/4, which corresponds to the area of a slit of length D/2 and width t/2, is judged to be conservative for the quantitative expression of loss of pipe integrity in the safety analysis of MONJU.

3. CONCLUSIONS

- Possible failure modes were investigated thoroughly. It is shown that fatigue (creep-fatigue, for the hot leg piping) failure is the most likely mode of loss of pipe integrity and that other modes can be eliminated.
- Postulating an initial flaw, the pipe integrity is confirmed under design duty loading conditions using a fracture mechanics technique.
- Even if the crack penetrates the pipe thickness under conditions beyond design duty cycles, unstable fast fractures would not be expected to occur and the mode of LBB is ensured. It is revealed that the postulated maximum leak path area, Dt/4, is conservative.

REFERENCES

[1] US Nuclear Regulatory Commission, "Standard Review Plan", NUREG-75/87, Section 3.6.1.

[2] SAKAKIBARA, Y., et al., "Fatigue Crack Propagation from Surface Flaw of Elbows", SMiRT-6 E7/3 (1981).

[3] ANDO, Y., YAGAWA, G., OKABAYASHI, K., "The Application of the Finite Element Method to the Analysis of Fracture of Cylindrical Shells", SMiRT-2 G5/4 (1973).

MAIN PIPE RUPTURE ACCIDENT ANALYSIS FOR THE CHINESE EXPERIMENTAL FAST REACTOR

YANG Hongyi, XU Mi
China Institute of Atomic Energy (CIAE), Beijing, China

Abstract

The main pipe rupture accident is the most serious one for the loss of coolant accident of pool type sodium cooled Fast Breeder Reactor (FBR). To simulate this accident, a model is developed based on the OASIS code, which is a French fast reactor system safety analysis code. To abide by the strict accident analysis principles, the main pipe rupture accident is calculated for various position of the pipe. Accident sequence and key parameters, including the fuel cladding temperature of reactor, are obtained for each case. The calculation results show that the fuel cladding temperature is below the safety limitation and the coolant temperature is lower then the saturation temperature of sodium in all cases.

1. INTRODUCTION

LOCA (Lost of Coolant Accident) is a type of serious event not only for a Pressure Water Reactor (PWR), but also for the Fast Breeder Reactor (FBR). The Main pipe Rupture accident is an important LOCA accident for the FBR.

For a typical pool type FBR, for example the SPX and BN-600, there are several pumps and circuits in the primary heat transfer system. So the consequence of one primary pipe rupture accident is not so severe as other FBR that have only two circuits in the primary heat transfer system. The China Experimental Fast Reactor (CEFR) is such a reactor.

The CEFR is a typical sodium cooled pool type fast reactor. The thermal power of the CEFR is 65 MW, matched with a 25 MW turbine generator. The CEFR is under construction now, and first criticality is expected in 2005.

The PSAR of the CEFR was finished in May of 1998, but the review lasted 2 years. The primary pipe rupture accident is the key accident and the most important topic in this review. The owners (us) think that the 0.25DT (D is the diameter of the pipe and T is the thickness of the pipe) size break initial event should be a DBA (Design Base Accident), but the double-ended guillotine break instantaneous should be a BDBA (Beyond DBA). However, the reviewer was of the opinion that the double-ended instantaneous guillotine break should be DBA. The owner should calculate the break position spectrum in order to find the most serious case.

The advantage is that the CEFR has a large sodium pool: it has 260 t of sodium in the primary loop and the good characteristic of the sodium coolant, low pressure in the primary loop, the material of the pipe has a good toughness, the large negative reactivity feedback, etc. However, the shortcoming is that the primary pipe is a one-layer tube and that there are only two circuits with 4 pipes in total.

In spite of the fact that the safety cases for Monju, CRBRp, SPX, and BN-600 have all considered that the double-ended guillotine instantaneous break should not be a DBA (Design

Base Accident), we calculated almost all the cases, the break position spectrum, the break continue time spectrum, the break position spectrum, the break size spectrum, and so forth.

In this paper we show the main result of the break position spectrum calculations. The restrictive reactor safety and conservative assumptions requested by the authorities are applied in these calculations.

The configuration related to the CEFR reactor protection system is also introduced in this simulation. The various rupture positions and all the transient parameters of the primary loop, as well as the accident sequence are obtained with the help of the system safety analysis code OASIS. This code is based on the original French code OASIS, modified to simulate the CEFR.

After comparing the results from these cases, the most critical position for the safety of the reactor core is confirmed. The results show that all the key parameters of the reactor core are within the safety limits during the course of the accident, and that the primary containment of the reactor is not destroyed.

2. INTRODUCTION OF CEFR

The CEFR is a sodium cooled 65MWt experimental fast reactor with $(Pu,U)O_2$ as fuel, but UO_2 as first loading, Cr-Ni austenitic stainless steel as fuel cladding and reactor block structure material, of bottom supported pool type, with two main pumps and two loops for primary and secondary circuit respectively. The water-steam tertiary circuit has also two loops, but the steam superheater is incorporated into one pipe that is connected with the turbine. Figure 1 shows the scheme of the CEFR main heat transfer system.

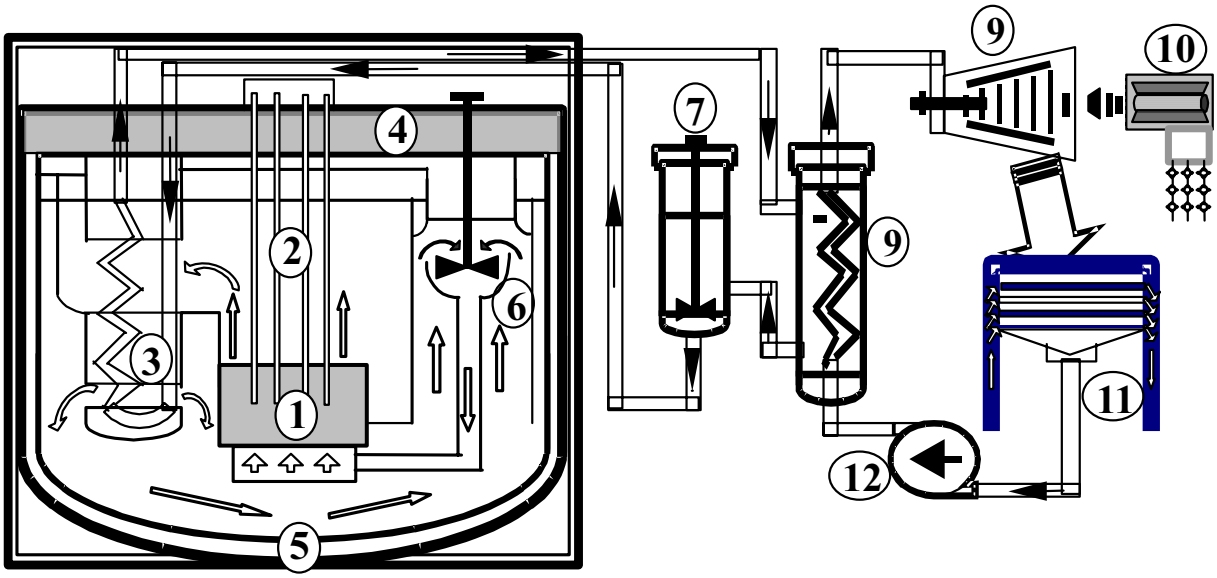

Primary Loop Intermediate Loop Water-Steam Loop

Legend of the Figure 1:

1	Core	7	Secondary pump
2	CRDM	8	Steam generator
3	IHX	9	Turbine
4	Top shield	10	Generator
5	Vessel	11	Condenser
6	Primary pump	12	Condenser

FIG. 1. Scheme of main heat transfer systems of CEFR.

The primary circuit of the CEFR is composed of two main pumps, four intermediate heat exchangers, reactor core support diagrid plenum, pipes, and cold and hot sodium pools. In the cold pool, the two primary loops are separated from each other, but in hot pool they are linked up. In normal operation the average sodium temperature in the cold pool is 360°C and in the hot pool it is 516°C. Figure 2 shows the CEFR primary pipe.

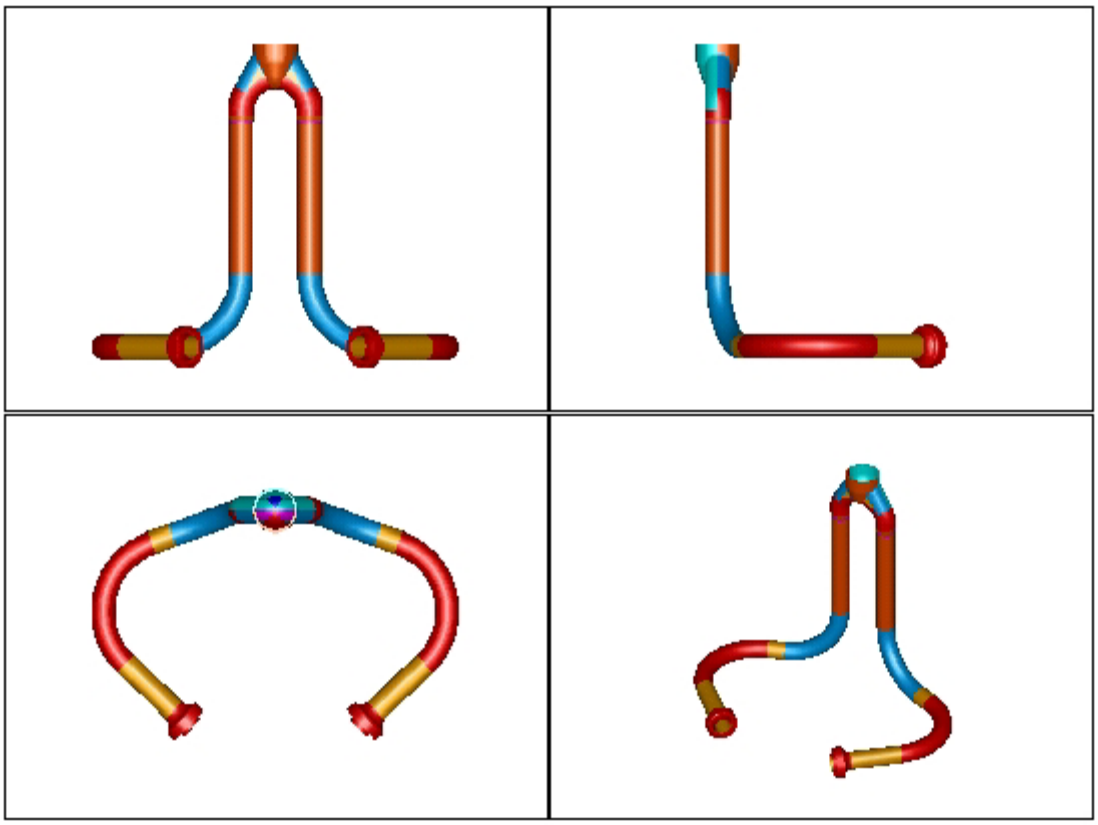

FIG. 2. CEFR primary sodium pipes.

Figure 3 shows the CEFR reactor block. The four primary sodium pipes connect the outlet of the primary pumps with the lower grid plate. There are two pipes for each pump in each of the two circuits.

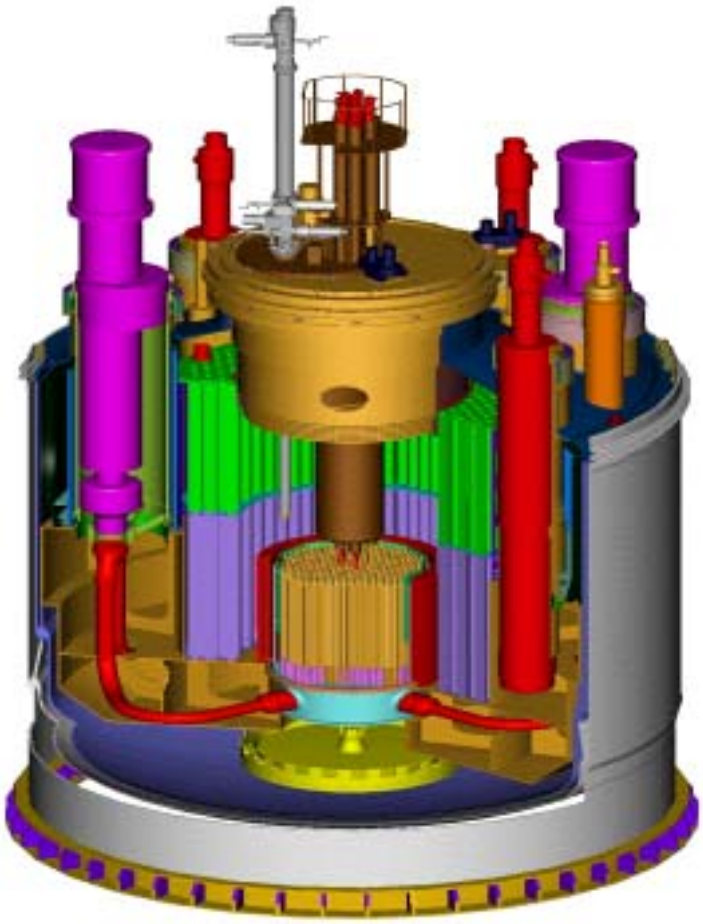

FIG. 3. Reactor block of CEFR.

3. IDENTIFICATION OF CAUSES AND ACCIDENT DESCRIPTION

The reactor is assumed to be operating at 102.5% of full power when one of the four main pressure pipes of the primary loop experiences a double-ended guillotine break. Then a great amount of sodium will leak out. Possible causes for this event are: fatigue rupture following a small break, large stress on the installation, faulty jointing, as well as any other unexpected accident. At the same time, according the conservation rule of the accident analysis requested by the national nuclear safety authorities, loss of the off-site power is supposed to occur. After the break occurs, the flow rate of two primary pumps will show a sudden increase and then the core flow rate will decrease sharply. As a result, the reactor protection system will be launched because of the power to flow rate ratio exceed the trigger threshold. So the reactor shutdown system will act. The procedure of this shutdown consists of following primary actions:

- The control rods begin to insert;
- The two primary pumps begin to coast down;
- The two secondary pumps begin to coast down;
- The main steam gate begins to close;
- The bypass valves begin to open;
- The main feed water pumps begin to coast down.

4. DETECTION SIGNALS

The possible related signals that could trigger protection are:

- Deviation of the power-to-flow rate ratio with the threshold of ±112%;
- High core outlet temperature > 565°C;
- Loss of off-site power.

5. INITIAL CONDITIONS AND CONSERVATIVE ASSUMPTIONS

Supplementing the normal parameters, the following additional conservative assumptions and conditions were used for the analysis:

- 102.5% power thermal hydraulic design condition operating points;
- Positive tolerance of the inlet temperature of the reactor is 3;
- The break is a double-ended guillotine break;
- The break is instantaneous;
- This event occurred at the end of the reactor life;
- Single shutdown rod with maximum worth is stuck:
- While the accident occurs, off-site electricity power is lost;
- Single Failure Criteria: after scram, the primary pump of the unaffected loop coasts down to stop;
- The intermediate loops are isolated after 60 s from scram;
- The function of the decay heat removal system is neglected;
- Taking into account the effect of an earthquake, the duration of control rod insertion is doubled.

6. ANALYSIS OF EFFECTS AND CONSEQUENCES

6.1. Simulation model

The main pressure pipe break accident analysis was conducted using the French OASIS Code, which is a dynamic system simulation program especially for the pool type sodium cooled FBR. It can simulate the thermal-hydraulics of the whole FBR plant circuits and reactor control and protection system, including the regulation system. So OASIS is a good simulation tool to study the operation and accident transients in a FBR Plant. An introduction and the physical models of the OASIS code are presented in the Ref. [1].

Reference [2] describes the establishment of a dynamic simulation system for the CEFR and modified OASIS. Figure 4 gives the simulation model of the CEFR primary heat transfer system using OASIS code. Figure 5 describes the simple calculation model of affected loop.

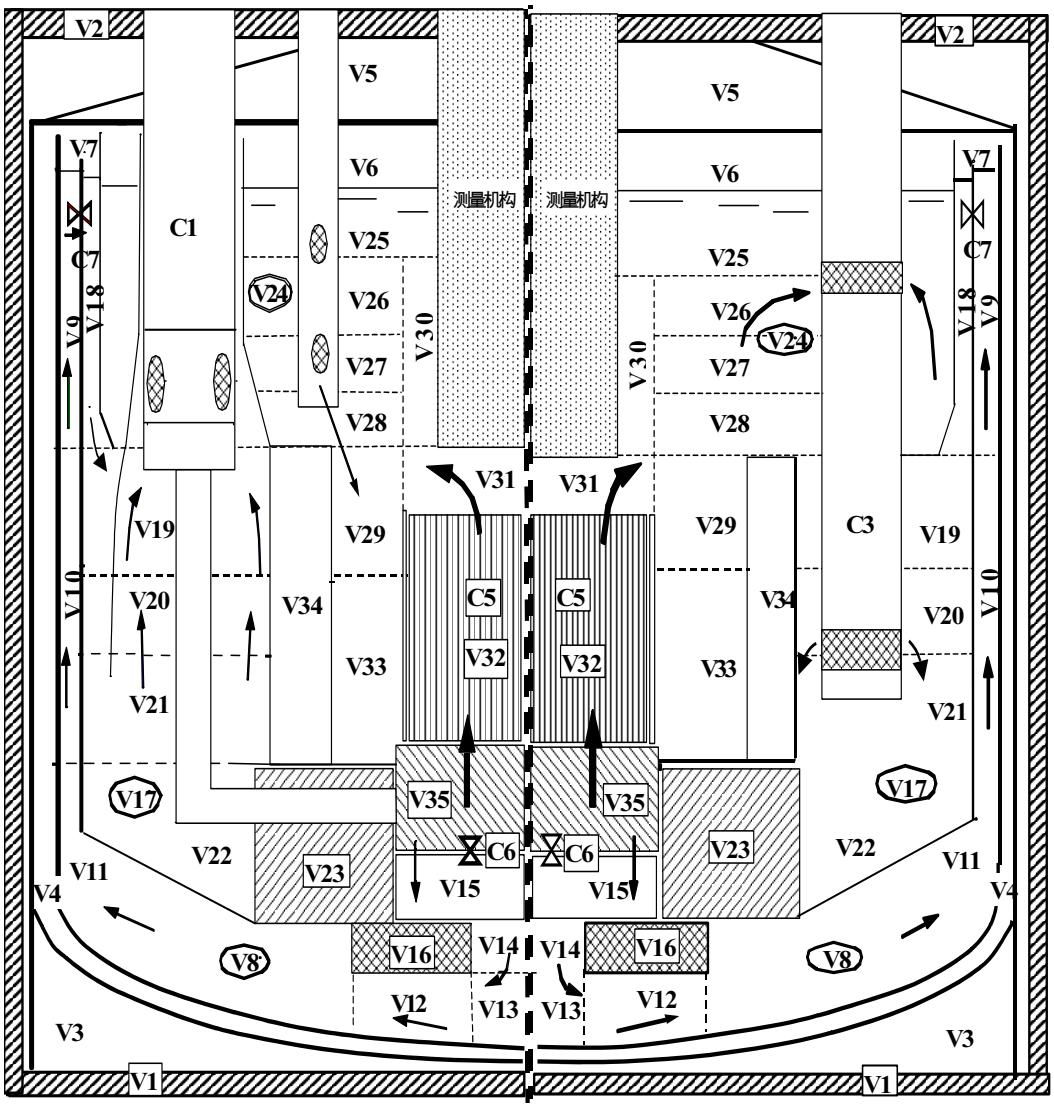

Components:

C1：Primary pump 1
C2：Primary pump 2
C3：IHX 1
C4：IHX 2
C5：Reactor core
C6：Valve under the lower grid plate
C7：Valve of the main vessel cooling system

Volume:

V1：Reactor pit
V2：Reactor top plate
V3：Argon seal outside of main vessel
V4：Gas gap of main vessel
V5：Reactor top seal
V6：Argon seal about the hot pool
V7：Argon seal about the cold pool
V8：Main vessel cooling pool (8 sous-volumes)
V17：Cold pool (6 sous-volumes)
V24：Hot pool (8 sous-volumes)
V33：Radial shielding zone
V34：Upper supporting plate
V35：Lower grid plate

FIG. 4. Primary loop configuration of CEFR.

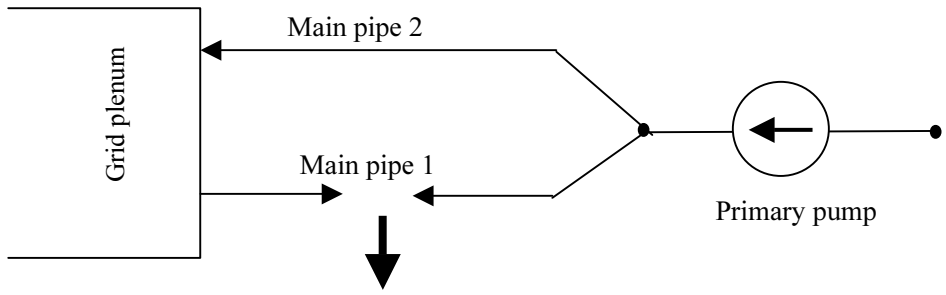

FIG. 5. Simple model for main pipe rupture accident analysis.

6.2. Various rupture position calculation results

According to the characteristic of the main pressure pipe, five typical rupture positions are selected and calculated, they are A, B, C, D, E in Fig. 6. The results of these calculations are listed in the Table 1.

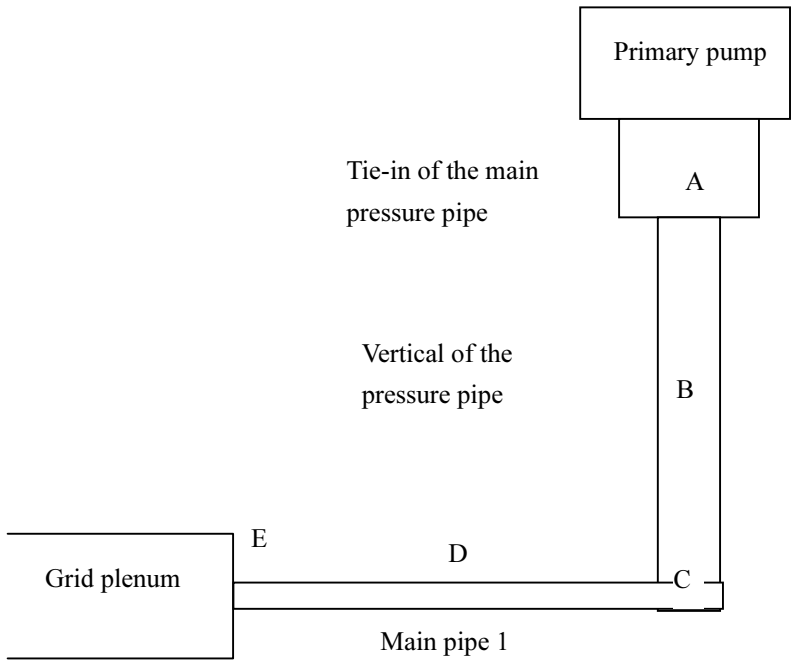

FIG. 6. Various positions in the calculation.

TABLE 1. MAIN CALCULATION RESULTS VARIOUS RUPTURE CASES

Position	Signal* arrival time (s)	Maximum flow rate of break point		Maximum core outlet temperature	
		Maximum flow rate (kg/s)	Time (s)	Maximum outlet temperature (°C)	Time (s)
A	0.01	329.7	0.46	792.576	1.79
B	0.02	310.37	0.37	764.517	1.71
C	0.03	315.20	0.495	801.773	1.93
D	0.03	327.56	0.345	808.58	1.83
E	0.03	338.83	0.14	814.596	1.76

* signal of power to flow rate ratio.

From Fig. 2 and the Table 1, we conclude that the most consequential position for the safety of the reactor core is the position E.

6.3. Sequence and consequences of the most serious case

Especially for the calculation for the position E case, the sequence during the accident development is listed in the Table 2.

TABLE 2. SEQUENCES OF EVENTS FOR ONE MAIN PRESSURE PIPE RAPTURE

Event	Time (s)
Guillotine break occurs	0
Loss of off-site electricity power: Affected primary pump began to coast down to 150 rpm Unaffected primary pump began to coast down to stop Secondary pumps began to coast down to stop Feed water pump began to trip	0
Maximum flow rate of total break	0.14
High power to flow rate ratio signal (one second delay considered)	1.03
Shutdown：control rods begin to insert	1.23
Secondary and water-steam circuits are wholly isolated	60.0

Figures 7-11 show the transient of maximum core outlet temperature, total break flow rate, core power and flow rate, and cladding maximum temperature respectively.

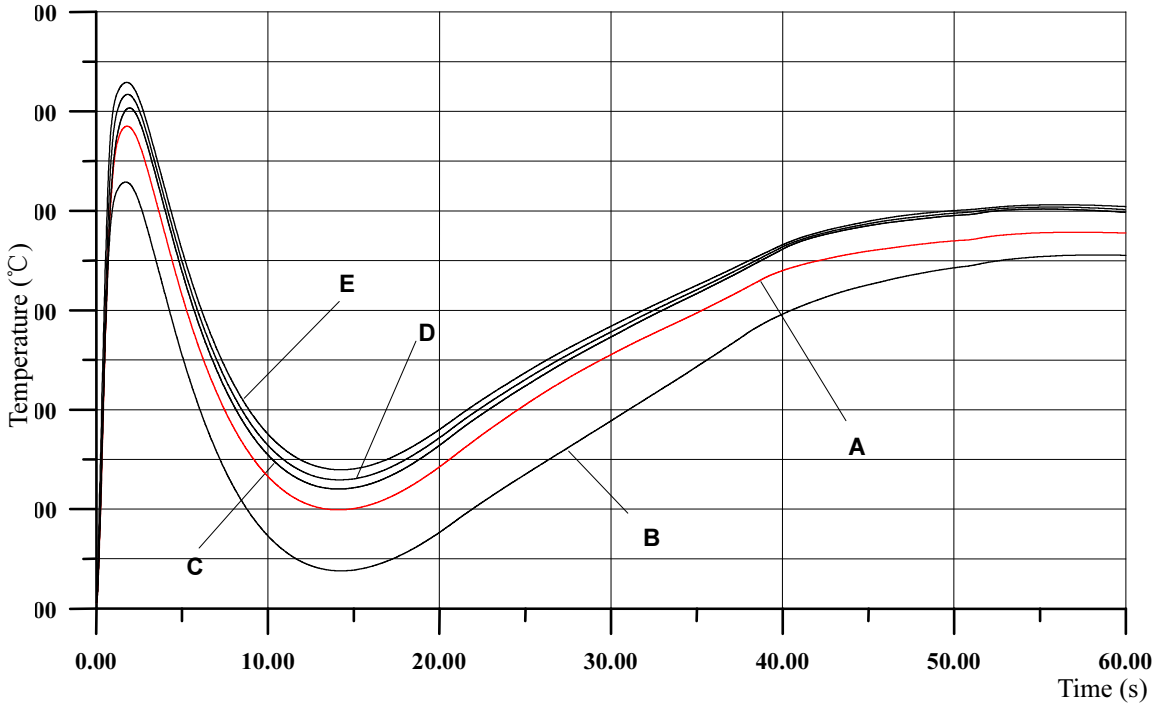

FIG. 7. Core outlet maximum temperature for various positions.

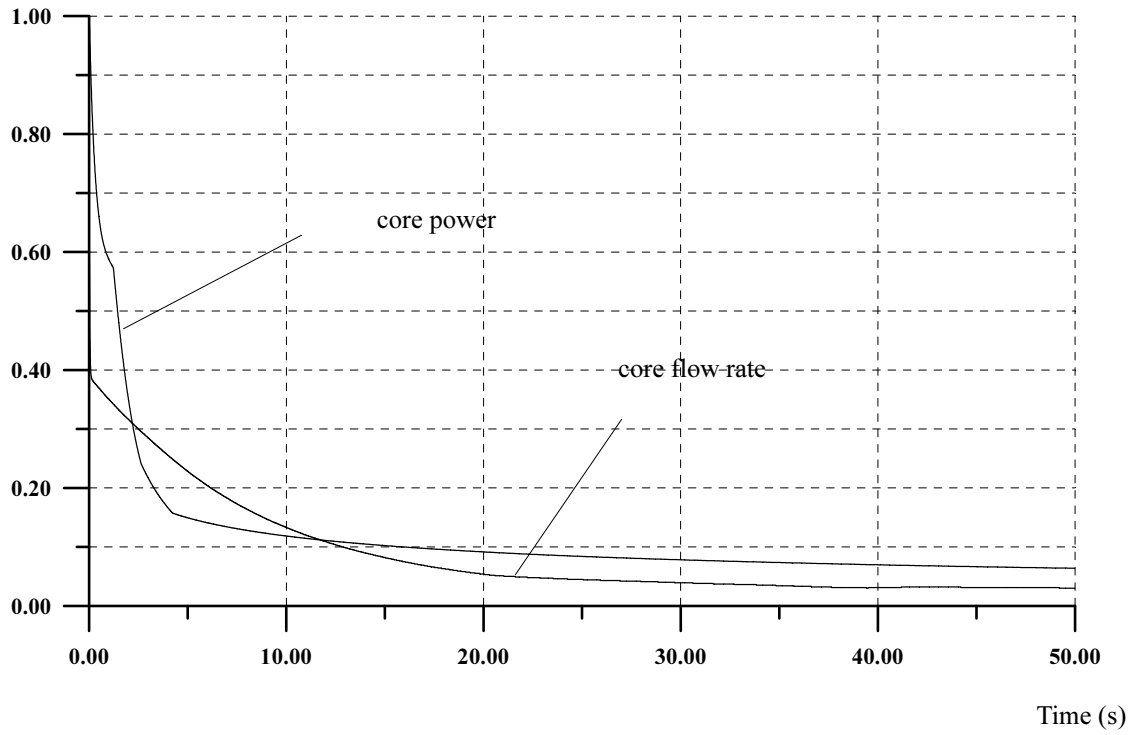

FIG. 8. Reactor core power and flow rate.

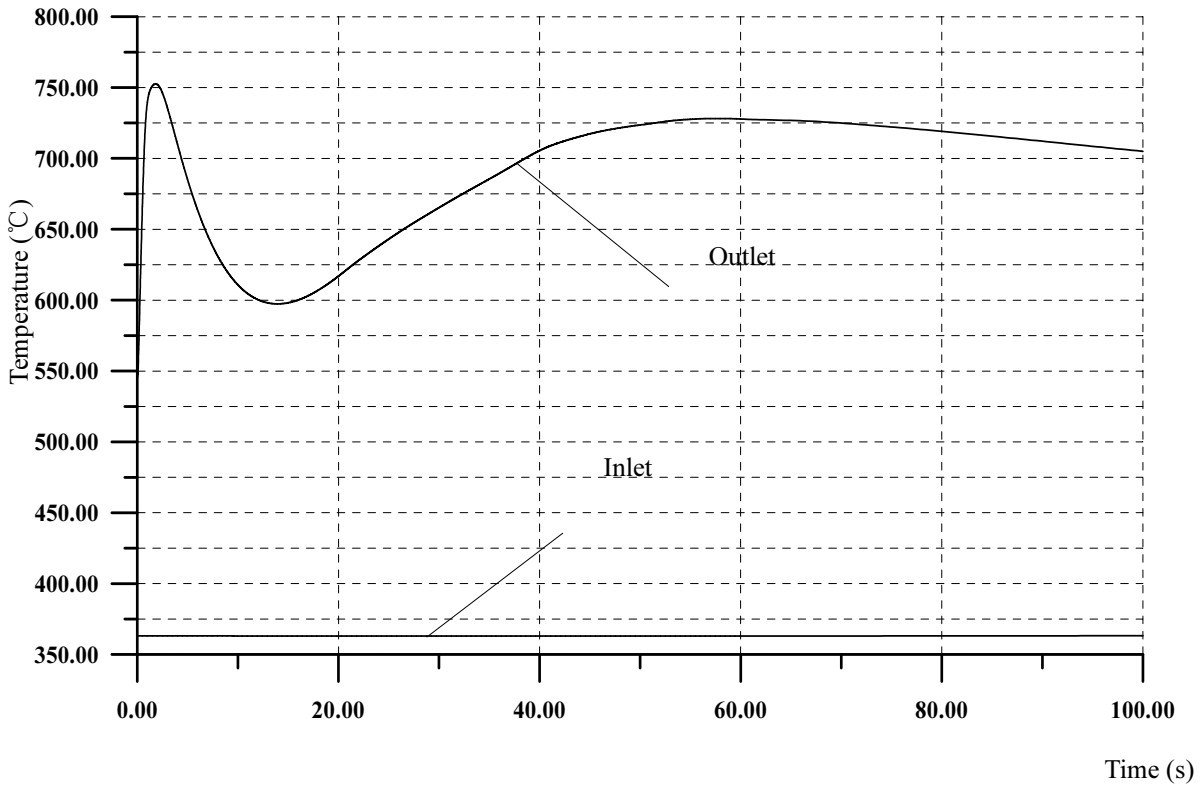

FIG. 9. Average sodium temperature of reactor core.

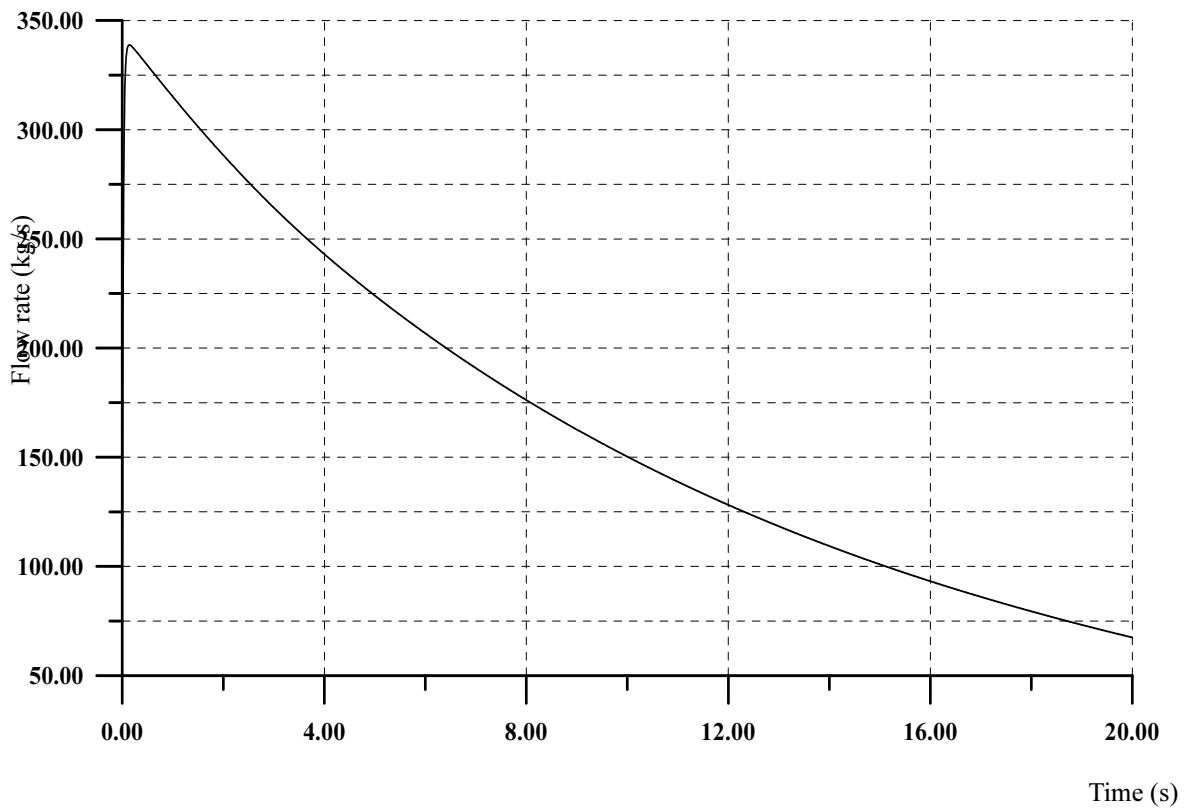

FIG. 10. Total break flow rate.

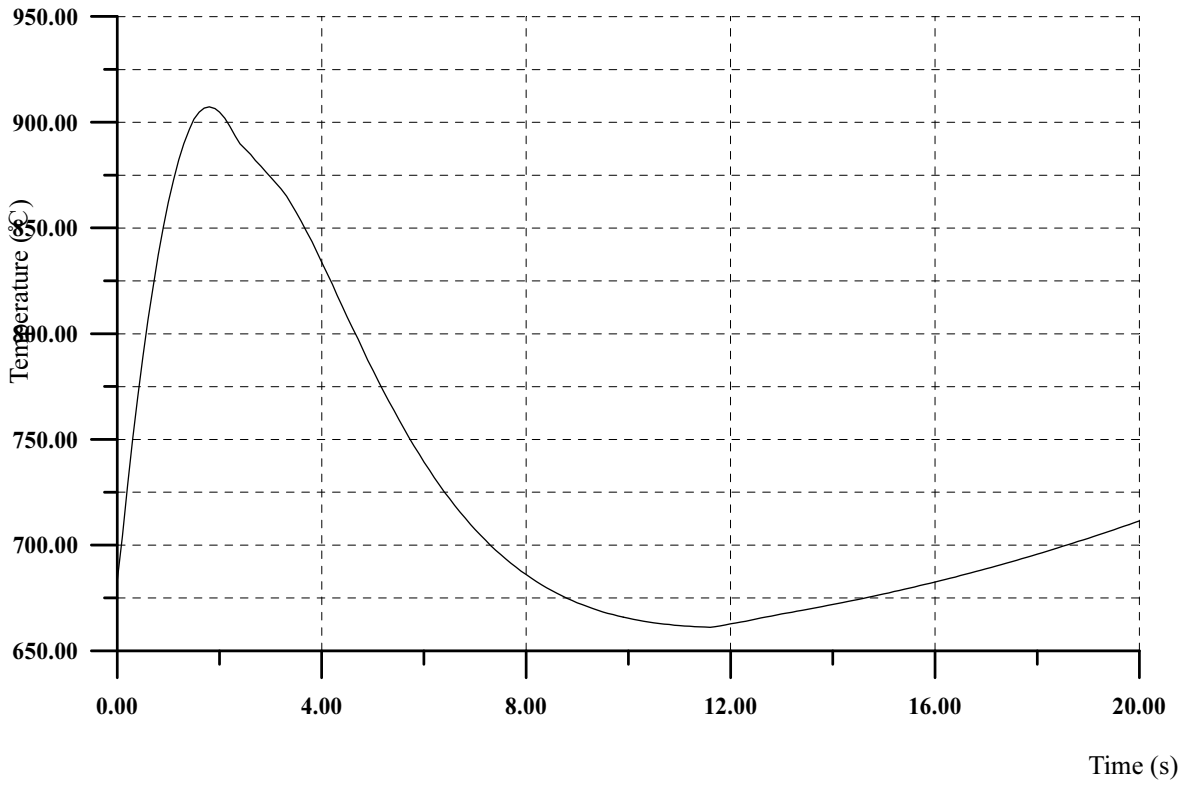

FIG. 11. Cladding maximum temperature.

7. CONCLUSIONS

During the accident development process, the temperature of the fuel is always lower than melting point. The temperature of the cladding is lower than safety limitation also. The integrity of the pressure boundary of the primary loop has not been destroyed.

REFERENCES

[1] DUFOUR, Ph., "OASIS: An Interactive Simulation Case", paper presented in the Simulation Multiconference, 9-13 April 1995, Phoenix, Arizona, U.S.A.

[2] YANG, H., "Establishment of a Dynamic Simulation System for China Experimental Fast Reactor", Atomic Energy Science and Technology, Vol.33, No. 2 (1999).

RUPTURE OF LIPOSO* IN SUPERPHÉNIX

PH. DUFOUR, J. LOUVET, P. LO PINTO
CEA DEN / Cadarache, St. Paul-lez-Durance, France

Abstract

After a review of the French safety approach for the fast breeder reactors and its application to the design basis of Superphenix, we describe the scenario of a primary pipe rupture from a phenomenological viewpoint. The first physical points involved in this accident are a fast partial loss of the core flow despite the natural increase of the pumps flow, and the dissymmetry in the pressure core inlet, in the grid plate, leading to local fuel channels overheating. In the pessimistic reference assumption of a practically instantaneous double-ended guillotine break, the potential consequences, due to a quick overheating of the sodium, are:

- The risk to reach a local sodium boiling in the core, starting from stable boiling conditions, but with possible propagation towards unstable conditions due to either, directly the flow reduction, or indirectly to a void reactivity effect;
- The risk of a cladding rupture with possible impact on the neighbouring fuel pins by gas release. This gas release could be an initiator for other cladding ruptures and associated gas releases and then introducing some phenomena for sodium boiling propagation and/or reactivity insertion.

Extensive studies of the LIPOSO accident, including experimental programmes, were performed on the understanding of the various phenomena involved in a pessimistic scenario, on the prevention and protection means and on the calculation models including all the uncertainties. The final result was that the Superphénix safety provisions were able, thanks to the reactor and the core design, to cope with this type of fast loss of core flow accident, despite pessimistic assumptions, which was initially considered as a main initiator of a core disruptive accident.

1. SAFETY APPROACH

1.1. Deterministic approach

The safety approach used in the Superphénix design was basically deterministic in comparison with existing probabilistic approaches. Indeed, for a conceptual design phase, a list of classified normal and abnormal operating conditions, retained as envelope of all the possible events in terms of occurrence frequency and consequence level, is set from an agreement between the Designer, the Utility and the Safety Authority.

This list of operating conditions is the starting point for both reactor dimensioning and safety analysis. Relating to the former (dimensioning), other main elements are needed: classification of the reactor equipments into safety classes according to specific safety rules and the regulatory guides for design and construction. Relating to the latter, pessimistic rules are used in the safety analysis of each already operating envelope condition, for instance uncertainties treatment or events combinations. The general safety objectives to be met (see Section 1.2) are translated into decoupling criteria, for instance a temperature limit, for each event class.

All these various rules and codes, either for dimensioning or safety analysis, need to be approved by the Safety Authority for each reactor plan. Regarding Fast Reactors, specific rules and codes were set for design, construction and safety analysis, and improved since the demonstrator Phénix time up to the most recent European project (EFR).

Probabilistic methods which, when applied to a new reactor generation, have as weak point a lack of experience feedback, are not excluded in the deterministic approach. Their application case by case, when needed, is useful argueing about possible changes in the classification of a

* **LI**aison **PO**mpe **SO**mmier

given event or to assess the reliability of some equipment. In general, probabilistic methods are applied to point out, among a given global reliability, the major weak components to be improved.

In the frame of FR system development, a semi-probabilistic method, named Lines-of-Defence method (LoD), was defined just after the Superphénix period (i.e., SPX2 conceptual phase) and extensively applied in the EFR project. This method makes up for the lack of a database on experience feedback.

1.2. Objectives and safety principle

Although the LWR and FR have specific safety approaches, their global safety objectives and fundamental safety principle are the same and can be summed up as follows:

- For each reactor condition (events or sequences), the more important the potential consequences are, the less should be its occurrence probability;
- The global probability that the plant could cause unacceptable consequences (i.e., needing off-site measures) must be less than 10^{-6} /year;
- Safety provisions should be taken against conditions having very low probability, but severe consequences, in order to reduce either their probability or their consequences.

These objectives are reached by application of the well-known Defence-in-Depth principle, consisting of several levels of prevention, protection and mitigation provisions.

1.3. Classification of the LIPOSO accident

In the frame of the French safety approach for FR, the postulated accident of one primary pipe break (LIPOSO, **LI**aison **PO**mpe **SO**mmier pipeline from pump to grid plate) is considered as the envelope condition of any fast loss of core-flow and then is classified in the last Design Base class of operating conditions (i.e., category 4).

In general, the choice of any classified condition takes into account possible initiator events, notably an earthquake impact on equipment having an existing critical crack. Since it is difficult to assess the probability for an equipment (even designed against seismic loading) to have an existing critical crack not detectable, the most penalizing break is chosen as reference condition. The limited capability for in-sodium inspection of FR internal equipments contributes towards this deterministic approach. Relating to the objectives of the category 4 (hypothetical events), loss of the investment (i.e., the reactor itself) is admitted by the utility, but the safety consequences must be within the safety targets. For Superphénix, the safety target of category 4 was 0.15 Sv permanently at the site boundary. Moreover the reactor must be brought back to a safe state. In practice, these safety objectives are translated into decoupling design criteria. Concerning the core zone, these decoupling criteria are as follows:

- The number of fuel cladding failures should be limited (according to the radiological target);
- Any phenomena leading to irreversible conditions (e.g., bulk sodium boiling) should be prevented;
- Core geometry with cooling capability must be kept (e.g., neither clad melting nor significant inner local fuel melting leading to material dispersion);
- The reactor must be brought back to a safe cold shutdown state.

1.4. Analysis rules for LIPOSO break

As mentioned above, pessimistic rules are applied for the analysis of each Design Basis condition and then in particular for the analysis of the LIPOSO accident. This approach involves:

- The choice of the most penalizing reactor operation initial state (e.g., full power);
- Pessimistic hypotheses for the LIPOSO accident scenario (double-ended guillotine break in 1 s);
- Simultaneous loss of station power if more penalizing;
- Application of 'single failure' criterion.

The choice of the most penalizing single failure depends on the accident type. After considerations about a LIPOSO break inducing a pump seizure risk, the single failure retained was a deterministic fuel cladding failure in the hottest core channel during the LIPOSO scenario. Indeed, the subsequent fission gas release could a priori, disturb the sodium flow, increase its boiling risk from the unfavourable 'core power / flow' ratio due to the pipe break, while a reactivity effect by sodium void could be inserted.

According to the LoD method, safety provisions by more than one safety system (i.e., emergency shutdown) should be planned against the LIPOSO accident (considered itself equivalent to the loss of a strong line of defence) in order to reject unprotected cases with severe consequences in the residual risk domain. Practice aspects of the LIPOSO accident treatment are presented below, based on the Superphénix analysis, including presentation of the induced phenomena, the efficiency of the detection means and the resulting consequences compared to the safety targets.

2. ACCIDENT SEQUENCE

2.1. General phenomena

The postulated accident, assuming an instantaneous double-ended guillotine break of a pipeline joining pump to the core grid plate, can be regarded as a fast loss of flow in the core, as opposed to the reference Core Disruptive Accident, initiated by a complete pumps trip and leading to a slow loss of flow. After break, pumps remain operating with a constant speed while the global hydraulic resistance of the circuit is reduced, which induces a modification of the pump operating mode, leading to a total pump flow rate increase. Nevertheless, cavitation effects, acting as self-control, restrict this pump flow rate increase. Eventual pump damage (by erosion) due to cavitation effects needs to be verified under long term testing, nevertheless these effects do not change the accident analysis. In the same time, the quick break (in about 1 s) contributes to a large sodium flow rate decrease through the core, depending on the reactor design (i.e. number of pumps and pipes) and on break assumption (i.e. pressure drop), in particular in the core zone corresponding to the broken pipe, where the pressure in the core grid plate is necessarily lower. Then, the sodium flow assymmetric redistribution through the core depends on the pressure repartition in the core grid plate. Assymmetric hydraulic characteristics in the core grid plate can be evaluated from reverse rotation pump testing. Due to the rapid and large sodium flow reduction through the core, the transient is then governed by thermal inertia of the primary sodium circuit and by power evolution, the latter being determined by reactivity feedback effects. The sodium temperature at the inlet remains constant at the beginning of the transient (over a few seconds). The rapid sodium heating up at core outlet, resulting from the large sodium flow reduction through the core, leads to a weak power increase (due to sodium thermal expansion effects on reactivity).

An earlier accident detection by controlling power and pump flow or pump rotation speed is not yet efficient (weak increase of core power and pump flow, no variation of pump rotation speed). At the same time, fuel is not already heated up, so that early thermal reactivity feedbacks (such as fuel expansion and Doppler effect) are not efficient to counterbalance consequences of the rapid sodium core flow reduction. Subsequently to the sudden sodium outlet temperature increase, cladding temperatures are increasing and local sodium boiling phenomena could occur and still accelerate the accidental sequence (by sodium voiding reactivity effect) and then enhance consequences (e.g., cladding dry out; gas release effect after cladding rupture on neighbouring pins, sodium boiling propagation through the pin bundle).

These consequences have to be considered not only in terms of cladding rupture risk, but mainly in terms of global core accident risk, taking into account the rapidity of the accidental sequence compared to the accident detection efficiency (sodium outlet temperatures, reactivity and power). Then, it is very important to analyse in detail the conditions for local sodium boiling stability in order to evaluate margins for cladding dry out propagation through the pin bundle in the subassembly, then to bulk boiling.

Large scale experimental and theoretical studies have been performed mainly to show that:

- Sodium flow reduction through the fuel bundle promotes sodium flow mixing and redistribution through the bundle;
- Gas release after cladding rupture occurring in a local boiling zone does not contribute to amplify cladding dry out and cladding rupture propagation through the pin bundle.

Then, precise evaluation of uncertainties is required for the accident scenario and consequences analysis mainly depending on:

- The break pressure drop characteristics and the pressure repartition in the core grid plate which influence the sodium flow reduction and repartition;
- The fuel thermo-mechanical behaviour under irradiation that determines both, fuel temperatures and associated reactivity feedbacks effects (fuel expansion and Doppler effects), fuel to clad heat transfers and interaction, as well as the consequent cladding thermo-mechanical behaviour and thermal expansion reactivity effects;
- The methodology for evaluating local sodium and cladding temperatures through the pin bundle (hot spot), consequent cladding failure rate and radiological risk.

Practically, the unprotected accidental scenario is firstly analysed without reactor protection, taking into account pessimistic assumptions and uncertainties, in order to determine detection capability and timing. Thereafter, the scenario sequence is reanalysed, in the same way, with taking into account the reactor protection (accident detection and reactor shutdown) to evaluate maximum clad temperatures reached.

2.2. Accident prevention

Prevention of accident firstly depends on design, dimensioning, and manufacturing:

- Number of pipes and pumps, for example four pumps, each connected by two pipes to the core grid plate in Superphénix, in order to minimize consequences of such a pipe rupture;
- Design concept for pump and core grid plate connections to allow flexibility in order to avoid consequences in case of differential thermal expansions, pump vibrations and pump seizure;

- Design and dimensioning to seismic loading;
- General rules and quality controls for manufacturing and welding;
- Specific tests (as pump seizure for example) and periodic inspections (by means of a MIR telemetry able to measure relative displacements at connections for example, as provided in the EFR project) during reactor startup and operating life.

3. THE SUPERPHÉNIX CASE

3.1. Prevention (1st level of defence in depth) by design

The design of the grid plate supply is:

- Four pumps, each connected by two pipes to the core grid plate;
- Seven wave dilatation compensators operating separation between hot and cold collectors;
- Design and dimensioning for seismic loading.

3.2. Studied case

Assumptions made for the study of this accident are:

- Double-ended guillotine break 1 s of a pipe joining a pump to the core grid plate in;
- Normal operating conditions at full power;
- First cycle core at 640 EFPD, i.e., in the most unfavourable conditions regarding the radioactivity release;
- Pumps speed is constant, equal to 421 r/min, in cavitation conditions;
- Pump flow increase is limited by the cavitation to 4 600 kg/s instead of 4 090 kg/s under nominal conditions.

3.3. Hydraulic transient

Figure 1 shows the hydraulic scheme in the grid plate after the liposo break.

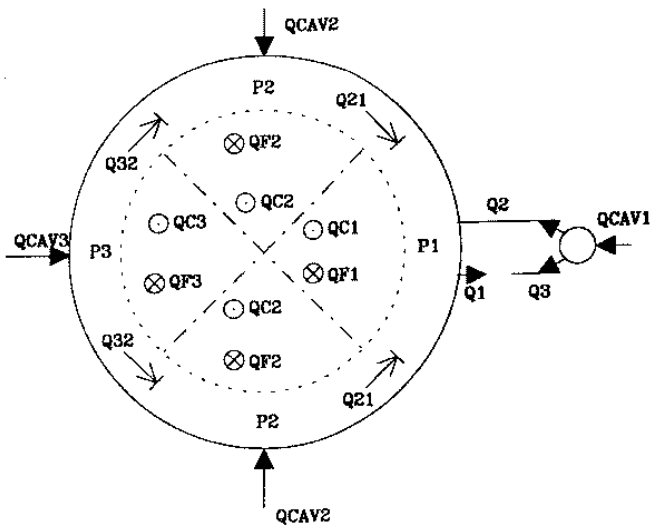

FIG. 1. Hydraulic scheme.

The repartition of pressure is related to the cold collector pressure:

- quarter 1: 0.89 bar;
- quarter 2: 1.22 bar;
- quarter 3: 1.26 bar.

This pressure repartition leads to flows through the core:

- quarter 1: 46.5% of the nominal flow;
- quarter 2: 54.3% of the nominal flow;
- quarter 3: 55.1% of the nominal flow.

Under this condition, the global core flow is 52.6% of the nominal flow.

3.4. Surveillance and detection (2nd level of defence in depth)

The integrated primary circuit does not allow a leak before break detection, thus the only surveillance possibility of this accident is limited to vibration measurement on pumps, resulting in an indirect and imprecise information when one's main concern is the status of the pumps.

An efficient measurement would be the power to core flow ratio (P/Q). Due to the pressure transducers positioning in Superphénix, the core flow measurement is not available, but only the pump flow, which is not relevant as core power and pump flow are both increasing during transient.

Three safety actions are able to actuate reactor scram, and are shown in Table 1.

TABLE 1. THREE SAFETY ACTIONS

Trip parameters	Nominal value	Alarm threshold	Scram threshold	Time constant
ΔTm	165°C	178°C	185°C	1.8 s
P/Pn	1	1.066	1.13	0.015 s
Reactivity	0	± 15 pcm	± 20 pcm	0.174 s

In Superphénix, taking into account uncertainties in an unfavourable way towards detection and time constants of detectors, the first trip parameter involved is the core outlet temperature that leads to the reactor shutdown, 3.8 s after beginning of the accident. The delay between this value and the one indicated in Fig. 2 is due to uncertainties. Later on (after 5 s), the scram threshold on reactivity is then reached, while the scram threshold on power ratio (P/Pn) is not reached.

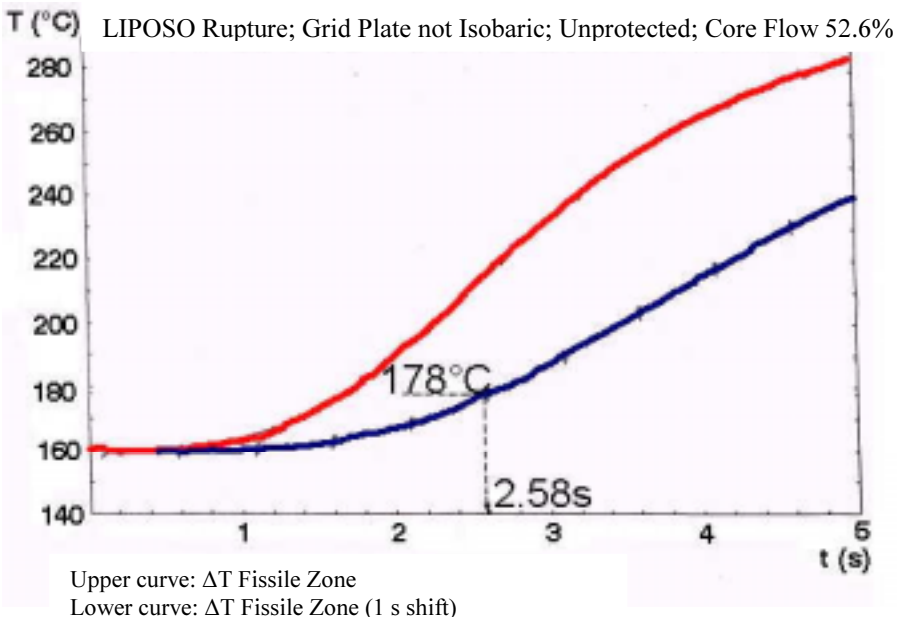

FIG. 2. Core outlet temperature.

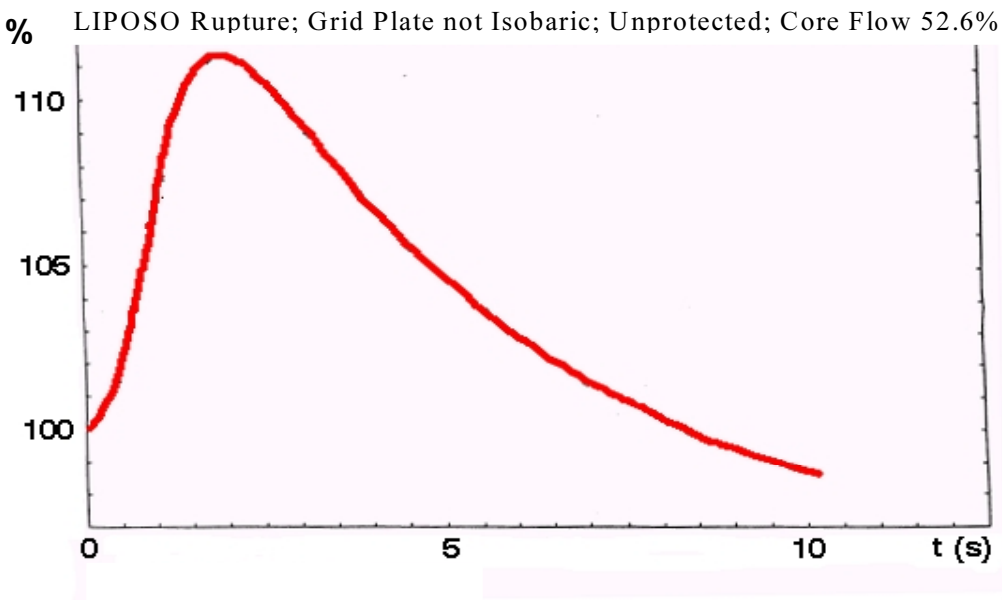

FIG. 3. Core power.

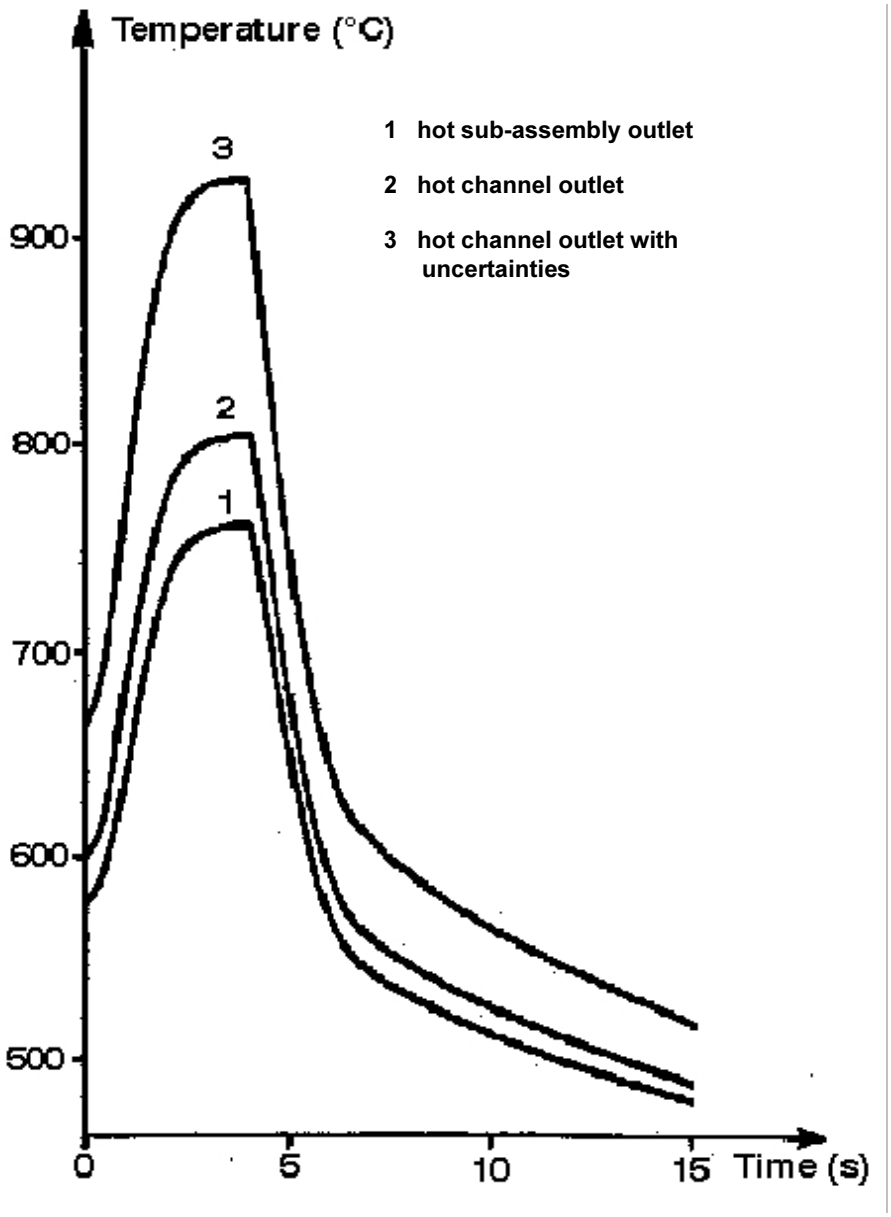

FIG. 4. Core temperature with scram.

The total power in the core reaches 112% of the nominal power (Fig. 3), then decreases under the feedback effects. At the time of shutdown, the core power is about 105% of the nominal power, with a positive reactivity of about 15 pcm. Towards the local, and a fortiori, bulk sodium boiling risk, the margin is large: the maximal outlet sub-assembly temperature is 760°C. Figure 4 shows the outlet temperature evolution in the hot sub-assembly with and without uncertainties.

On the basis of this calculation and using dimensioning rules and methodology, the cladding failure risk analysis has shown sufficient margins. So that, it can be concluded that there is no radiological risk.

4. THE EFR CASE

In the EFR, at the prevention level, periodic inspections by means of MIR telemetry is able to measure relative displacements at connections, for example, during reactor startup and operating life. At the detection level, the core flow measurement (Fig. 5) is provided (as in Phénix) through pressure measurement between pump inlet and outlet. The unprotected transient analysis (natural behaviour) has shown that the event is not likely to escalate towards a core disruptive accident. The residual core flow is about 42%. At short term, local sodium boiling is limited to the hottest pin coolant sub-channels and margins to the bulk sodium boiling are large thanks to the core power decrease due to reactivity feedback effects (mainly the Doppler effect) after a short over-power of about 20% at beginning of the transient. Two trip parameters are available, both providing a LoD, the power ratio (P/Q) and the Individual Sub-Assemblies outlet Temperature (ISAT). The most relevant trip parameter able to detect the LIPOSO break is P/Q. It allows a very early detection (at 0.4 s) and leads to control rods insertion (within 0.7 s) before the core power is reaching 105% of the nominal power. In these conditions, margins to bulk sodium boiling are large, more than 300°C.

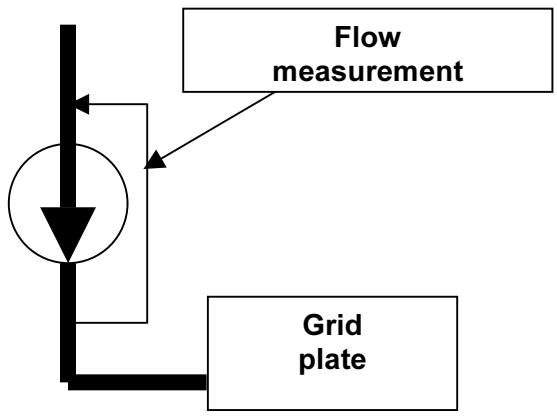

FIG. 5. EFR cores flow measurement.

5. CONCLUSIONS

In protected conditions the LIPOSO break accident does not lead to any significant core damage.

The accident resulting from the initial fault, the LIPOSO break (classified in category 4), combined with the failure of the first trip parameter, which is a strong line of defence (LoD), is in the beyond-design-base. Studies have been undertaken to investigate this case and have shown that consequences remain globally similar, notably towards margins to bulk sodium boiling, indicating that the reactor protection can be considered sufficient.
In conclusion, the safety objectives as defined in § 1.3 are met:

- The number of fuel cladding failures is limited (according to the radiological target);
- Bulk sodium boiling risk is avoided;
- Core geometry with cooling capability is kept;
- In all conditions, the reactor can be brought back to a safe cold shutdown state.

THEORETICAL AND EXPERIMENTAL ASSESSMENT OF STRUCTURAL INTEGRITY OF PRIMARY PIPE

P. CHELLAPANDI, A. BISWAS, S.C. CHETAL, S.B. BHOJE
Indira Gandhi Centre for Atomic Research (IGCAR), Kalpakkam, India

Abstract

This paper deals with the theoretical and experimental structural mechanics analysis carried out for the primary sodium pipes for the 500 MWe Prototype Fast Breeder Reactor (PFBR) towards demonstrating its structural integrity. The analysis is carried out to determine the stresses under pressure and thermal loads including seismic forces. Based on this, an optimum layout and pipe thicknesses have been arrived at. Subsequently, creep-fatigue damage values for the imposed thermal transients, in conjunction with the assumption that the spherical header gets stuck up, are estimated. Structural integrity is ensured further by detailed fracture mechanics analysis and experimental investigations.

1. INTRODUCTION

In the 500 MWe Prototype Fast Breeder Reactor (PFBR), two primary sodium pumps (PSP) circulate the sodium through the core to remove the nuclear heat. Primary sodium flows through the primary pipes from the spherical header (where PSP supplies sodium) into the grid plate. Each spherical header has two primary pipes, thus there are four pipes connected to the grid plate (Fig. 1).

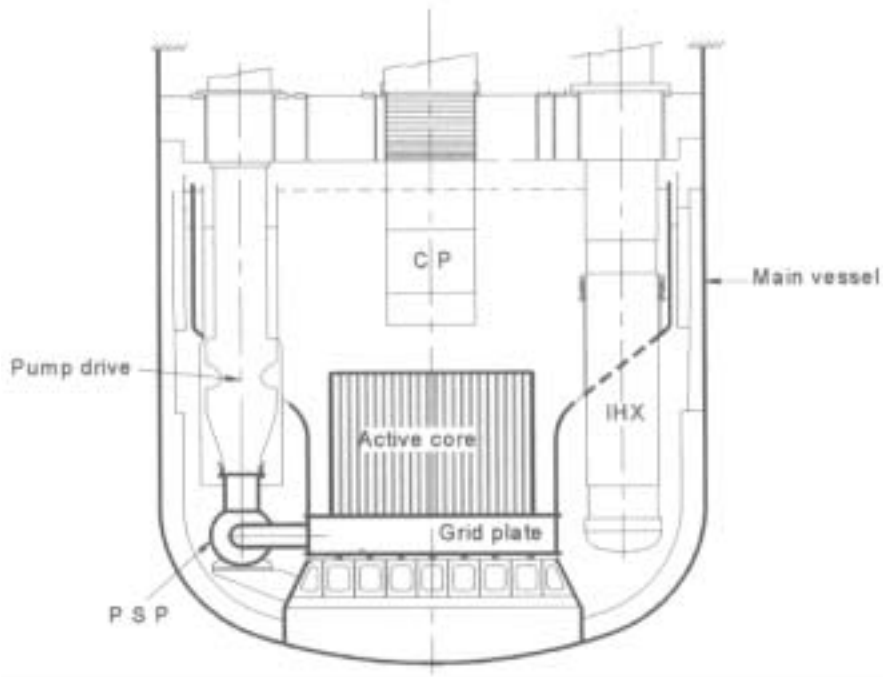

FIG. 1. Location of primary pipe in RA.

The outer diameter of 630 mm is selected in order to have proper flow distribution in the grid plate. An optimum layout is arrived at, based on flexibility requirements to accommodate thermal expansion, availability of space in the cold pool and compactness. Accordingly, the layout consists of a short straight portion connected to a single curvature bend having a radius R equal to 945 mm. The important geometrical details are shown in Fig. 2.

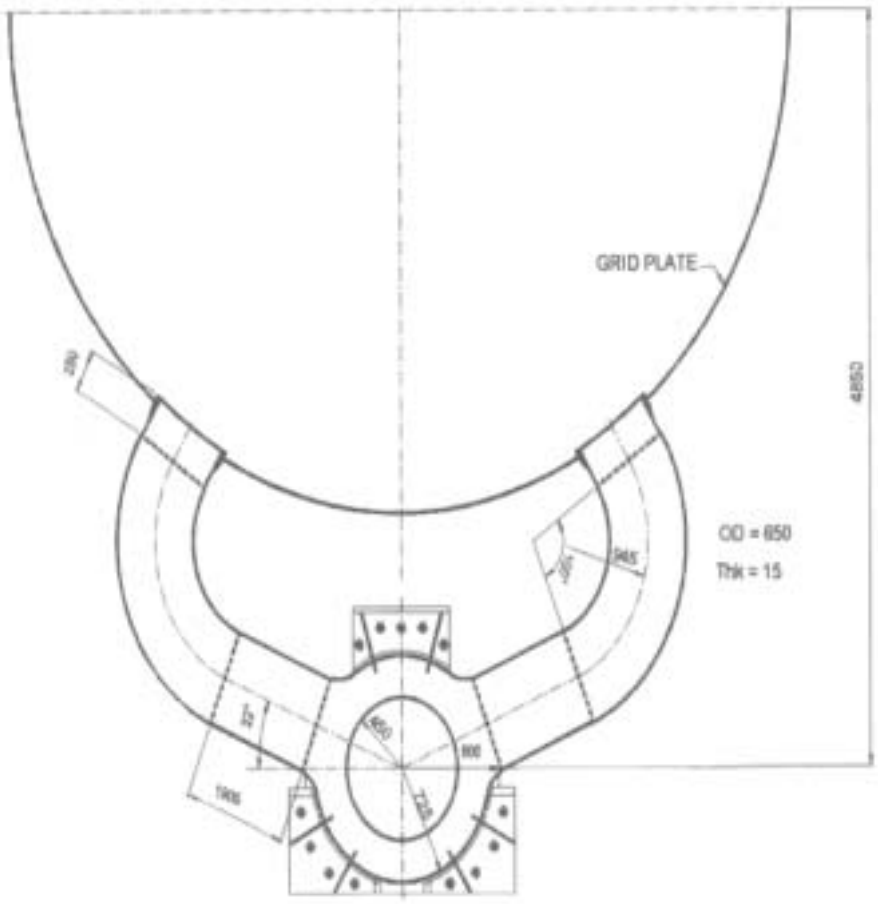

FIG. 2. Primary pump details.

In the reference design shown here, the pipe wall thickness is 15 mm.

1.1. Structural mechanics features of primary pipe

The pipe is operating in a relatively comfortable environment. The neutron dose values are low (< 0.1 dpa) and hence irradiation effects are negligible. Sodium corrosion is negligible. The pipes operate at the cold pool temperature (670 K) where the creep effects are insignificant. Thermal loadings are insignificant during normal operating conditions, since it is at the isothermal temperature of cold pool (670 K). Thermal transients, following secondary sodium and feed water pumps trips impose thermal loadings. By providing a sliding type arrangement for the spherical header, free movement of the pipe under thermal transients is ensured without sacrificing the rigidity requirements under seismic events. The material of construction is austenitic stainless steel SS 316 LN that is highly ductile. The component is designed and constructed as per the class 1 rules of RCC-MR – 1993 edition [1].

1.2. Scope of the paper

Each pipe forms a primary coolant pressure boundary and its failure in the form of a large leak or rupture is of great concern to safety. Hence, the structural reliability requirements are high for the component. With the view of this, detailed stress analysis has been carried out to optimize the thickness, and subsequently creep fatigue damage is estimated. Apart from postulating a pessimistic surface crack at a highly stressed location, fracture mechanics

analysis has been carried out. In order to raise the confidence further, experiments were conducted on 1/15th scale models. Besides, respecting the defense-in-depth philosophy, a double ended guillotine rupture (DEGR) is postulated and subsequently, by means of detailed thermal hydraulic investigations, it is demonstrated that resulting temperatures due to reduction in core flow, do not exceed the appropriate temperature limits for the coolant and cladding. Thermal hydraulic investigations are covered in a companian paper [2]. In this paper, the results of structural mechanics studies are reported.

2. DEFINITION OF LOADS

Under normal operating condition, each pipe is subjected to an internal pressure of 0.8 MPa. The steady state vibration force induced by the pump is insignificant (± 2 t), even at 120% of nominal speed (Fig. 3).

Under safe shutdown earthquake (SSE) conditions, the pipe is subjected to forces and bending movements due to inertial force imposed by the primary pump at the top of header nozzle. The peak value of the force is < 20 t (Fig. 4). The corresponding value under OBE is ~ 12 t. The details of seismic analysis can be found in Ref [3].

Among possible thermal transients following power failure, pump trips etc., a secondary sodium pump trip is the critical event, during which the temperature of sodium exiting from IHX outlet is raised by 100 K over 1 m. This causes a radial temperature gradient of 75 K (ΔT_R), and mean temperature rise of 50 K (ΔT_m) with reference to grid plate [4].

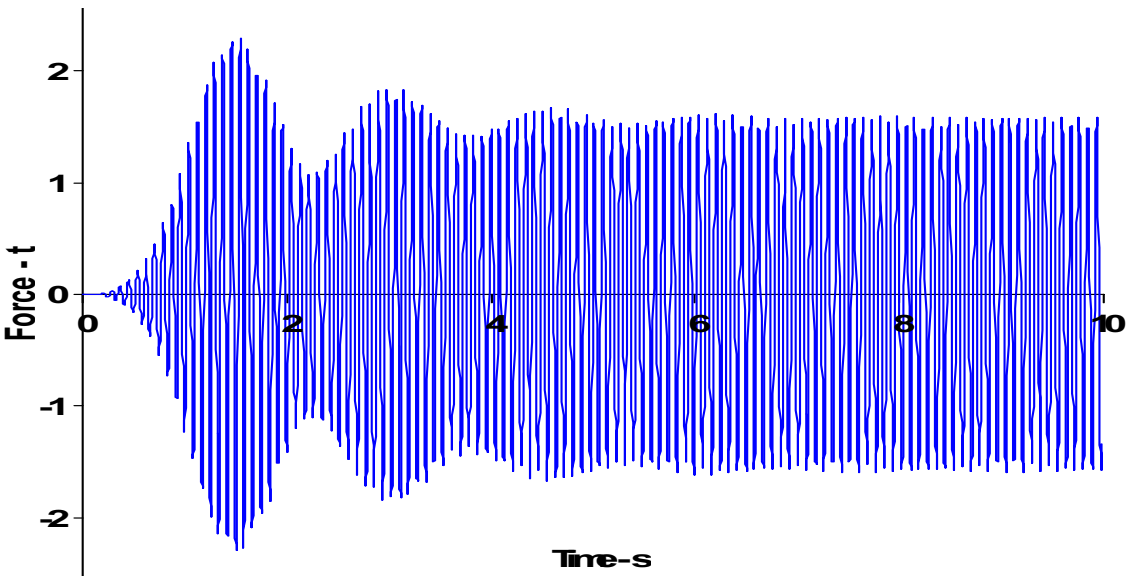

FIG. 3. Vibratory force on header.

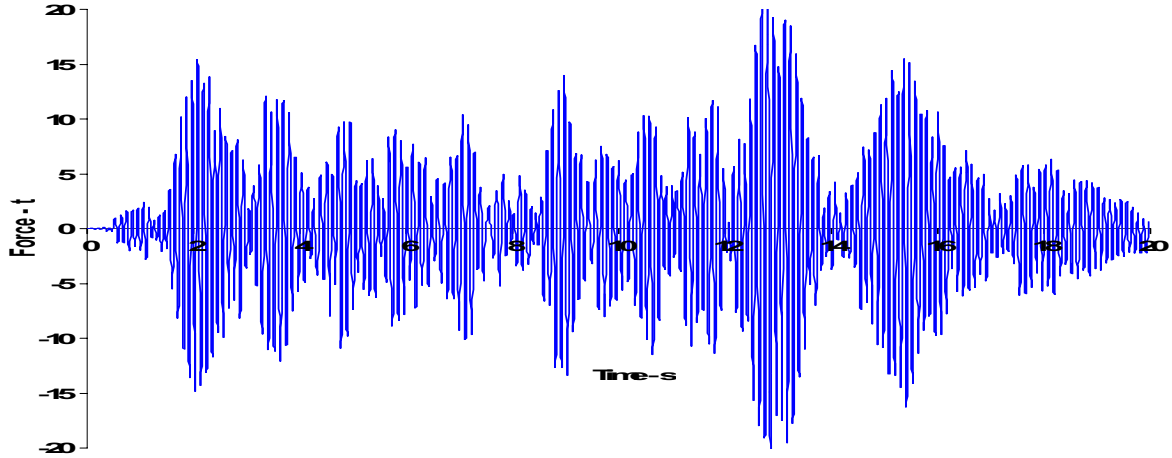

FIG. 4. Force on header under SSE.

Since the header can slide freely on the support plate, ΔT_m does not cause any significant stresses. Considering the lack of inspection of the sliding joint, a pessimistic assumption of a stuck up condition is made. Accordingly, ΔT_m can induce additional stresses.

For the cumulative fatigue damage assessment, five OBE contributing 50 cycles, one SSE contributing 10 cycles and 170 hot shocks are considered in the analysis.

3. STRUCTURAL ANALYSIS

As far as structural behaviour is concerned, two pipes along with one spherical header behave as an integral part of the grid plate. Further, the pipe has a R/d ratio of ~1, unlike the conventional piping. Hence, for the structural analysis, the pipe is modelled with shell elements rather than classical pipe elements and the design limits relevant to components are applied instead of design rules for the class 1 piping of RCC-MR. The finite element model of the primary pipe including the spherical header at one end and grid plate on the other end has been generated with the CASTEM 2000 code using three/four nodded thin shell elements. Figure 5 shows a 180° symmetrical portion of the model.

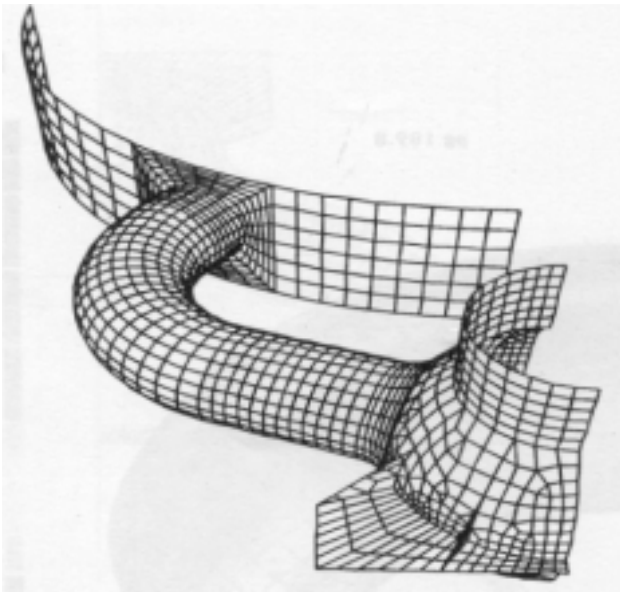

FIG. 5. FEM mesh.

It is to be noted that the model also includes the sliding support structure for the spherical header with restraints for the movements only in the vertical direction.

The overall deformations of pipe under thermal shock and SSE are depicted in Fig. 6.

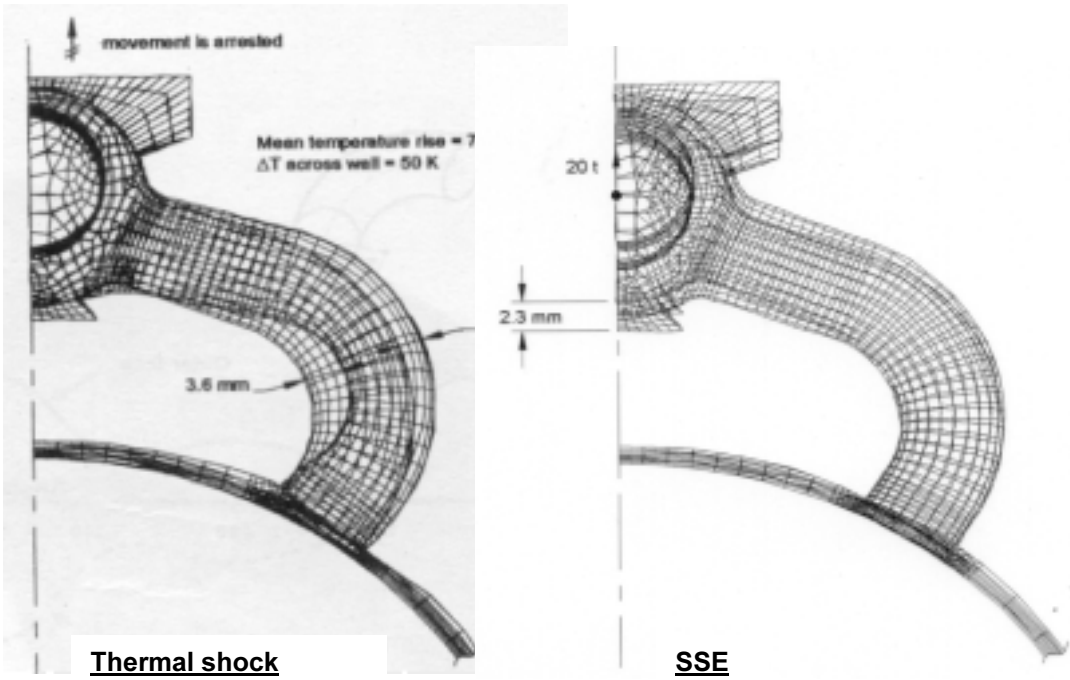

FIG. 6. Deformation under thermal shock and SSE.

The associated hoop stress distributions on the outer skin are shown in Fig. 7.

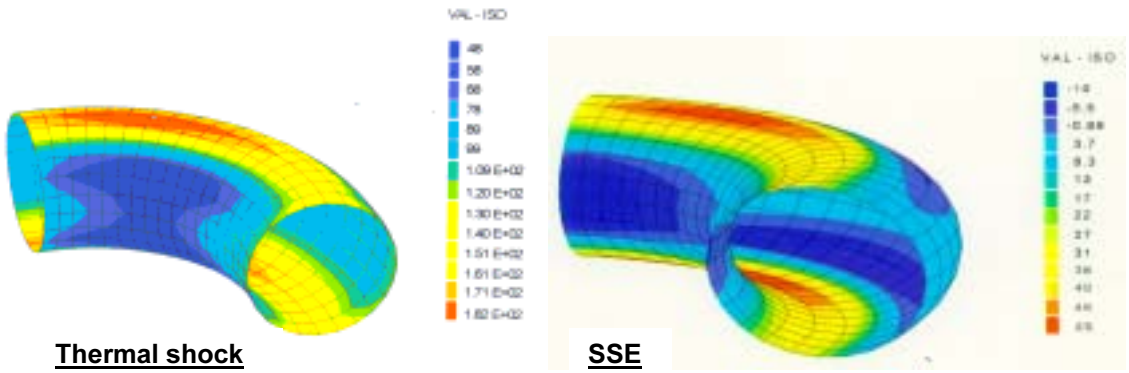

FIG. 7. Hoop stress contours.

Similarly, the circumferential variations of hoop stress on the outer surface at the centre of the pipe bend is depicted in Fig. 8.

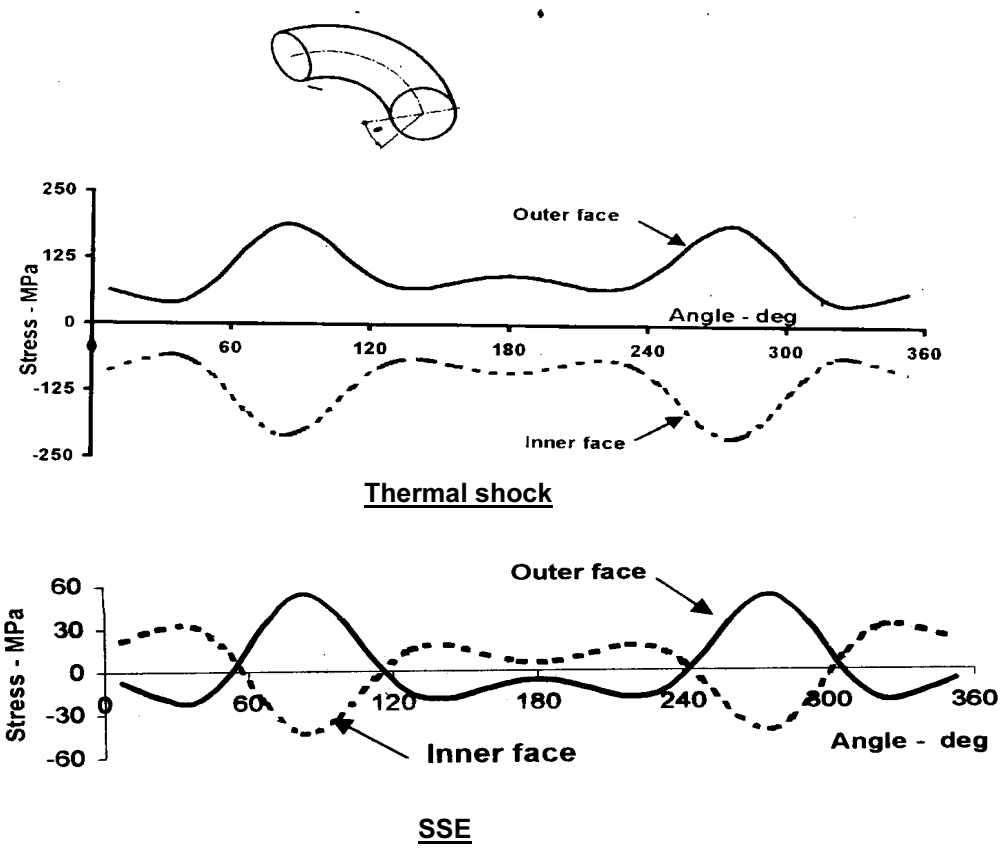

FIG. 8. Circumferential variation of hoop stress.

It is seen that, the top surface of the crown portion, where ovalisation occurs, is the critical location. The stresses at this location under various operating conditions are presented in Table 1, where m and b represent middle and bottom surface, respectively, σ_m and $\sigma_m+\sigma_b$ are membrane and membrane-plus-bending stress intensities.

TABLE 1. STRESSES (MPA) AT THE CROWN

Case	Loading condition	Level	σ_m	$\sigma_m+\sigma_b$
1	Pressure	A	30	45
2	Pressure + OBE	A	43	52
3	Pressure + SSE	D	52	74
4	Pressure + hot shock	C	197	502

4. DESIGN CHECK

The σ_m and $(\sigma_m+\sigma_b)$ values for the first three load cases, as indicated in the Table 1, are the primary membrane (P_m) and primary membrane plus bending stress intensity (P_m+P_b). $(\sigma_m+\sigma_b)$ for case 4 is primary plus secondary stress intensity (P_m+P_b+Q).

P_m should not exceed S_m and (P_m+P_b) should not exceed 1.5 S_m for level A loadings. The corresponding limits are 2.4 S_m and 3.6 S_m for level D loading conditions.

(P_m+P_b+Q) should not exceed 3 S_m limits. Since the S_m value is 104 MPa at 773 K, while the induced stress intensities have high margins. For a better thermo-mechanical behaviour and economy, the pipe thickness is reduced to 10 mm.

The resulting P_m and (P_m+P_b) values are found to have comfortable margins. However, thermal shock and corresponding stress intensities were decreased from 502 to ~ 400 MPa which is considered for the fatigue damage assessment.

5. CREEP FATIGUE DAMAGE ASSESSMENT

The creep fatigue damage is assessed as per the 'elastic analysis procedure' of RCC-MR [1]. The total stress range associated with hot shock is 412 MPa which envelopes all other transients. The stress range associated with OBE is 67 MPa for 10 mm thickness. Conservatively, $\Delta\sigma_t$ is assumed as 480 MPa for the total number of OBE and hot shock cycles (50+170 = 220), accounting for other minor transients. Including the creep damage and its interaction with fatigue, accumulated during the high temperature duration of the hot shock, the computed creep-fatigue damage is 0.2, which is much less than the RCC-MR allowable limit (0.9).

6. FRACTURE MECHANICS ANALYSIS

Assuming a severe deviation from manufacturing standards, a surface crack with a crack depth/wall thickness (a/t) = 0.25 and crack length/wall thickness (2c/t) = 6 is postulated.
Crack propagation is predicted by integrating the Paris law as recommended in A16 [5]: $da/dN = C(\Delta K_a)^n$ and $dc/dN = C(\Delta K_c)^n$ for the growth depth and length respectively. As per A16 [5], $C = 6.2\times10^{-8}$ and n = 3.28 at 773 K. The stress intensity values ΔK_a and ΔK_c are computed using Raju-Newman's correlations as given in A16 [5].

The growth of the initial crack of 3.5 mm depth and 90 mm length is depicted in Fig. 9. A through-wall crack is possible after application of 1270 load cycles. The total number of design load cycles is only 220. Hence there is a factor of safety of ~ 6. That is, six plant life load cycles are to be applied to produce a leak in the pipe.

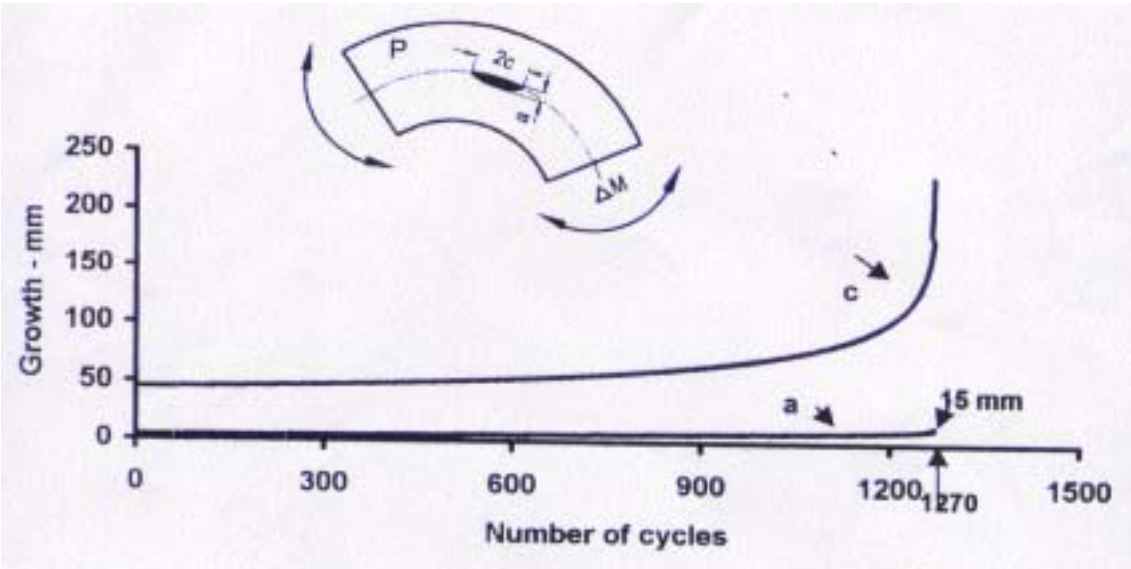

FIG. 9. Surface crack propagation at crown.

7. LBB ANALYSIS

The purpose of the analysis is to check, whether a double ended guillotine rupture (DEGR) in any of the four pipes can be detected by knowing the associated core flow reduction and temperature rise across the core.

In PFBR, a core flow reduction of about 43 kg/s results in a temperature rise of 1 K on the mixed mean core outlet temperature. Based on the temperature measurement sensitivity, it is judged that a minimum temperature rise of 2 K can be detected. The method of analysis is given below:

Extraction of net bending moment and axial force computed under SSE loadings at a section passing through the critical location;

- Computation of $2C_G$ as per the A16 for the above mentioned loadings;
- Computation of $2C_S$ from master curve assuming pure bending stresses;
- Computation of $2(C_G - C_S)$, which is considered the maximum admissible detectable crack length ($2C_L$);
- Knowing the $2C_L$ as well as the state of stress under normal operating conditions, crack opening displacement and consequent leak rate (Q_L) are estimated following the procedure of A16;
- Knowing the conversion factor (temperature rise per unit leak rate), the temperature rise that is associated with Q_L is calculated.

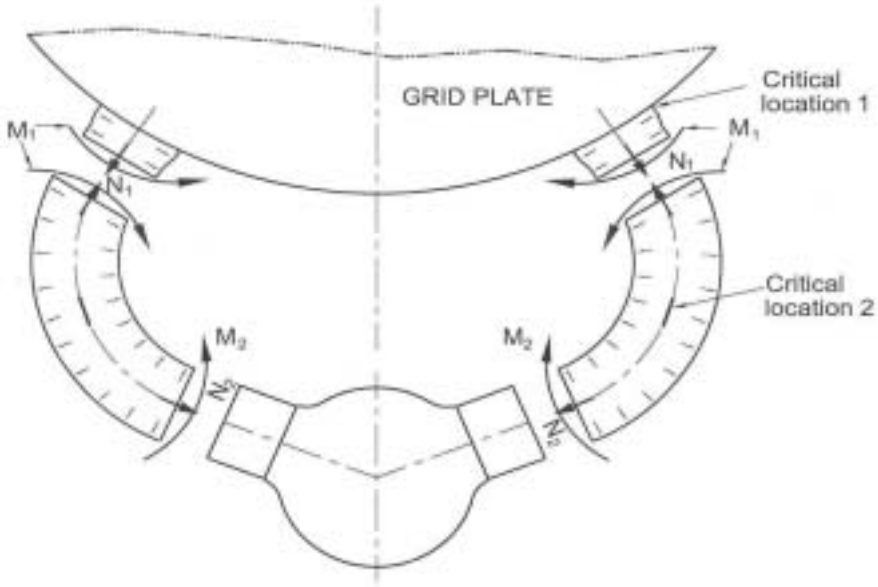

FIG. 10. Loadings.

7.1. Input data

Internal pressure is 0.8 MPa. Bending moments under SSE at the grid plate nozzle end = 66.53 kN-m and at the bend portion = 62.33 KN-m.

Material data used for the analysis at 670 K are as follows:

Sm = 109 MPa; $E = 1.61\times10^5$ MPa;
σ_y = 151 MPa; σ_o = 313 MPa; density of Na = 856.2 kg/m^3 ; viscosity of Na = 0.2792×10^{-5} Pa-s; $J_{IC} = J_{0.2}$ = 150 kJ/m^2 and $J_{\Delta a}$ = 130 + 100×c MPa.

7.2. At the grid plate nozzle junction (weld is assumed)

$2c_s$ = 144 mm. J_S = 430 n/mm. $2c_G$ = 1356 mm. $2c_L$ = 1212 mm. Crack mouth opening displacement δ = 0.24 mm. Leakage area = 230 mm^2. Leak rate = 6.83 kg/s. Temperature rise across core = ΔT = 0.16 K. Hence, it is not possible to detect the crack.

7.3. In the crown of the bend portion (no weld)

$2c_s$ = 144 mm. J_S = 430 n/mm. $2c_G$ = 342 mm. $2c_L$ = 198 mm. Crack mouth opening displacement δ = 0.08 mm. Leakage area = 120 mm^2. Leak rate = 4.3 kg/s. Temperature rise across core ΔT = 0.1 K. Hence, it is not possible detect the crack. It is seen that the crown is more critical than the grid plate nozzle junction.

It is concluded that LBB of the primary pipe can not be demonstrated with the resulting core flow reduction and associated temperature rise.

8. EXPERIMENTAL INVESTIGATIONS

The following are the main objectives of experiments:

- To validate the crack propagation behaviour based on tests on plate bending specimen (10) and ring specimens (3);
- To validate the finite element prediction of ovalization and strains at various pipe cross sections under combined bending and torsional moments, due to a radial force, imposed by the pump at the top of the spherical header nozzle during a seismic event (1);
- To simulate ratcheting on pipes subject to combined internal pressure and cyclic in-plane bending moment developed during thermal shock with the assumption that the free movement of spherical header is completely arrested (1);
- To identify the critical locations where cracks can develop on the structure that has welds at the junctions and initial manufacturing imperfections (in progress).

8.1. Tests on plate bending specimen

Master curves, as termed in A16, have been generated for SS 316 LN and G91 steel at room temperature. For the plates of uniform thickness h, subjected to pure bending stress, the asymptotic crack length $2C_S = 8\times h$ for G 91 steel (Fig. 11), as opposed $18\times h$ for 316 LN. A test series is in progress to quantify the same at high temperatures.

The asymptotic crack length has been predicted theoretically as 8.4 at room temperature and 6 at 923 K as shown in Fig. 12. With creep effects, the C_S is lower, predominantly under bending stresses. There is no effect under tensile stresses.

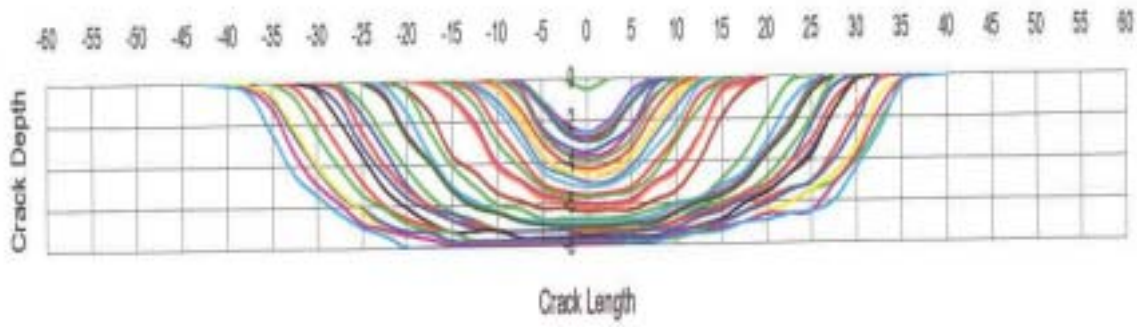

FIG. 11. Crack propagation in 10 mm thick G91 plate.

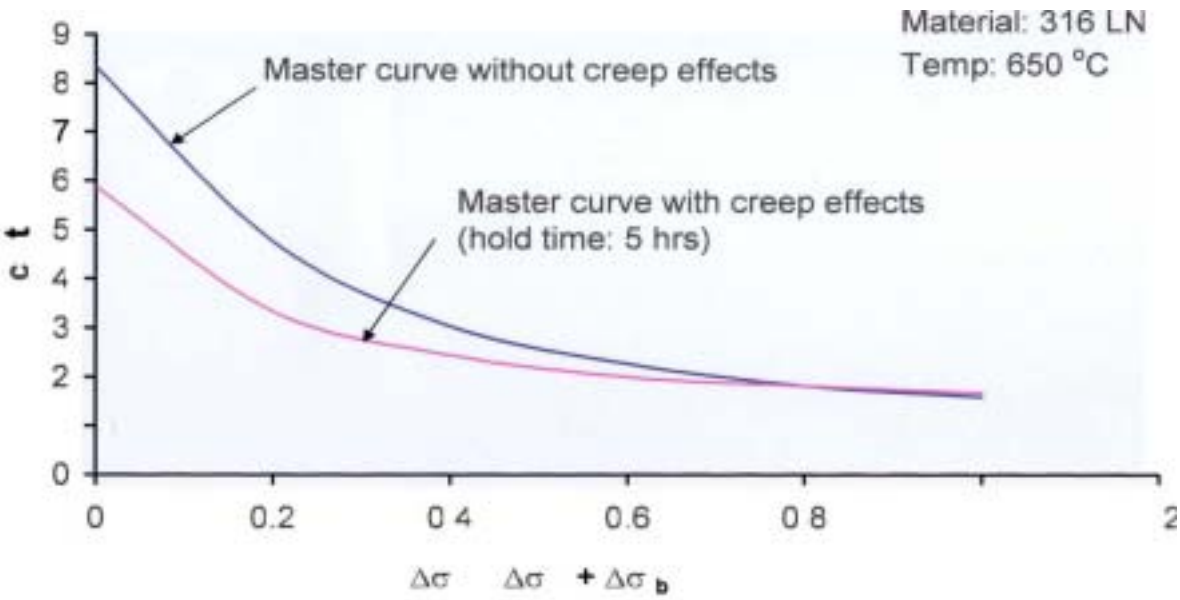

FIG. 12. Effect of creep on master curve.

8.2. Ring specimen

Finite element mesh of the test setup is shown in Fig. 13. The crack propagation prediction is compared with test data in Fig. 14.

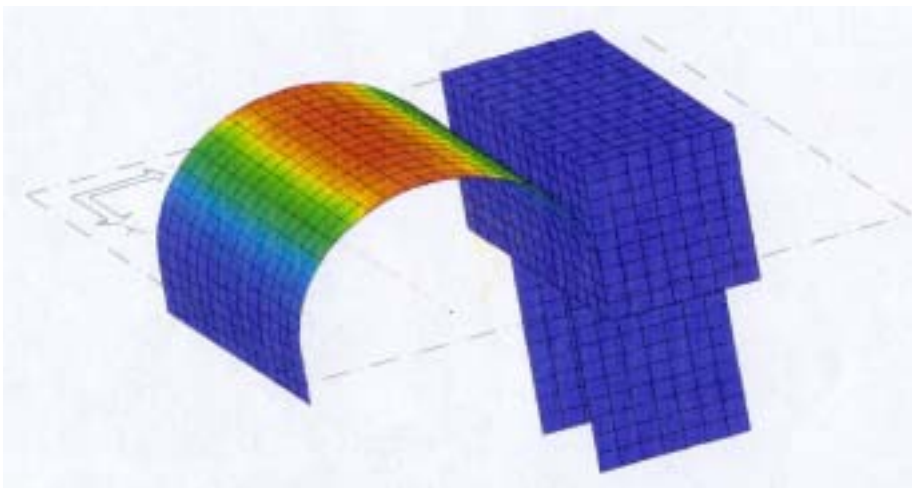

FIG.13. FE Mesh for ring specimen.

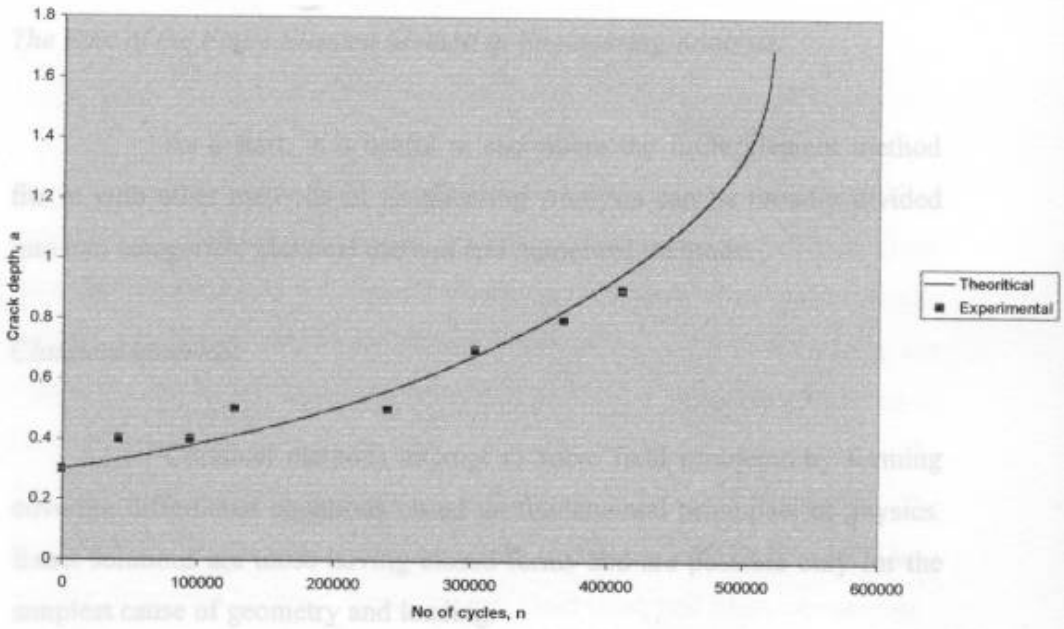

FIG. 14. Crack propagation behaviour.

8.3. Test results for combined bending and torsion moments

The test setup is shown in Fig. 15.

FIG. 15. Test setup.

The test results are compared with finite element predictions in Fig. 16.

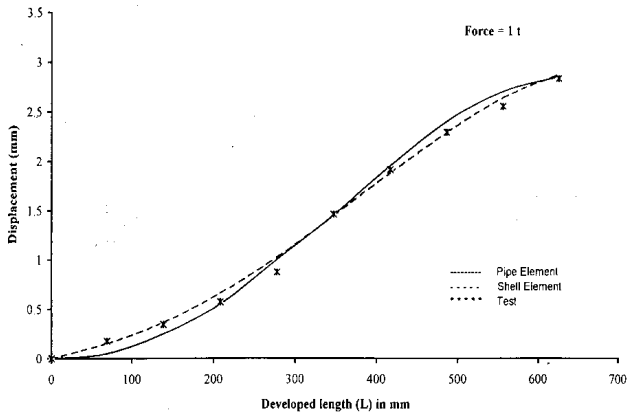

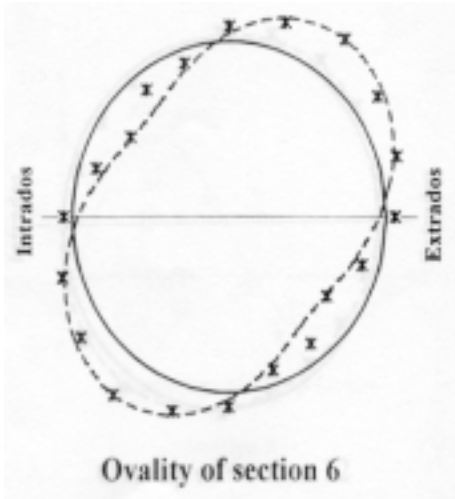

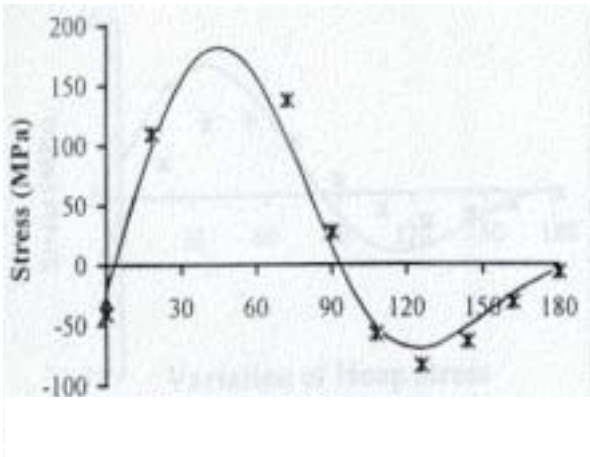

Variation of Hoop stress

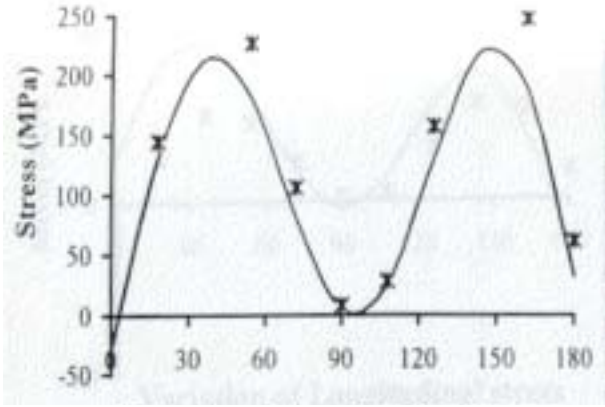

Variation of Longitudinal stress

FIG. 16. A few important results.

8.4. Predictions of ratcheting

FIG. 17. Ratchetting tests on a PSP model.

The test was conducted with a constant internal pressure of 1 MPa and a cyclic in-plane displacement equivalent to given ΔT_m. Tests indicated that the stabilized strain growth at the crown per unit ΔT_m is 7×10^{-3}% / K at room temperature. Extrapolation to the prototype under operating temperature yields 174 K. Since the maximum ΔT_m is only 50 K, ratcheting is not possible for prototype pipe.

Tests were continued on the model to initiate a visible crack. Even after application of more than 100 000 simulated load cycles, no crack has been seen. However, tests continued on the same model to quantify the crack initiation cycles.

9. CONCLUSION

Comfortable margins on the primary stresses, very low accumulated creep-fatigue damage, absence of ratcheting, and crack initiation even after application of more than ~ 500 simulated plant load cycles, and extensive experimental validation of finite element results, assures the structural integrity of primary pipe under all the normal and severe loading situations. Analysis shows that the maximum temperature rise of the core outlet sodium temperature (< 0.2 K), due to the leak through critical crack size, cannot be detected. Therefore, LBB demonstration by this mean is not possible.

REFERENCES

[1] RCC-MR, Regeles de Conception et de Construction des materiels Mecaniques des ilots Nucleaires RNR, Vol B (1993).

[2] KASINATHAN, N. et al., 'Thermal hydraulic consequences of primary pipe rupture', IAEA–TECDOC–1406, Vienna, (2004) 91–107.

[3] CHELLAPANDI, P., et al., 'Seismic analysis of Primary Sodium Pump for PFBR', paper presented in the National Seminar on Seismic Design of Nuclear Power Plants, 21–22 February 2003, at Structural Engineering Research Centre (SERC) Chennai, India.

[4] KASINATHAN, N., et al., 'Transient thermal loading on the primary pipe', PFBR/31290/DN/R/0 (2000).

[5] A16, 1995, Guide for defect assessment and leak before break, Rapport DMT 95/659.

A SIMPLIFIED CRACK GROWTH ASSESSMENT PROCEDURE FOR PCP IN FBR

T. WAKAI, K. AOTO

Abstract

This paper describes a creep-fatigue crack growth evaluation procedure applicable to the structural integrity assessment of primary coolant piping in a large scale liquid metal cooled fast breeder reactor. Simplified creep-fatigue crack growth evaluation procedure is proposed. In the crack growth analysis of the FBR components, plastic and creep deformation must be taken into account. The procedure evaluates crack growth rates based on stress intensity factor database obtained by linear elastic fracture mechanics approach, accounting for plastic and creep deformation. The predictions obtained by the procedure, based on the reference stress approach, are compared to some experimental data. It is found that the predicted fatigue crack growth behaviour is in good agreement with the observations and that the procedure exhibits some conservatism in creep-fatigue crack growth evaluation.

1. INTRODUCTION

It is essential to establish structural integrity assessment procedures for liquid metal cooled fast breeder reactor (LMFBR) components. JNC proposes a creep-fatigue crack growth evaluation procedure to apply to the structural integrity assessment of primary coolant piping (PCP) in large scale LMFBR. In the crack growth analysis of the FBR components, plastic and creep deformation must be taken into account. The procedure evaluates crack growth rates based on a stress intensity factor database obtained by linear elastic fracture mechanics approach, accounting for plasticity and creep. The procedure is verified by some experimental results.

2. JNC SIMPLIFIED CREEP-FATIGUE CRACK GROWTH EVALUATION PROCEDURE

In the procedures, JNC simplified creep-fatigue crack growth evaluation procedure, the interaction between fatigue and creep damages is not taken into account. The creep-fatigue crack growth rate da/dN is calculated as a linear summation of the fatigue and creep contributions as follows:

$$\frac{da}{dN} = \left(\frac{da}{dN}\right)_f + \left(\frac{da}{dN}\right)_c \tag{1}$$

1.1. Fatigue contribution

The fatigue crack growth rate $(da/dN)_f$ is calculated according to Paris rule:

$$\left(\frac{da}{dN}\right)_f = C_f \cdot \Delta J_{ep}{}^{m_f} \tag{2}$$

where ΔJ_{ep} is the elastoplastic J-integral range and C_f and m_f are material constants.

In the calculation, plasticity is taken into account. The membrane stress σ_m is obtained using the cyclic stress-strain curve and a parameter q_{ep} as shown in Fig. 1(a). For the bending stress, ($\varepsilon_{\mu+\beta}$,σ_{m+b}) and (ε_{m-b}.,σ_{m-b}) are determined using the cyclic stress-strain curve of the material and a parameter q_{ep} as illustrated in Fig. 1(b). The resulting elastoplastic stress distribution through the wall thickness is shown in Fig. 1(c). Assuming that the thickness of the plate equals to 2, the equivalent bending moment corresponding to such a stress distribution on the notch side and the opposite side is estimated using the following simplified equations:

$$M_{+b} = \int_0^l \left[f\{\varepsilon_m + (\varepsilon_{m+b} - \varepsilon_m)x\} - \sigma_m \right] x dx$$

$$M_{-b} = \int_{-l}^0 \left[f\{\varepsilon_m + (\varepsilon_m - \varepsilon_{m-b})x\} - \sigma_m \right] x dx$$

The elastoplastic bending moment M_{ep} can be calculated as follows:

$$M_{ep} = Min.[(M_{+b} + M_{-b}), M_e] \tag{4}$$

where M_e is the bending moment derived from an elastic calculation:

$$M_e = \int_{-l}^{l} (S_b x) x dx = \frac{2}{3} S_b \tag{5}$$

The equivalent elastoplastic bending stress σ_b can be calculated using the following equation:

$$\sigma_b = \frac{6 \cdot M_{ep}}{2 \cdot w \cdot t^2} = \frac{3}{2} M_{ep} \tag{6}$$

The elastic J-integral range ΔJ_{el} is estimated using a crack closure factor qw:

$$\Delta J_{el} = \frac{\{q_w \cdot (K_{max} - K_{min})\}^2}{E^*}$$

with (7)

$q_{clos} = (1\text{-}R)^{n-1}$

where K_{max} and K_{min} are the maximum and minimum stress intensity factors in the loading cycle, respectively, and $E^*=E$ for plane stress conditions and $E^*=E / (1-\nu^2)$ for plane strain conditions.

Assuming that compressive loads do not contribute to crack growth and crack closure effect is negligible, n is defined by:

for $R \geqq 0$	$n = 1$	$q_w = 1$
for $R < 0$	$n = 0$	$q_w = 1 / (1-R)$

The elastoplastic J-integral range ΔJ_{ep} is obtained from ΔJ_{el} using a plastic correction factor fep:

$$\Delta J_{ep} = f_{ep} \cdot \Delta J_{el}$$

$$f_{ep} = \frac{\sigma_{ref}^{\ 3}}{2\sigma_y^{\ 2} \cdot E \cdot \varepsilon_{ref}} + \frac{E \cdot \varepsilon_{ref}}{\sigma_{ref}}$$

where σ_{ref} is the reference stress calculated at the maximum load of the cycle and ε_{ref} is the corresponding reference strain. σ_y is the 0.2% proof stress derived from the cyclic stress-strain curve of the material. The reference stress is determined using a net section shape function F_{net}:

$$\sigma_{ref} = F_{net}(p_m \cdot \sigma_m + p_b \cdot \sigma_b) \tag{9}$$

JNC proposes F_{net}, p_m and p_b corresponding to the shape of structure and the loading conditions.

2.2. Creep contribution

The creep crack growth rate $(da/dN)_c$ is calculated according to Paris rule:

$$\left(\frac{da}{dN}\right)_c = C_c \cdot \Delta J_c^{\,m_c} \tag{10}$$

where ΔJ_c is the equivalent creep J-integral range and C_c and m_c are material constants.

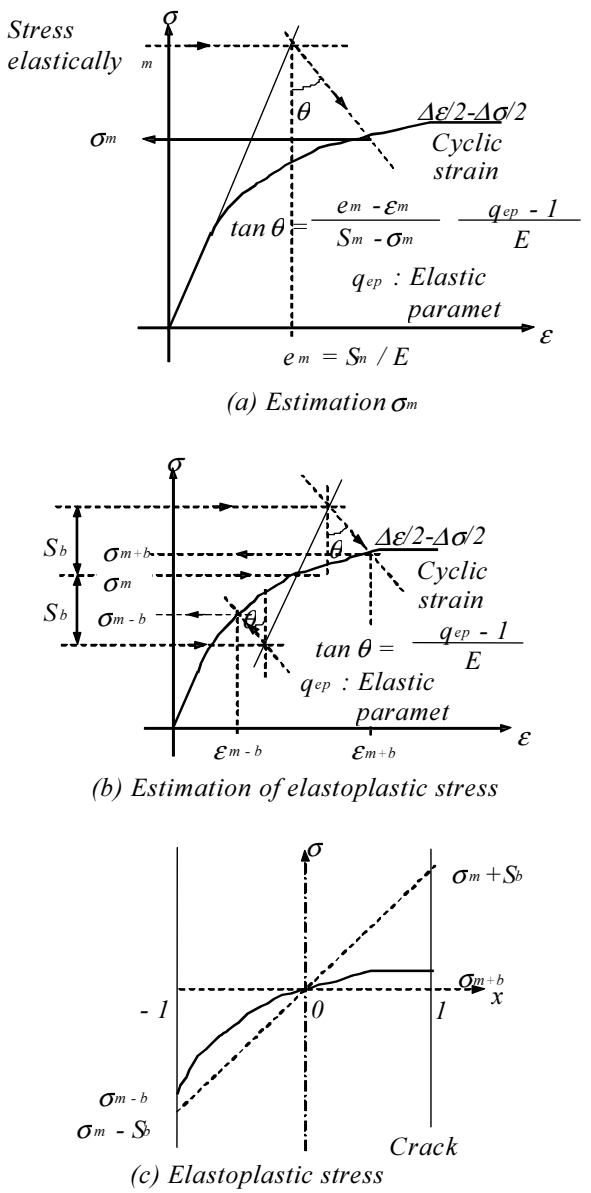

FIG. 1. Determination of σ_m and σ_b according to the JNC method.

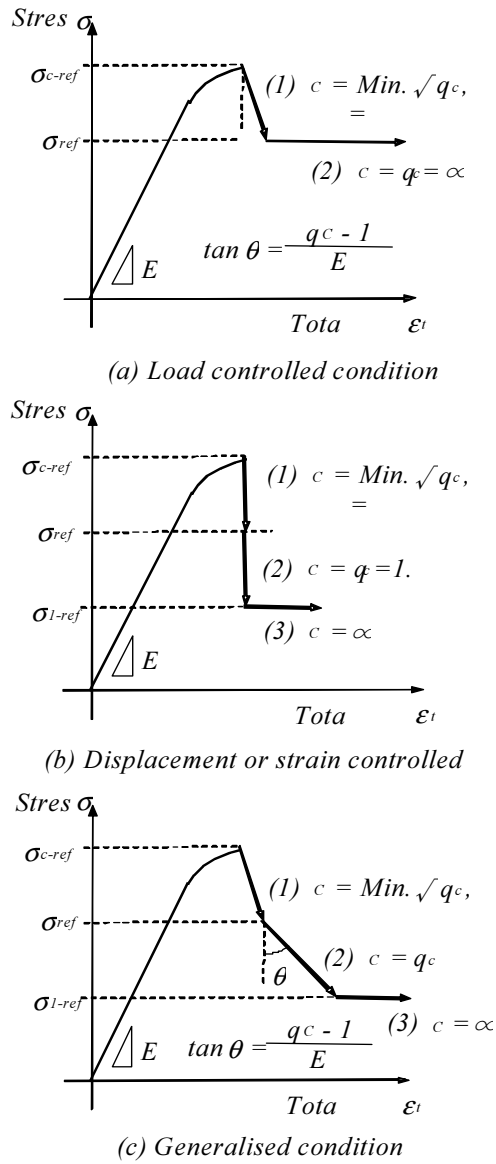

FIG. 2. Stress relaxation in the JNC method.

JNC assumes that the time dependent creep J-integral $J_c(t)$ is obtained from the elastic J-integral J_{el} at the maximum load of the cycle using a creep correction parameter f_c defined by:

$$J_c(t) = f_c \cdot J_{el} = \frac{E \cdot \dot{\varepsilon}_{c-ref}(t)}{\sigma_{c-ref}} \cdot J_{el} \tag{11}$$

with

$$f_c = \frac{E \cdot \dot{\varepsilon}_{c-ref}(t)}{\sigma_{c-ref}}$$

where $\varepsilon_{c\text{-ref}}(t)$ is the time dependent reference creep strain rate and $\sigma_{c\text{-ref}}$ is the reference stress at the beginning of the hold time. The creep strain rate $\varepsilon_{c\text{-ref}}(t)$ is estimated taking stress relaxation into account, but the reference stress at the beginning of the hold time is used in the creep correction procedure. The equivalent creep J-integral range ΔJ_c has to be integrated over the hold time t_c as follows:

$$\Delta J_c = \int_0^{t_c} J_c(t)dt$$

$$= \frac{E \cdot K_{max}^{\ 2}}{E^* \cdot \sigma_{c-ref}} \int_0^{t_c} \dot{\varepsilon}_{c-ref}(t)dt$$

$$= \frac{E \cdot K_{max}^{\ 2} \cdot \varepsilon_{c-ref}(t_c)}{E^* \cdot \sigma_{c-ref}} \tag{12}$$

where $\varepsilon_{c\text{-ref}}(t_c)$ is the reference creep strain at $t = t_c$, that is at the end of the dwell and can be calculated by time integration of the creep strain rate $\varepsilon_{c\text{-ref}}(t)$ from 0 to t_c. In the calculation of $\varepsilon_{c\text{-ref}}(t_c)$, stress relaxation is considered using a parameter q_C given in Fig. 2. $\varepsilon_{c\text{-ref}}(t_c)$ is calculated using the creep law of the material, reinitialised at each cycle.

The time dependant reference creep strain rate $\dot{\varepsilon}_{c\text{-ref}}$ is determined from the reference stress $\sigma_{c\text{-ref}}$. σ_{ref} is given by Eq.(9).

For small scale yielding conditions, JNC observed that too small creep J-integral values are obtained if σ_{ref} is used as $\sigma_{c\text{-ref}}$. Therefore, JNC assumes that the reference stress at the beginning of the hold time $\sigma_{c\text{-ref}}$ depends upon the yielding conditions:

for $\sigma_{\rho\varepsilon\phi} < \sigma_y \rightarrow$ Small scale yielding condition: $\sigma_{\chi-\rho\varepsilon\phi} = \sigma_{\rho\varepsilon\phi} (\sigma_\psi / \sigma_{\rho\varepsilon\phi})^{\pi}$

for $\sigma_{\rho\varepsilon\phi} \geqq \sigma_\psi \rightarrow$ Large scale yielding condition: $\sigma_{\chi-\rho\varepsilon\phi} = \sigma_{\rho\varepsilon\phi}$

where σ_y is the 0.2% proof stress derived from the cyclic stress-strain curve of the material and p is a parameter that allows to take the heterogeneous stress distribution in the ligament into account for small scale yielding condition. JNC gives an expression of p as a function of crack size:

$$p = p_1 + p_2 (a / t) \tag{13}$$

and recommends that $p_1 = p_2 = 0.2$. This is based on the results obtained from creep finite element analyses for plates containing a through wall notch subjected to uniaxial tension. Since such a heterogeneous stress distribution will disappear immediately with strain redistribution, the stress is allowed to relax from $\sigma_{c\text{-}ref}$ to the value of $\sigma_{\rho\varepsilon\phi}$ given by eqn.(9). This is illustrated in Fig. 2. The stress relaxes during the hold time in accordance with the following expression:

$$d\sigma_{relax} = \frac{E \cdot d\varepsilon_c}{q_C} \tag{14}$$

$$d\varepsilon_c = \int_t^{t+dt} \dot{\varepsilon}_c(t)dt \tag{15}$$

In the stress relaxation process, JNC assumes a strain hardening rule for the calculation of the creep strain rate.The loading conditions, the geometry of the plates and the dimensions of the initial notches are given in Table 1. The membrane stress σ_m and the bending stress σ_b can be calculated elastically. The material properties are given in Table 2. The cyclic stress-strain curve at 650°C is expressed as follows [5].

$$\Delta\varepsilon = 100 \times \frac{2(1+\nu)}{3E}\Delta\sigma + \left(\frac{\Delta\sigma}{K}\right)^{1/m}$$

where, $\Delta\varepsilon$ is the total strain range in %, $\Delta\sigma$ is the stress range in MPa, E and n are Young's modulus and Poisson's ratio at the corresponding temperature and K and m are constants. For this material, K = 718 and m = 0.319.

3. COMPARISON WITH SOME EXPERIMENTAL DATA

3.1. Fatigue crack growth

A fatigue crack growth test consists of a plate made of an austenitic stainless steel 316L(N) containing a semi-elliptical surface notch subjected to a cyclic bending moment at a load ratio R = 0.1. Two tests were performed at 650°C [3, 4]. The experimental setup is shown in Fig. 3.

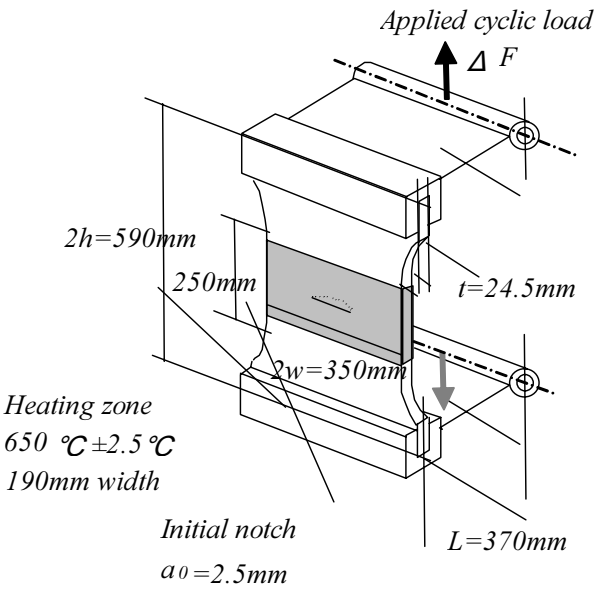

Fig.3 Experimental setup

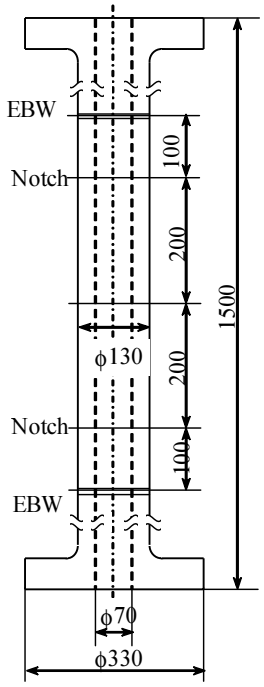

Fig.4 Shape and dimensions of the specimen

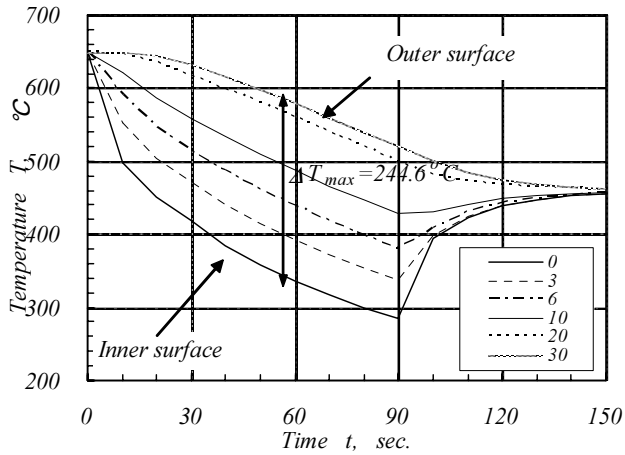

Fig.5 Temperature history of a thermal transient

3.2. Thermal fatigue crack growth

For small scale yielding condition, JNC observed that too small creep J-integral values are obtained if σ_{ref} is used as $\sigma_{c\text{-}ref}$. Therefore, JNC assumes that the reference stress at the beginning of the hold time $\sigma_{c\text{-}ref}$ depends upon the yielding conditions: A thermal fatigue crack growth test consists in a thick wall cylinder made of a type 304 stainless steel (SUS304) containing axisymmetrical notches on the inner surface [6]. The shape and dimensions of the specimen are shown in Fig. 4. The specimen has axisymmetrical initial notches machined by electric discharging on the inner surface and fatigue pre-cracking was not performed prior to start the experiment

The specimen was first heated uniformly up to a temperature of 650°C using an electric furnace. Then, the specimen was subjected to cyclic thermal transients for 90 s using pressurised air on the inner surface. No mechanical load was imposed onto the specimen and the thermal expansion was not accelerated. The temperature history at several depths through the wall thickness is shown in Fig. 5. These temperature gradients were measured experimentally with a defect-free specimen prior to the thermal fatigue crack growth test. As shown on this figure, a large temperature gradient is obtained up to 90 seconds. Then the gradient reduces with time as the air flow is stopped. The maximum temperature gradient is obtained at t = 60 s, (ΔT_{max} = 244.6°C).

The temperature dependant mechanical properties and the cyclic stress-strain curve of the type 304 stainless steel material constituting the specimen are given in Table 3. The fatigue crack growth rate is estimated using the Paris law expressed as a function of the J-integral range, as given in Table 3. The Paris law is assumed to be temperature independent for 450°C $\leq$ T < 650°C.

3.3. Creep-fatigue crack growth

A creep-fatigue crack growth test consists of a plate made of an austenitic stainless steel 316L(N) containing a semi-elliptical surface notch subjected to a cyclic bending loads at 650°C [4]. The load controlled creep-fatigue loading cycle consists of a triangular wave form with a 1 hour dwell at the maximum load of the cycle. The experimental setup is shown in Fig. 3. The loading conditions, the geometry of the plate and the dimensions of the initial notch after fatigue pre-cracking are given in Table 4. The membrane stress σ_m and the bending stress σ_b can be calculated elastically. The mechanical properties, the cyclic curve and the creep curve available in the RCC-MR [5] are given in Table 5 together with the Paris law and the creep crack growth characteristics [4].

Table 1 Description of the fatigue crack growth tests

Test conditions					Plate geometry		Length of Bending arm	Initial notch	
Temp. T (^oC)	Load ratio R -	Min.Load F_{min} (kN)	Max.Load F_{max} (kN)	Dwell t_c (hour)	Thickness t (mm)	Width $2w$ (mm)	L (mm)	Depth a (mm)	Length $2c$ (mm)
650	0.1	1.9	19.0	-	24.5	350	370	2.5	85.0

Table 2 Material propeties for 316L(N) used in the fatigue crack growth tests

Temperature T (^oC)	Mechanical properties			Fatigue crack growth Characteristics	
	Young's modulus E (MPa)	Poisson's ratio ν -	0.2% proof stress σ_y (MPa)	C_f -	m_f -
650	140600	0.30	125	3.2×10^{-7}	2.46

Table 3 Material properties for SUS304 used in the thermal fatigue crack growth test

- Temperature dependant cyclic stress-strain curve

$\Delta\sigma \leqq 2\sigma_p$ $\quad \Delta\varepsilon=\Delta\sigma/E$ (mm/mm)

$\Delta\sigma > 2\sigma_p$ $\quad \Delta\varepsilon=\Delta\varepsilon_e+\Delta\varepsilon_p$ (mm/mm)

$$\Delta\varepsilon_e=\Delta\sigma/E$$

$$\Delta\varepsilon_p=\left\{\frac{\Delta\sigma-2\sigma_p}{10^{A_o}}\right\}^{1/A_1}$$

Young's modulus $\quad E=2.06031\times10^5-9.52457\times10^1\times T$ (MPa)

Yield stress $\quad \sigma_y=2.50542\times10^2-5.47758\times10^{-1}\times T+1.02296\times10^{-3}\times T^2-7.27684\times10^{-7}\times T^3$ (MPa)

Proportional limit $\quad \sigma_p=\sigma_y-K(0.002)^m$ (MPa)

$K=4.34207\times10^2-1.75354\times10^{-1}\times T$

$m=2.79395\times10^{-1}+7.74900\times10^{-5}\times T$

$A_0=1.968789+6.446708\times10^{-3}\times T-4.675557\times10^{-6}\times T^2-3.724201\times10^{-9}\times T^3$

$A_1=3.690128-1.847969\times10^{-2}\times T+3.544927\times10^{-5}\times T^2-2.297822\times10^{-8}\times T^3$

(T : Temperature in ^oC)

- Fatigue crack growth characteristics

$$\frac{da}{dN}=C_f\cdot(\Delta J)^{m_f}$$

(da/dN(mm/cyc), ΔJ(N/mm))

C_f $\quad 1.4953\times10^{-5}$

m_f $\quad 1.8158$

Table 4 Description of the creep-fatigue crack growth tests

Test conditions					Plate geometry		Length of Bending arm	Initial notch	
Temp. T (^oC)	Load ratio R -	Min.Load F_{min} (kN)	Max.Load F_{max} (kN)	Dwell t_c (hour)	Thickness t (mm)	Width $2w$ (mm)	L (mm)	Depth a_0 (mm)	Length $2c_0$ (mm)
650	-1.0	-14.0	14.0	1.0	24.5	350	350	7.9	87.2

Table 5 Material propeties for 316L(N) used in the creep-fatigue crack growth test

- Mechanical properties

Young's modulus	E	140600 (MPa)
Poisson's ratio	ν	0.30
0.2% proof stress	σ_y	125 (MPa)

- Cyclic stress-strain curve

$$\Delta\varepsilon=100\times\frac{2(1+\nu)}{3E}\Delta\sigma+\left(\frac{\Delta\sigma}{K}\right)^{1/m}$$

$K=718$

$m=0.319$

($\Delta\varepsilon$(%), $\Delta\sigma$(MPa))

- Fatigue crack growth Characteristics

$$\frac{da}{dn}=C_f\cdot\Delta K_{eff}^{m_f}$$

$C_f=6.2\times10^{-8}$

$m_f=2.46$

(da/dN(mm/cyc), ΔK_{eff}(Mpa $\sqrt{m}$))

- Creep curve

for $t<t_{ffp}$:

$$\varepsilon_c=C_1\cdot t^{C_2}\cdot\sigma^{n_1}$$

for $t\geqq t_{ffp}$:

$$\varepsilon_c=C_1\cdot t^{C_2}\cdot\sigma^{n_1}+100\times C\cdot\sigma^n(t-t_{ffp})$$

$$t_{ffp}=\left(\frac{C\cdot\sigma^{n-n_1}}{C_1\cdot C_2}\right)^{1/(C_2-1)}$$

$C_1=6.78\times10^{-14}$

$C_2=0.4845$

$n_1=5.469$

$C=1.70\times10^{-20}$

$n=6.999$

(ε_c(%), σ(MPa), t_{ffp}(hour))

- Creep crack growth Characteristics

$$\frac{da}{dt}=A\cdot(C^*)^q$$

$A=7.1\times10^{-3}$

$q=0.73$

(da/dt(mm/hour), C^*(N/mm))

4. RESULTS AND DISCUSSIONS

4.1. Fat crack growth

The calculated crack shapes as a function of number of cycles are compared with the experimental data in Fig. 6. The elastoplastic calculation gives very good prediction of the crack shape. Under these experimental conditions, the influence of crack closure on crack growth does not need to be accounted for. Validity of crack closure factor in the procedure must be verified.

4.2. Thermal fatigue

The calculated crack dimensions as a function of number of cycles are compared with the experimental data in Fig. 7.

The predictions are found to be in good agreement with the experimental data. The method allows to predict crack growth acceleration in the early stage of the experiment and crack growth deceleration after 1 000 cycles. Since the procedure accounts for the parabolic stress component, the stress distribution through the wall thickness used in the procedure agrees well with the one calculated from a thermo-elastic FE analysis.

4.3. Creep-fatigue

The crack dimensions as a function of number of cycles are compared with the experimental data in Fig. 8. As shown in Fig. 8, the procedure exhibits some conservatism when predicting crack growth. There is evidence that reinitializing the creep curve of the material at each cycle is too conservative [7]. This figure also shows the predictions using an alternative model to integrate the creep law of the material. This model consists in integrating the creep curve continuously during the experiment [8]. The calculation results employing this model are also shown in Fig. 8 and indicated as solid lines. This model is found to underestimate the creep crack growth behavior.

In the determination of the reference stress, JNC accounts for the creep strain intensity due to heterogeneous stress distribution in the ligament for small scale yielding condition. However, since the recommended values of p_1 and p_2 in eqn. (13) are based on creep finite element analyses for plates containing a through wall notch subjected to uniaxial tension, the applicability to the semi-elliptical surface crack has not been verified yet.

In fact, in this work, the JNC predictions are too conservative. Although not fully verified yet, some calculations substituting σ_{ref} for $\sigma_{c\text{-}ref}$ were performed. The calculation results are shown in Fig. 9. Better agreement with the experimental data is obtained.

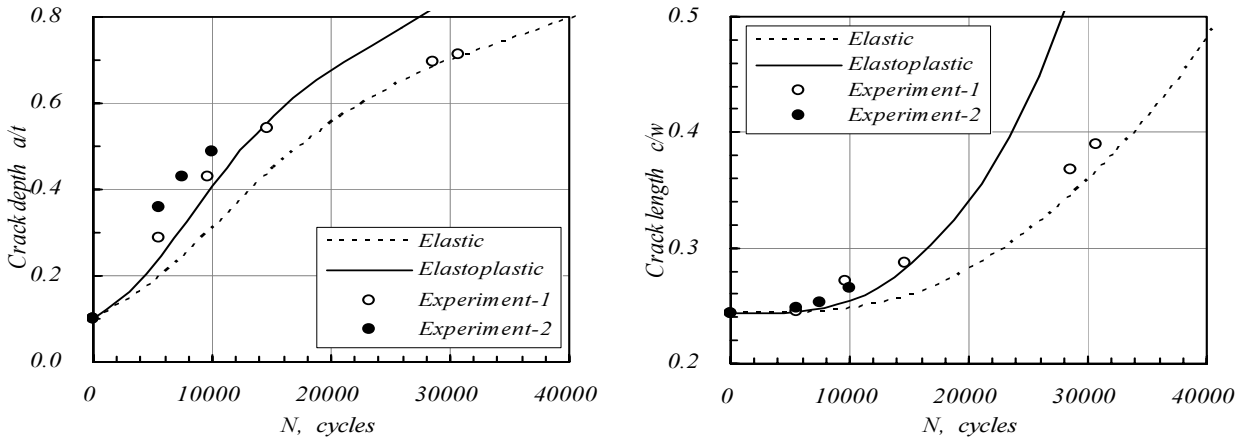

(a) Crack depth (b) Crack length

FIG. 6. Comparison between calculated fatigue crack growth behavior and experimental data.

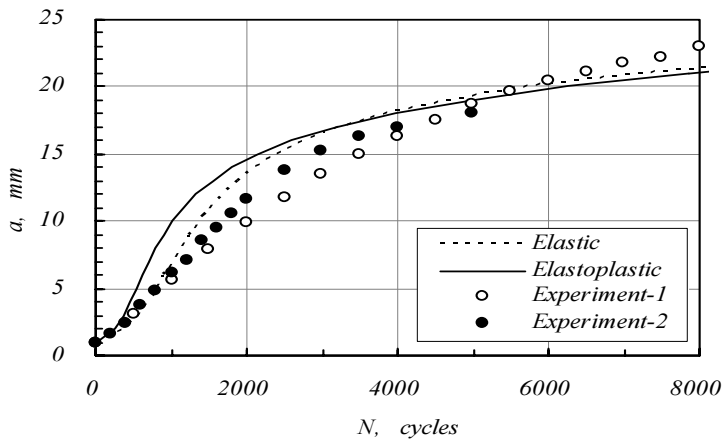

FIG. 7. Comparison between calculated thermal fatigue crack growth behavior and experimental data.

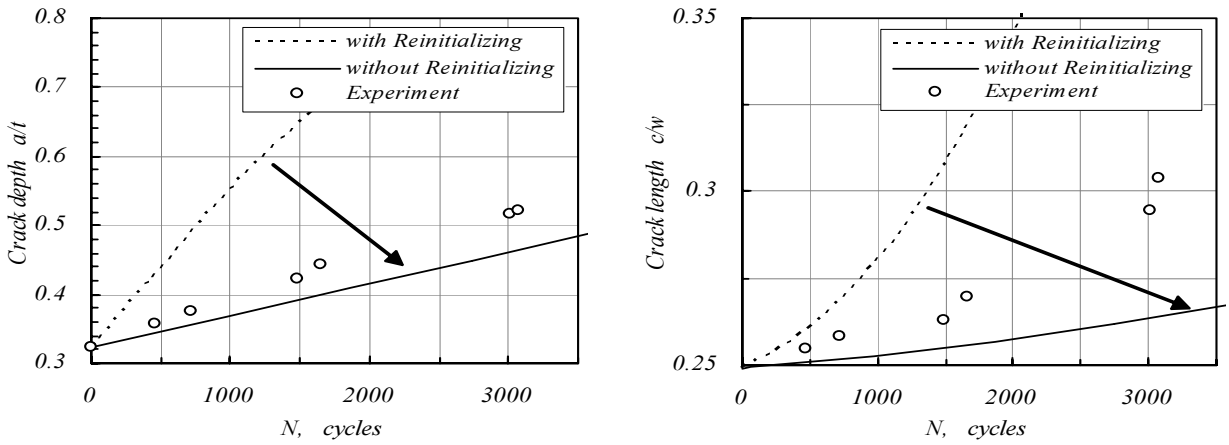

(a) Crack depth (b) Crack length

FIG. 8. Comparison between calculated creep-fatigue crack growth behavior and experimental data.

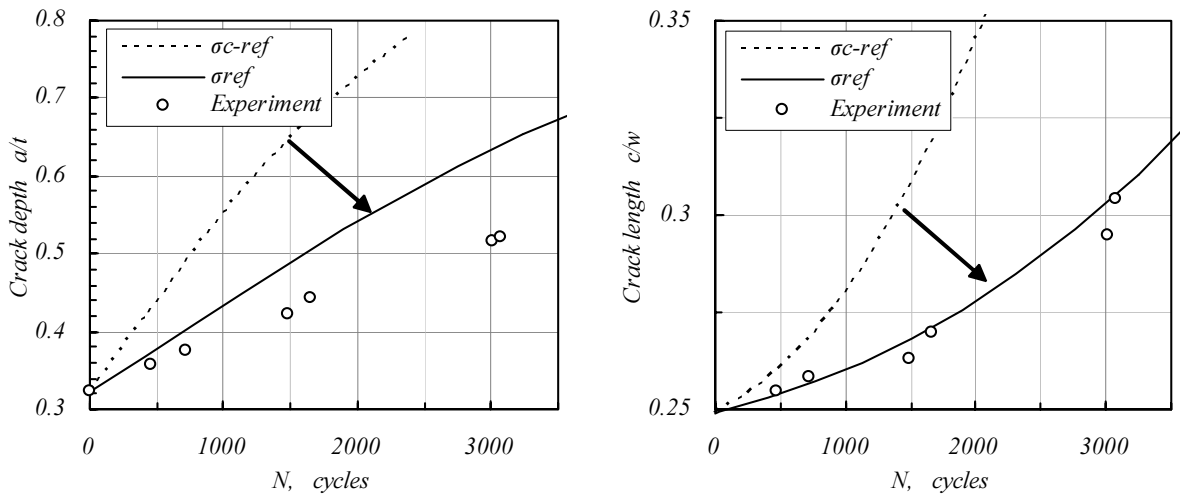

(a) Crack depth *(b) Crack length*

FIG. 9. Influence of reference stress on crack growth predictions.

5. CONCLUSIONS

JNC proposes a simplified creep-fatigue crack growth evaluation procedure. The predictions obtained by the procedure are compared to some experimental results.

For load controlled fatigue crack growth, at R = 0.1, the procedure well predicts the fatigue crack growth behavior observed experimentally.

For thermal fatigue crack growth, the simulation results are in good agreement with the experimental data. For load controlled creep-fatigue crack growth, it is found that the simplified methods exhibit conservatisms that are significantly reduced when using alternative model to integrate the creep law of the material.

REFERENCES

[1] WAKAI, T., POUSSARD, C., DRUBAY, B., "A Comparison between Japanese and French A16 Defect Assessment Procedures for Fatigue Crack Growth", paper presented in the 15th Intl Conf Structural Mechanics in Reactor Technology (SMiRT-15), 15–20 August 1999, Seoul, Rep. of Korea.

[2] POUSSARD, C., WAKAI, T., DRUBAY, B., "A Comparison between Japanese and French A16 Defect Assessment Procedures for Creep-fatigue Crack Growth", paper presented in the 15th Intl Conf Structural Mechanics in Reactor Technology (SMiRT-15), 15–20 August 1999, Seoul, Rep. of Korea.

[3] POUSSARD, C., et al. "High temperature leak before break experimental studies of austenitic stainless steel centre cracked plate", Proc 14th Intl Conf Structural Mechanics in Reactor Technology (SmiRT-14), 17–22 August 1997, Lyon, France, G13/5 (1997).

[4] POUSSARD, C., et al. “Creep-fatigue Crack Growth in Austenitic Stainless Steel Centre Cracked Plates at 650°C - Part I: Experimental Study and Interpretation”, Proc Intl “HIDA” Conference on Creep and Fatigue Crack Growth in High Temperature Plant, 15–17 April 1998, CEA Saclay, France, S3-22 (1998).

[5] RCC-MR, 1993, Design and Construction Rules for Mechanical Components of FBR Nuclear Islands, 3rd edition, AFCEN, France.

[6] WAKAI, T., HORIKIRI, M., POUSSARD, C., DRUBAY, B., “A Comparison between Japanese and French A16 Defect Assessment Procedures for 2D Crack in the Thick-wall Cylinder Subjected to Thermal-Transient”, Ninth International Conference on Pressure Vessel Technology (ICPVT-9), 9–14 April 2000, Sydney, Australia.

[7] POUSSARD, C., et al., “Creep-fatigue Crack Growth in Austenitic Stainless Steel Centre Cracked Plates at 650°C - Part II: Defect Assessment According to the A16 Document”, Proc Intl “HIDA” Conference on Creep and Fatigue Crack Growth in High Temperature Plant, 15–17 April 1998, CEA Saclay, France, S7-48 (1998).

[8] POLVORA, J.P., et al., “Creep fatigue Crack Growth on CT25 Specimens in 316L(N) stainless steel at 650°C”, Proc 14th Intl Conf Structural Mechanics in Reactor Technology (SmiRT-14), 17–22 August 1997, Lyon, France, G13/2 (1997).

THERMAL HYDRAULIC CONSEQUENCES OF PRIMARY PIPE RUPTURE

N. KASINATHAN, K. NATESAN, P. SELVARAJ, P. CHELLAPANDI, S.C. CHETAL
Indira Gandhi Centre for Atomic Research (IGCAR), Kalpakkam, India

Abstract

Thermal hydraulic analyses of primary pump pipe rupture event have been carried out with the objective of (i) estimating the temperature rise in the fuel, cladding and coolant, (ii) investigation of possible flow redistribution in subassemblies and (iii) investigation of the formation of vapour bubbles due to flashing, resulting in reactivity addition in the core. For this purpose one dimensional studies using thermal and hydraulic models of the core SA and primary sodium circuit, three dimensional studies of grid plate using the CFD code PHOENICS and one dimensional studies using pressure transient codes have been carried out. Analysis indicates that the core flow is reduced to 30% during the transient and specified temperature limits of this category of events are respected. There is no flow redistribution among various subassemblies and no formation of vapour in subassemblies.

1. INTRODUCTION

The primary sodium circuit consists of hot and cold sodium pools with an inner vessel separating them. Sodium from the cold pool is circulated through the core by two centrifugal Primary Sodium Pumps (PSP) operating in parallel. Each PSP is located inside a standpipe. Sodium flows from the cold pool to the standpipe and then is pumped to the grid plate. Each pump feeds the grid plate through two 600 mm diameter primary pipes. Sodium from the hot pool flows through four Intermediate Heat Exchangers (IHX) to the cold pool. IHX transfers heat produced by the core to a secondary sodium circuit. A schematic of primary sodium circuit is shown in Fig. 1.

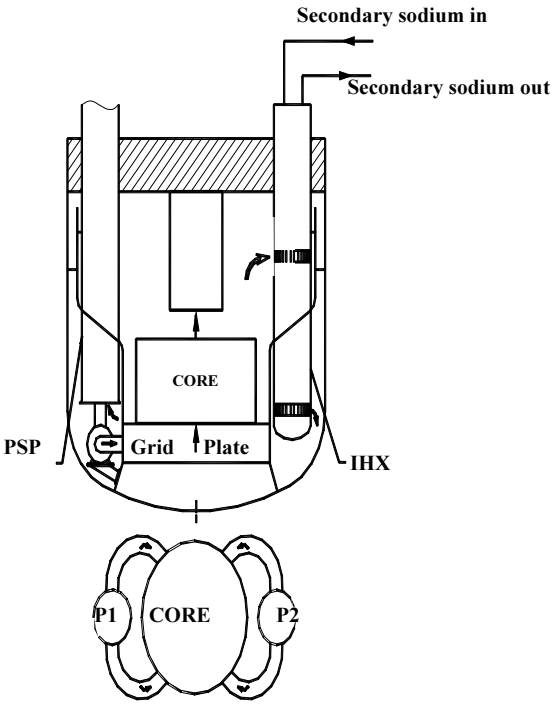

FIG. 1. Schematic of primary sodium circuit.

Schematic of standpipe flow and PSP flow is shown in Fig. 2.

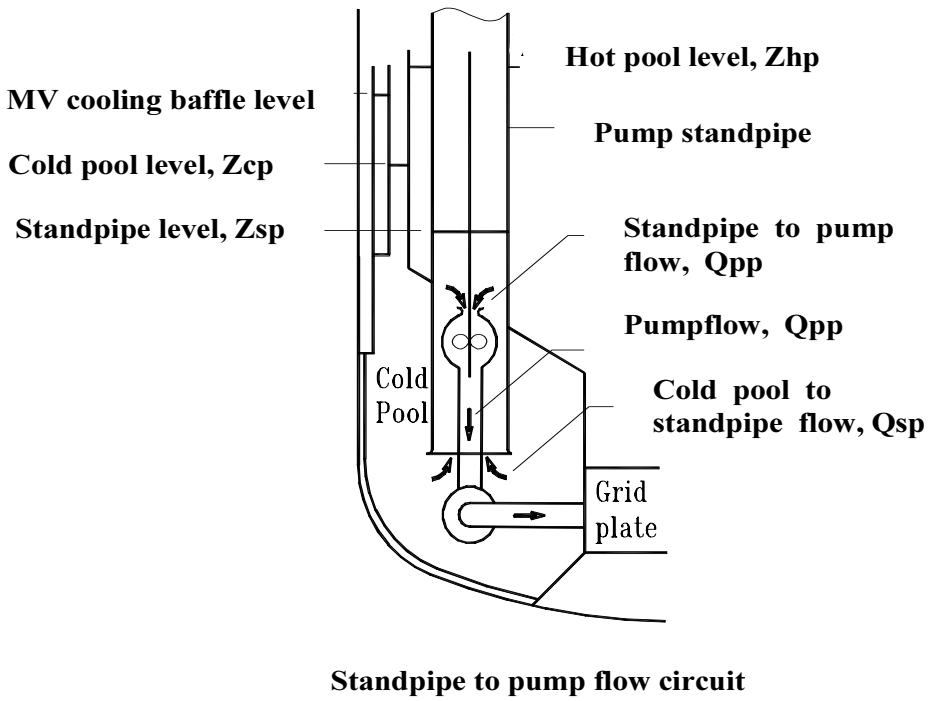

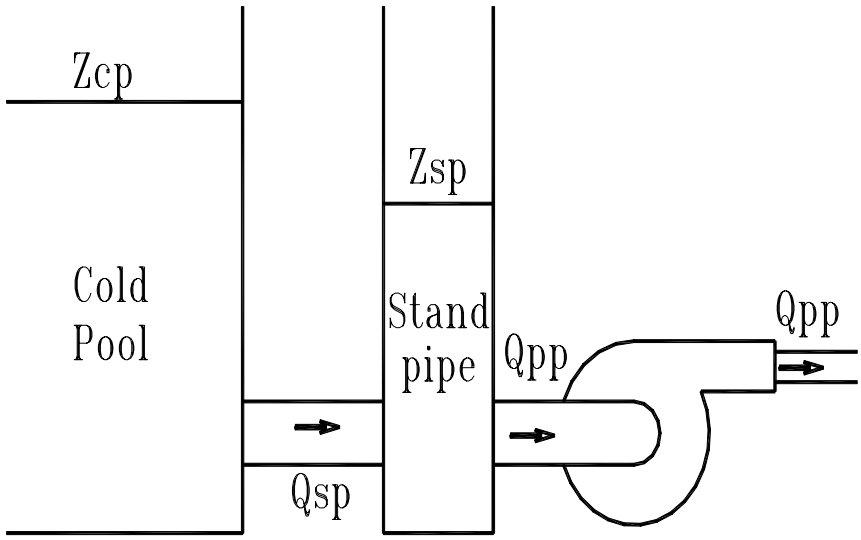

FIG. 2. Schematic of the stand pipe and pump sodium flows.

Because of resistance offered by the standpipe for flow, the sodium level in the standpipe would be lower than the cold pool level by an amount equal to head drop suffered by sodium flow in the standpipe. Primary pipes are designed according to safety class 1 rules and to withstand a design basis earthquake. High structural reliability is ensured by selecting highly ductile SS 316 LN material. Further, it is subjected to relatively low operating temperature (less than 673 K) where creep effects are insignificant during normal operation and for high quality manufacturing. Structural mechanics studies have indicated low operating stress. These aspects render the Double Ended Guillotine Rupture (DEGR) of the pipe a very low probability event. However, due to the inability of LBB justification because of the difficulty in leak detection, and as a measure of defence in depth, instantaneous and total DEGR in a single primary pipe has been considered as a Category 4 Design Basis Event (DBE).

In a DEGR of a single primary pipe, primary sodium flow bypasses the core through the ruptured path back to the cold pool and the core flow decreases to a low value at a rapid rate and in turn causes sodium and cladding temperatures to rise. Any one among the scram parameters (for automatic emergency shutdown of the reactor), enabled by the Power to Flow Ratio (P/Q), Reactivity (ρ), Linear Power (Lin P), and Central SA Sodium Outlet Temperature (θ_{CSAM}), would shutdown the reactor. Other important consequences in this event are as follows: The resistance against which both pumps have to supply comes down sharply, which causes the pump flows to increase suddenly. Such sudden change of pump flow does not affect standpipe flow immediately. Hence, a sudden increase in the pump flow causes reduction in the standpipe sodium level during the transient. This results in the reduction of available net positive suction head ($NPSH_A$) for the pump. Increase in the pump flow also results in an increase of the required net positive suction head ($NPSH_R$) of the pump. Thus, a situation of $NPSH_A$ becoming less than $NPSH_R$, leading to cavitation of the pump, occurs during this event. There may be a concern of a sudden decrease in pressure in the core and consequent vapour bubble formations (due to flashing), resulting in reactivity addition. This paper gives a summary of thermal hydraulic studies carried out for the primary pipe rupture event.

1.1. Cladding and coolant temperature limits

Design Safety Limits (DSL) for a Category 4 event are that the Cladding Hotspot Temperature (T_{Cl}) should be less than 1473 K, and SA mean Sodium Hotspot Temperature (T_{Na}) should be less than the boiling point of sodium.

2. ANALYSES OF THE EVENT

The analyses have been carried out in three steps. In the first step, evolutions of flow and temperature of the primary circuit and core [1] respectively are obtained using the plant dynamics code DYANA-P. Details of the DYANA-P code have been published earlier [1]. In the second step, the possibility of flow redistribution in the core under pipe rupture condition is analyzed [2]. In the third step, the possibility of void formation in the core is analyzed [3].

2.1. Analysis to obtain flow and temperature evolutions

One-dimensional (1-D) thermal hydraulic analysis is carried out using the DYANA-P code to obtain transient evolutions of primary circuit flows and hotspot temperatures. Maximum temperatures are compared against the DSL and safety margins are established. Important input data and features of the primary circuit model are given in the following sections.

2.1.1. Input data

Pump characteristics obtained from the pump designer are shown in Fig. 3.

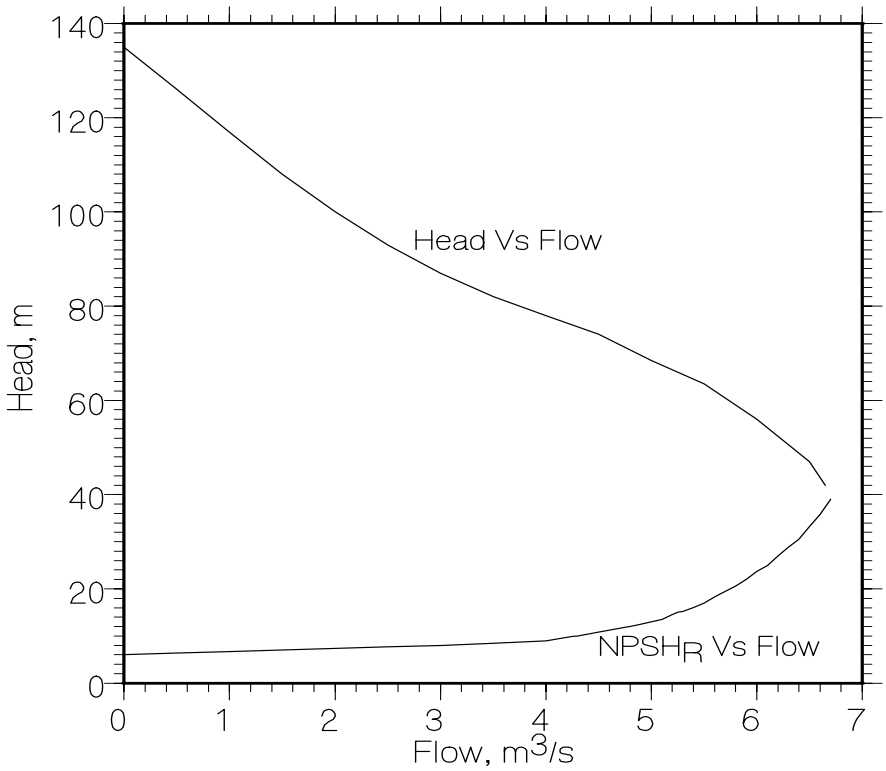

FIG. 3. PSP characteristics at 590 rpm.

T_{Na} and T_{Cl} are obtained by multiplying the nominal average central subassembly temperature rise (ΔT_{CSA}), sodium film drop (ΔT_{flm}) and cladding middle to outer surface drop (ΔT_{cl}) with appropriate hotspot factors as follows:

$$T_{Na} = T_{RI} + F_{SA}\,\Delta T_{CSA}$$

$$T_{Cl} = T_{Na} + f_{ch}\,\Delta T_{CSA} + f_{flm}\,\Delta T_{flm} + f_{cl}\,\Delta T_{cl}$$

Values of these hot spot factors are: $F_{SA} = 1.1672$, $f_{ch} = 1.2119$, $f_{flm} = 2.3920$ and $f_{cl} = 1.4213$. The same hotspot factors are also used for transient calculation. Pressure drop (in m of sodium column) values considered in the analysis at nominal power and flow conditions are: core pressure drop of 64 m, standpipe entry pressure drop of 2 m, primary pipe pressure drop of 2 m, grid plate pressure drop of 4.5 m and IHX pressure drop of 1.5 m. Pressure drop at the ruptured end of the primary pipe is modeled by using unity velocity head loss coefficient.

While the measurement time constant for P/Q, Lin P and ρ scram parameters is 0.05 s, it is 0.3 s for θ_{CSAM}. In addition to this, trip logic delay time is 0.2 s. Control rod drop time is 0.8 s. Plant design incorporates two diverse shutdown systems of worths 8000 pcm (Control

and Safety Rods or CSR) and 3000 pcm (Diverse Safety Rods or DSR). On a scram command, it is envisaged that both the shutdown systems are actuated and inserted into the core. However, safety criteria prescribes that it is needed to consider that only one shutdown system works and in the working system, the highest worth rod gets stuck. Accordingly, analysis has also been carried out for a negative reactivity insertion of 2000 pcm following scram.

2.1.2. Features of primary circuit model

Sodium flow in any segment is considered to be incompressible. The grid plate is considered as a plenum with single pressure. $NPSH_R$ vs flow curves for various speeds of PSP have been obtained by applying the affinity laws $Q \propto N$ and $NPSH_R \propto N^2$ on the nominal curve. The torque consumed by the impeller under cavitating condition is assumed to be equal to its value at the incipient cavitation point. The torque consumed by friction in the drive system at various points is obtained through an empirical correlation [4].

Pressure drop coefficients are taken as inversely proportional to $Re^{0.25}$. Kazimi and Carelli's correlation [5] is considered for calculating the film heat transfer coefficient from the cladding surface to the sodium. Bypass flow through the break is assumed to be not subjected to the grid plate resistance, whereas, the same is considered for core flow as shown in Fig. 4.

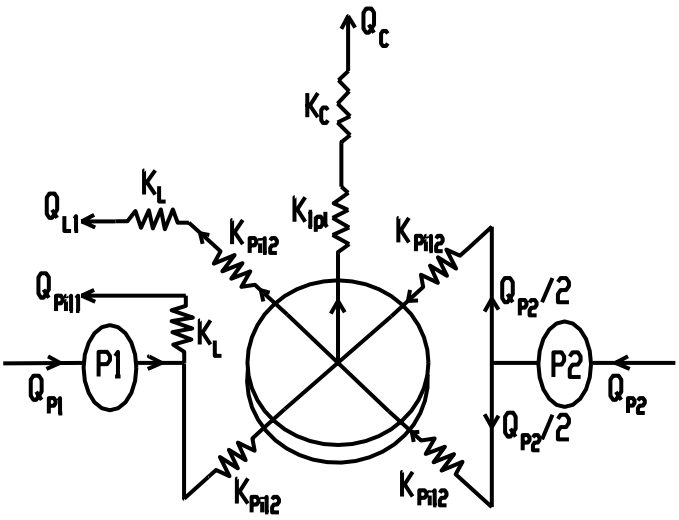

FIG. 4. Equivalent resistance model for the primary sodium circuit with the rupture at header end.

The detailed governing equations are shown in Sections 2.1.2.1. and 2.1.2.2.

2.1.2.1. Governing equations for 3-D primary circuit model

$$A_I \frac{dQ_{Il}}{dt} = (Z_{HP} - Z_{IE})\, \rho_{HP}\, g - (Z_{CP} - Z_{IO})\, \rho_{CP}\, g - K_I\, Q_{Il}\, |Q_{Il}| - g \int_{Z_{IE}}^{Z_{IO}} \rho_l dZ, \quad \text{for } l=1,2 \qquad (1, 2)$$

$$A_{PP1} \frac{dQ_{PP1}}{dt} = (Z_{CP} - Z_{IO})\, \rho_{CP}\, g - P_{J1} + D_{PP1} - K_{PPS}\, Q_{PP1}\, |Q_{PP1}| \qquad (3)$$

$$A_{Pi11} \frac{dQ_{Pi11}}{dt} = P_{J1} - (Z_{CP} - Z_{IO})\, \rho_{CP}\, g - (K_{pi11} + K_L)\, Q_{Pi11}\, |Q_{Pi11}| \qquad (4)$$

$$A_{Pi12} \frac{dQ_{Pi12}}{dt} = P_{J1} - \Delta P_{core} - (Z_{HP} - Z_{CT})\, \rho_{HP}\, g - (K_{Pi12} + K_{Ipl})\, QPi12\, |Q_{Pi12}| \qquad (5)$$

Where:

$$\Delta P_{core} = P_{CE} - P_{CT}$$

$$A_{L1} \frac{dQ_{L1}}{dt} = \Delta P_{core} + (Z_{HP} - Z_{CT})\, \rho_{HP}\, g - (Z_{CP} - Z_{IO}) \rho_{CP}\, g - (K_{L1} + K_L + K_{Ipl})\, Q_{L1}\, |Q_{L1}| \qquad (6)$$

$$A_{PP2} \frac{dQ_{PP2}}{dt} = (Z_{CP} - Z_{IO})\, \rho_{CP}\, g - (Z_{HP} - Z_{CT})\, \rho_{HP}\, g - \Delta P_{core} - K_P\, Q_{PP2}\, |Q_{PP2}| + D_{PP2} \qquad (7)$$

Where:

$$K_P = K_{PPS} + K_{Pi12} + K_{IPL}$$

$$K_{Pi12} = K_{L1}$$

Using the relation:

$$\frac{dQ_{PP1}}{dt} = \frac{dQ_{Pi11}}{dt} + \frac{dQ_{Pi12}}{dt} \qquad (8)$$

and

$$\sum_{r=1}^{10} n_r \frac{dQ_{cr}}{dt} = \frac{dQ_{Pi12}}{dt} + \frac{dQ_{PP2}}{dt} - \frac{dQ_{L1}}{dt} \qquad (9)$$

A detailed expression for ΔP_{core} and P_{J1} can be obtained from:

$$\rho_{HP}\, S_{HP}\, \frac{dZ_{HP}}{dt} = \left[\sum_{l=1}^{2}(Q_{PPl}-Q_{Il})\right] - (Q_{L1} - Q_{Pi11}) \tag{10}$$

$$\rho_{CP}\, S_{CP}\, \frac{dZ_{CP}}{dt} = \left[\sum_{l=1}^{2}(Q_{Il}-Q_{PPl})\right] + (Q_{L1} + Q_{Pi11}) \tag{11}$$

$$I_{PP}\, \frac{d\omega_{PPl}}{dt} = \beta_{PDrl} - \beta_{PPl}, \qquad \text{for } l=1,2 \tag{12, 13}$$

$$D_{PPl} = f1(Q_{PPl}, \omega_{PPl}), \qquad \text{for } l=1,2 \tag{14, 15}$$

$$\beta_{PPl}(tot) = \beta_{PPl}\,(impeller) + \beta_{PPl}(fri), \qquad \text{for } l=1,2$$

$$= f2(Q_{PPl}, \omega_{PPl}) + \beta_{PPl}\,(fri) \tag{16, 17}$$

Where f1 and f2 are the functions evaluating the homologous characteristics.
The empirical relation used for the friction in the pump drive system $\beta_{PP}\,(fri)$ other than the impeller is:

$$\frac{\beta_{PP}(fri)}{\beta_{PP}(tot)} = \begin{cases} 14.77\alpha, & |\alpha| \le 0.005 \\ 0.117 - 8.797\alpha, & 0.005 < |\alpha| \le 0.0117 \\ 0.023\alpha + 0.012, & |\alpha| > 0.0117 \end{cases} \tag{18}$$

For individual core zones we have:

$$A_{cr}\frac{dQ_{cr}}{dt} = \Delta P_{core} - K_{cr}\, Q_{cr}\, |Q_{cr}| - g\int_{Z_{CE}}^{Z_{CT}} \rho_r\, dh, \;\; for\ r = 1\ to\ 10 \tag{19,…..,28}$$

$$\sum_{r=1}^{10} n_r\, Q_{cr} = \left(\sum_{l=1}^{2} Q_{PPl}\right) - Q_{L1} - Q_{Pi11} \tag{29}$$

2.1.2.2. Numerical solution procedure

The numerical solution of the primary circuit is carried out in two stages. In the first stage, IHX flow, pump flows, pump speeds and the sodium levels are calculated utilizing a standard ordinary differential equation solver based on the Hamming's predictor-corrector method.

Using the total core flow obtained from the first stage as input for the second stage, core zone equations are solved. For this, a semi-implicit finite differencing and linearization technique is applied to the governing equations for the individual core zone flows [4]. Also by utilizing the fact that the change in the total core flow (δQRI) computed in the first stage described above is equal to the total of the changes in the individual zone flows, the calculation of the current time individual zone flows are obtained as follows:

$$\Delta P_{core} = \left[\frac{\delta Q_{RIj} + \sum_{r=1}^{10} n_r a_r b_r}{\sum_{r=1}^{10} n_r a_r} \right] \tag{30}$$

$$Q_{crj} = Q_{cr\,j-1} + \Delta P_{core}\, a_r - a_r b_r, \quad .for\ r=1\ to\ 10 \tag{31}$$

Where:

$\delta t \quad = t_j - t_{j-1}$

$$\delta Q_{RIj} = \left[\sum_{l=1}^{2} Q_{PPlj} \right] - \left(Q_{L1j} + Q_{Pi1j} \right) - Q_{RIj-1}$$

$$a_r = \frac{1}{\frac{A_{cr}}{\delta t} + K_{cr} \left| Q_{crj-1} \right|}$$

$$b_r = K_{cr} \left| Q_{crj-1} \right| Q_{crj-1} + \overline{d_r}$$

$$\overline{d_r} = g \int_{Z_{CE}}^{Z_{CT}} \rho_r \, dh$$

LEGEND

Nomenclature		Subscripts	
A	flow inertial coefficient, m^{-1}	CE	core inlet
D	pump developed head, Pa	CP	cold pool
I	moment of inertia, kg m^2	CT	core top
K	pressure drop coefficient, Pa / (kg s^{-1})^2	HP	hot pool
P	pressure, Pa	I	Intermediate Heat Exchanger (IHX)
Q	mass flow rate, kg s^{-1}	IE	IHX inlet
S	area of cross section, m^2	IO	IHX outlet
Z	elevation, m	IPL	Inlet Plenum
g	acceleration due to gravity, m s^{-1}	J	junction
n	number of SA in a radial group	L	leak flow
t	time, s	PDr	primary pump drive
α	normalised pump speed	PE	primary pump inlet
β	torque, N m	PP	primary pump
ρ	density, kg m^{-3}	PPS	primary pump suction
		Pi	primary pipe
		RI	reactor inlet
		c	core channel

2.1.3. Results

The evolution of NPSH of pump, reactor power and reactivity, primary circuit flows and temperatures during DEGR of a primary pipe near the header end are shown in Figs 5 - 8.

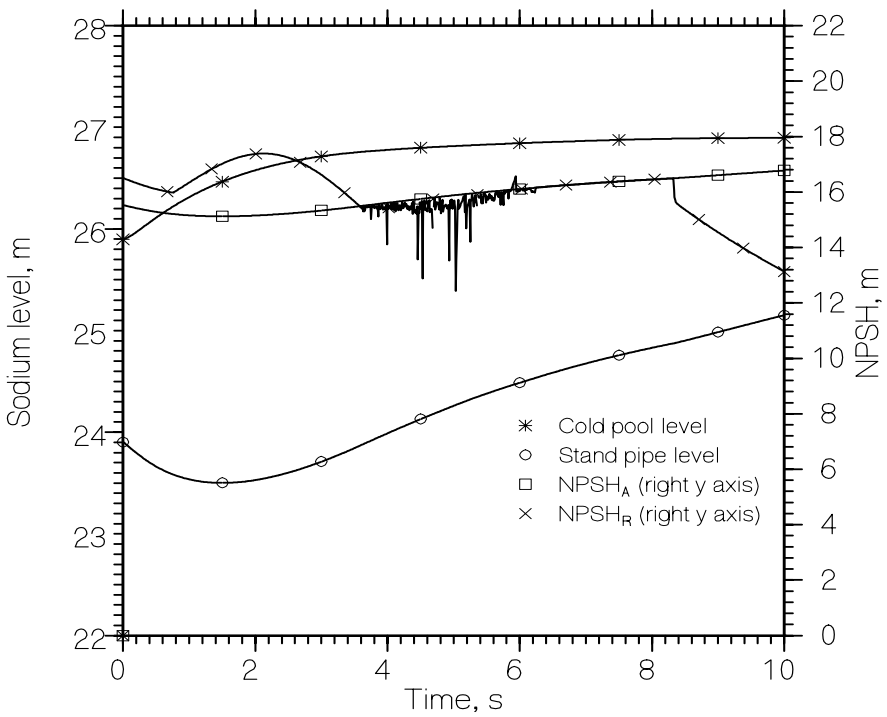

FIG. 5. Evolution of sodium levels and NPSH.

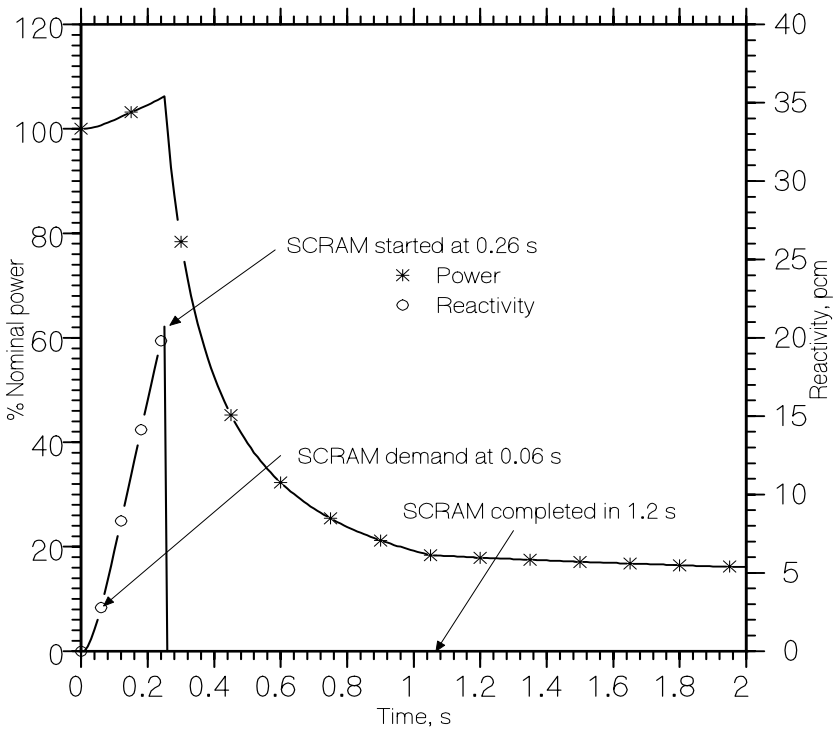

FIG. 6. Evolution of power and reactivity.

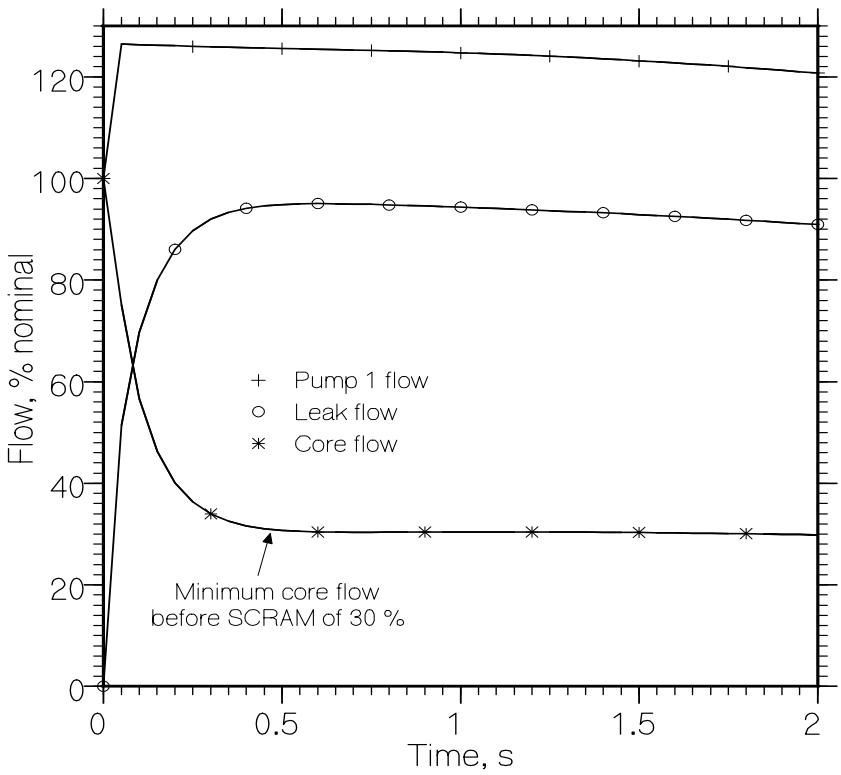

FIG. 7. Evolution of sodium flows.

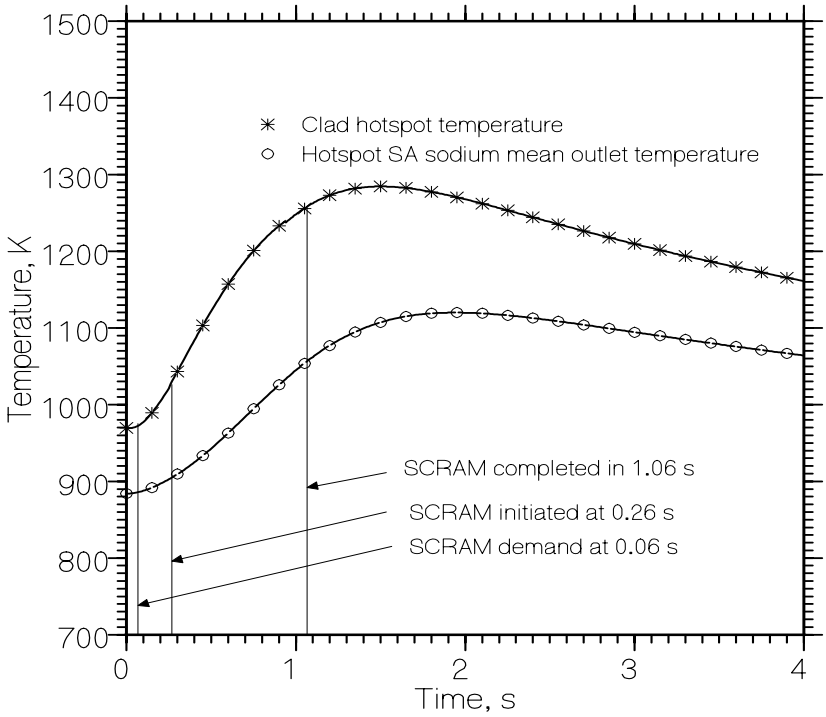

FIG. 8. Evolution of temperatures.

The scram parameters, their appearance time, and maximum values of T_{Cl} and T_{Na} reached during the event are given in Table 1.

TABLE 1. MAXIMUM VALUES OF TEMPERATURES REACHED DURING THE EVENT

Scram parameter and its demanded time (s)	Maximum CHST, K		Maximum SASHST, K	
	DSR alone actuated	Both CSR and DSR actuated	DSR alone actuated	Both CSR and DSR actuated
P/Q at 0.06	1284	1267	1120	1107
Reactivity at 0.2	1302	1286	1132	1120
Lin P at 0.45	1333	1323	1154	1144
θ_{CSAM} at 1.1	1406	1398	1209	1201

CSR: Control and Safety Rods
DSR: Diverse Safety Rods

The pumps start cavitating within 0.05 s and their flows increase to 126% instantaneously. Core flow reaches a minimum value of 30% of nominal at 0.7 s. The power to flow ratio scram parameter crosses its threshold (1.1) at 0.06 s. However, due to the trip logic delay time, maximum reactivity and power of 21 pcm and 106% respectively are reached at 0.25 s before they are rapidly reduced by scram.

PSP speed reduction following scram causes $NPSH_R$ to fall and it becomes equal to $NPSH_A$ at 3.4 s. $NPSH_R$ follows $NPSH_A$ up to 8.3 s and then falls sharply. There would not be cavitation of the pump beyond this time. The PSP speed and flow at this time are 57% and 95% respectively.

Due to this envisaged condition of the PSP operating under cavitating conditions for a short duration following such an event, testing of a 1:2.75 scaled model pump under severe cavitation (80% head drop) condition has been carried out. The pump was operated for about 10 minutes. No flow fluctuation or vapour locking was observed.

Similar analyses have been carried out at various initial power conditions between 15% and 100% also. It has been seen that at least two scram parameters are available for the event occurring at all initial power conditions. At power levels less than 40%, fuel and coolant DSL is not be crossed even without any safety actions.

Analysis has also been carried out for the DEGR at the grid plate end of pipe. Reduction in the resistance of flow passage from grid plate to ruptured end causes leakage flow through that path to increase. However, increase in flow resistance in the path from pump header to ruptured end causes flow in that path to decrease and flow through the other unruptured pipe to increase. As a consequence of these two effects core flow falls to a minimum value (before scram) of 31%, which is better than the rupture at the header end.

An iterative algorithm for calculating the steady state values of primary flows during a pipe rupture event occurring at various operating speeds of PSP has also been developed separately. The final steady state values of flows calculated using this algorithm differ from those estimated using the transient calculation procedure in DYANA-P code by only a maximum of 1%.

2.2. Investigation of flow redistribution in the core

A three Dimensional (3-D) hydraulic analysis of the grid plate under pipe rupture conditions has been carried out using the CFD code PHOENICS to investigate the possible redistribution in the core flow among various SA and to study the influence of a calming zone on the bypass leak flow.

Under pipe rupture conditions, the flow rates of sodium through four pipes supplying sodium to the grid plate are different from each other. Hence, there is no symmetry in the angular direction for the ruptured state of the grid plate. Therefore, a full 360° model has been considered for this study. Grid pattern and boundary conditions adopted are shown in Figs 9 and 10.

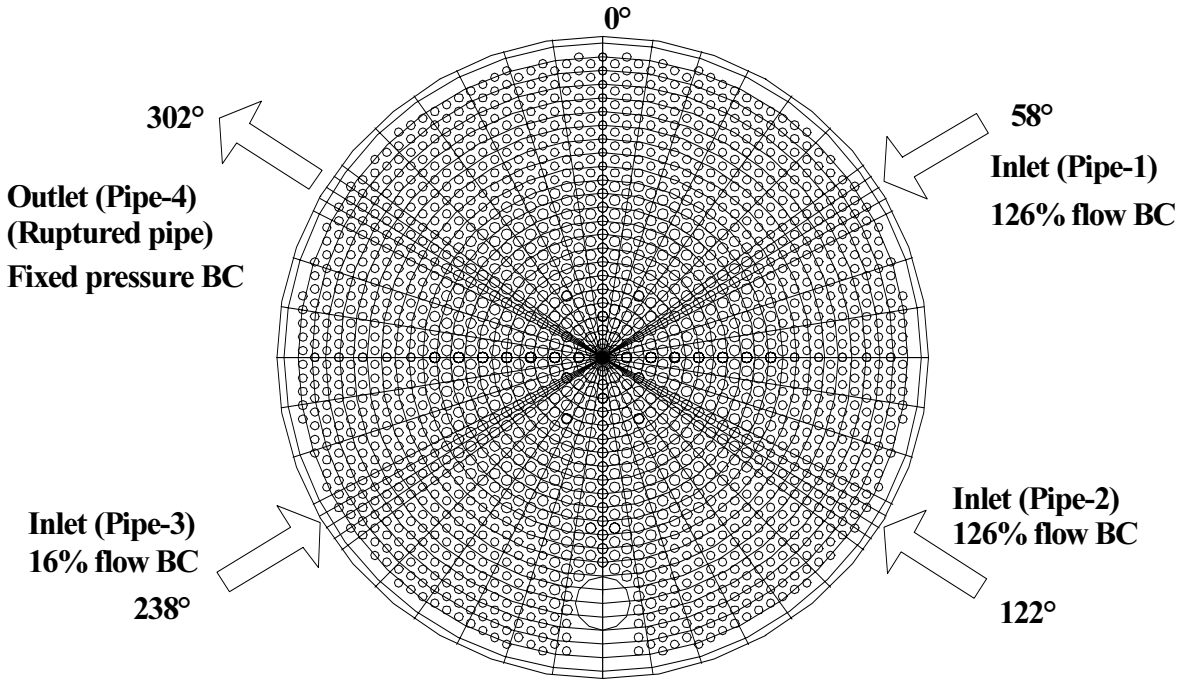

FIG. 9. Grid plate 3-D model (plan).

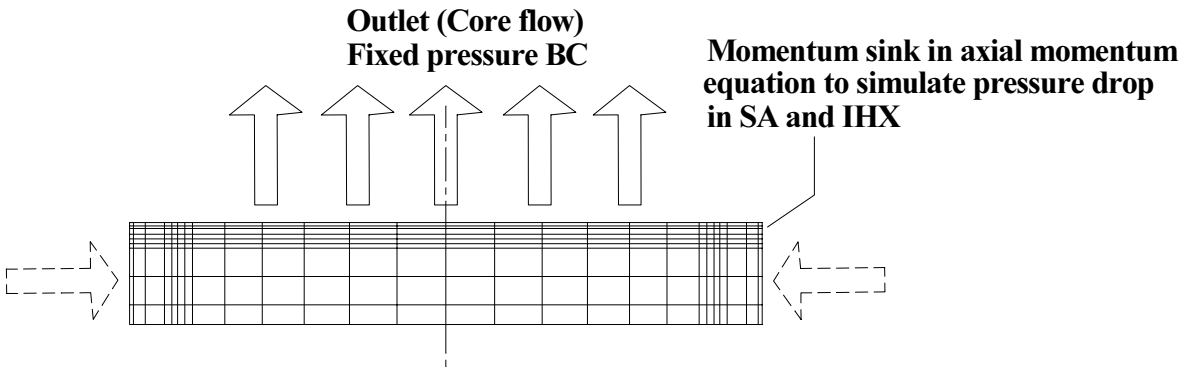

FIG. 10. Grid plate 3-D model (elevation).

The presence of sleeves in the grid plate has been represented by porosities in various coordinate directions. Pressure drop in the radial and angular directions is modeled using a correlation reported in literature [6] for cross flow over a bank of sleeves. Pressure drop coefficients for various SA are calculated from the core pressure drop of 64 m of sodium for the nominal flows through them. Pressure drop on the bypass flow through the ruptured pipe is represented as a sum of pipe resistance (rupture considered at the header end of pipe) and

the resistance due to free expansion to the cold pool (k = 1). Grid pattern considered for the study in the (r - θ - Z) directions is 24×52×8. The K-∈ turbulence model has also been used.

A flow rate of 126% of nominal (PSP flow under cavitating conditions) has been considered through pipe-1 and pipe-2 supplying the grid plate. A flow rate of 16% of nominal is considered to enter the grid plate through pipe-3. Pipe-4 is ruptured. These data correspond to the final steady state condition results (without PSP speed reduction) of 1-D analysis. The resulting velocity field in the grid plate is shown in Fig. 11.

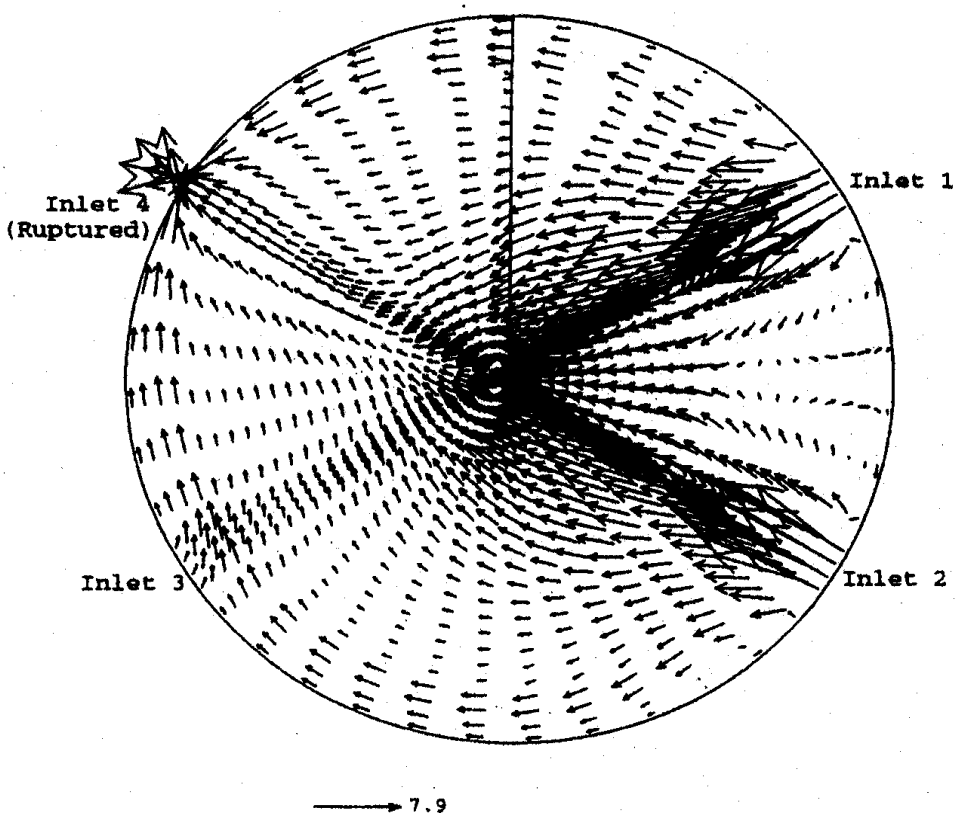

FIG. 11. Velocity profile within the grid plate under pipe rupture condition in the circumferential plane of the inlet pipes.

Core flow has been estimated to be 33% of nominal. The rest of the flow bypasses through the ruptured pipe. The core flow rate estimated by 1-D calculation is 31%. It can be seen from Fig. 10 that the sodium in the grid plate flows towards the ruptured pipe along the calming zone without being subject to the resistance in the sleeves. Thus, it can be concluded that it is a reasonable approach to neglect inlet plenum pressure drop on the by pass leak flow and considering the same in series with core flow in the 1-D study. Mean velocities within core SA at various radial and angular locations are shown in Fig. 12.

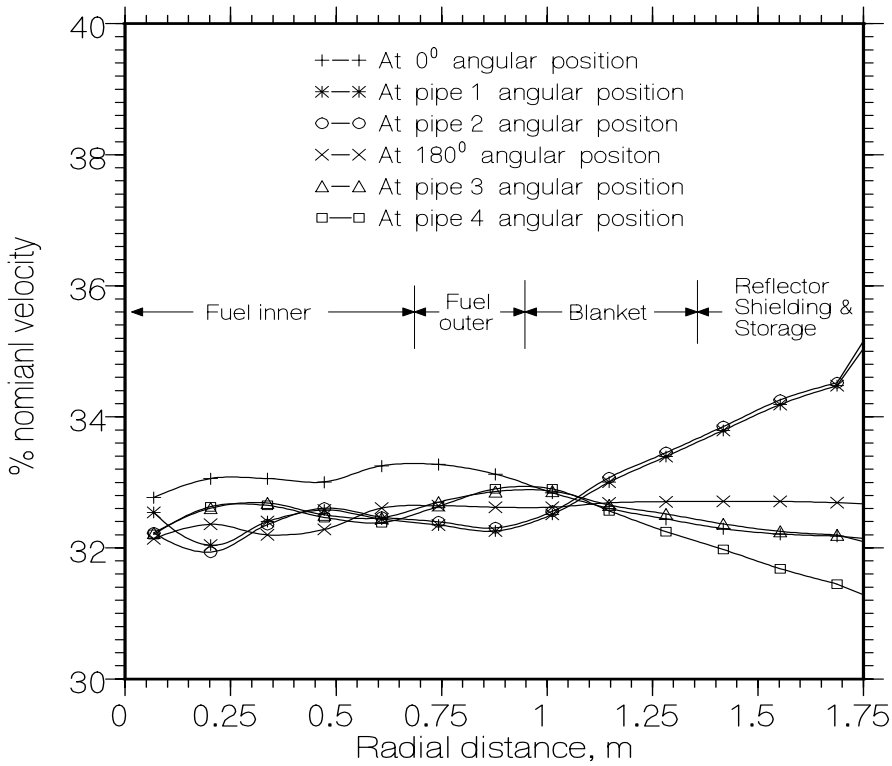

FIG. 12. Mean velocities within SA at various radial and circumferential locations under pipe ruptured conditions.

It can be seen that maximum variation in the flow through various SA from the mean core flow value is of the order of +0.5% to -1% in the fuel region. The deviation is more in the peripheral SA (reflector and shielding), where sodium flow itself is very small. Thus, it can be concluded that there is no significant flow redistribution through core SA under pipe rupture condition, which is also in agreement with experimental observations made in a 1/3 scale air model test.

2.2. Investigations on void formation

The computer code SWEPT [7] is used for this analysis. SWEPT is a system pressure wave propagation analysis code adequate for the analysis of short-term transients in a closed network due to many engineering issues such as sudden valve closure, sodium-water reactions, pump start up. The primary sodium circuit is modeled as a closed piping network with hot pool, cold pool, and PSP forming pipe junctions. Sodium is assumed to be isothermal at the average temperature of 745 K. Pipe rupture at the header end is analyzed here.

Following pipe rupture, the pump flow increases due to reduced flow resistance. The flow through core reduces and more flow is diverted towards the leakage point as flow resistance across the core is higher than that of the ruptured pipe. Following the breach in the pipe, the primary system is suddenly exposed to low pressure at the leakage point. This low-pressure wave travels both upstream and downstream pipes, causing pressure fluctuations at various system components. Fig. 13 shows the variation of pressure at the SA inlet, middle point and at the exit.

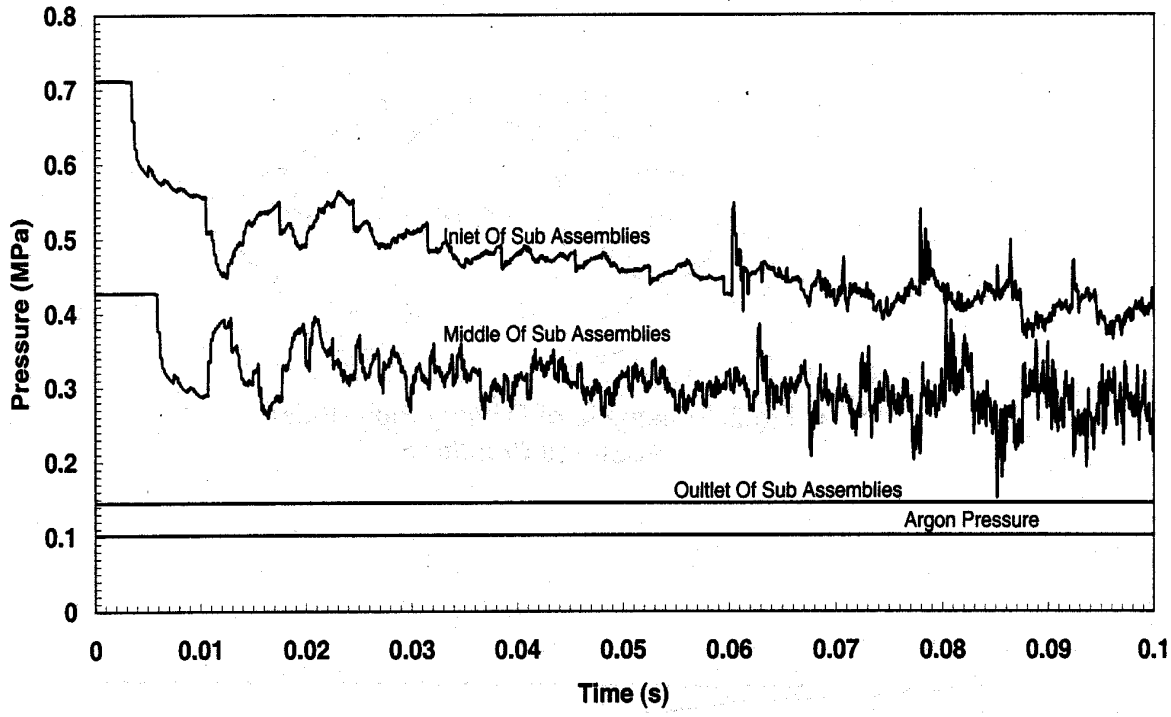

FIG. 13. Evolution of pressure in the SA during pipe rupture event.

As core flow reduces, pressure drop across the core reduces. Pressure fluctuations are seen only for 1 s. As and when the pump flow, leakage flow and core flow stabilizes, pressure fluctuation also subsides. It can be seen that there is no void formation in any SA since pressure at all points in the system stays above the vapour pressure of sodium at the operating temperature (278 Pa). Core flow estimates also compare well with the incompressible flow model estimates.

3. CONCLUSIONS

Even though the structural integrity of the pipe is ensured under all the conditions with a comfortable factor of safety, DEGR of one of the four primary pipes is considered as a Category 4 event. 1-D thermal hydraulic analysis predicts a minimum core flow of 30% during the transient. Maximum T_{Cl} and T_{Na} are 1302 K and 1132 K respectively, which respect the specified temperature limits. 3-D steady state hydraulic analysis of grid plate predicts a final steady state core flow of 33%, which matches well with the 1-D prediction of 31%. The 3-D study also concludes that there is no significant flow redistribution among various SA following this event. This study also confirms the influence of calming zone in the grid plate on core flow and validates the approach of neglecting inlet plenum resistance on bypass leak flow and considering the same in series with core flow in the 1-D study. Pressure transient analysis of this event has also found that there is no void formation at any SA during the transient. Pressure fluctuations are seen only for 1 s following the breach. Final steady state values of flows estimated using 3-D hydraulics of the grid plate, the SWEPT code, and an independent final steady state algorithm are all in good agreement with that of the 1-D estimate.

REFERENCES

[1] NATESAN, K., et al., "Thermal Hydraulic Analysis of Primary Pump Pipe Rupture Event in PFBR", Proc 8th Intl Conf on Nuclear Engineering (ICONE-8), 2000, Baltimore, MD, USA, American Society of Mechanical Engineers (ASME), New York (2000).

[2] NATESAN, K., et al., "3D Hydraulic Analysis of Grid Plate Under Pipe Ruptured Conditions in PFBR", paper presented in the 27th National Conference on Fluid Mechanics and Fluid Power (FMFP), Palghat, India, 2000.

[3] SHAMSHEER, et al., "Pressure Transient Analysis for an Instantaneous Guillotine Rupture of a Pipe", paper presented in the 27th National Conference on Fluid Mechanics and Fluid Power (FMFP), Palghat, India, 2000.

[4] AGARWAL, A.K., KHATIB RAHBAR, M., "Dynamic simulation of LMFBR Systems", Atomic Energy Review, Vol. 18, No. 2, pp. 329-552 (1980).

[5] KAZIMI, M.S., CARELLI, M.D., Heat Transfer Correlations for Analysis of CRBRP Assemblies, ibid.

[6] ZUKAUSKAS, A., ULINSKAS, R., Heat Exchanger Design Handbook, Vol. 2, Hemisphere Publishing Corporation (1983).

[7] RAJPUT, A.K., "Pressure Transient Resulting From Sodium-Water Reaction Following a Large Leak in LMFBR Steam Generator", paper presented in the IAEA Specialists' Meeting on Theoretical and Experimental Work on LMFBR Steam Generator Integrity and Reliability with a Particular Reference to Leak Development and Detection, Hague, Netherlands, 1983.

ANALYSIS OF PRIMARY PIPE BREAK FOR THE KOREAN ADVANCED LIQUID METAL REACTOR (KALIMER)

H.Y. JEONG, W.P. CHANG, Y.B. LEE, D. HAHN
Korea Atomic Energy Research Institute (KAERI), Daejon, Republic of Korea

Abstract

A postulated break in the primary pump discharge pipe is analyzed to assure the inherent safety of the Korean Advanced Liquid Metal Reactor (KALIMER), a pool-type liquid metal-cooled reactor generating 392 MWth of power in the core. The main concern of the analysis is the amount of increase in the fuel and the coolant temperatures. The stabilization of the transient due to reactivity feedback is also important. In the present analysis, it is assumed that one of the four pipes connecting the pump discharge to the core inlet plenum is broken. The break is located 3.7 m below the pump outlet and the diameter of the break is 0.4 m. It is also assumed that the reactor is not scrammed after the initiation of the break, therefore, the pumps keep on running during the accident. The analysis is performed with the SSC-K code, which was developed for the analysis of the transient system response of a pool-type reactor. As soon as the break occurs, the core flow decreases drastically to 65% of full flow in the base case. A more conservative case is also analyzed, in which the core flow is reduced artificially to 50% full flow. The reactor power stabilizes by the reactivity feedback effects in about 10 minutes. The increase of the fuel and coolant temperatures due to the sudden reduction of the core flow are also mitigated with a large margin to coolant saturation temperature. The gas expansion module plays an important role providing the dominant reactivity feedback when the core flow is reduced to less than 50% full power. It is evident from these results that both a sufficient subcooling margin of more than 400 K and a stable system response are maintained in the KALIMER design during the primary pipe break accident, which guarantees the inherent safety of KALIMER against a pipe break.

1. INTRODUCTION

The inherent safety characteristic against postulated events is the most remarkable superiority of a liquid metal cooled reactor (LMR) to other type of reactors. One of the major threats to the safety of LMR is a loss of flow event accompanied a failure of reactor shutdown systems. This situation is usually referred to as an unprotected loss of flow (ULOF). The inherent safety of the Korean Advanced Liquid Metal Reactor (KALIMER) during the ULOF [1] has been assessed for the situation of all pump trips followed by coastdown. It was assumed that the decay heat is removed by four intermediate heat exchangers (IHXs) and the safety grade system of passive safety decay heat removal system (PSDRS). The results showed that the power was stabilized by the reactivity feedback of the system even though the effect of the gas expansion module (GEM) was not taken into account.

Other possible mechanisms of loss of flow include the seizure of one or more pumps and the rupture of a primary pipe [2]. In a loss-of-flow-type accident, the power-to-flow ratio is the key parameter that determines the consequences of the accident. Thus, the initial pump behavior plays an important role for the plant safety when the pump is still running. On the other hand, a more severe mismatch between the power and flow is possible in a pump seizure or a pipe break accident because the core flow drops more abruptly. Therefore, it is required to analyze the loss of flow due to the break of the inlet pipe connecting the pump discharge and the core inlet plenum.

The present study analyzes a postulated break in the primary pump discharge pipe to assure the inherent safety of KALIMER. KALIMER is a pool-type liquid metal sodium cooled fast reactor plant. The main concern of the accident is the amount of subcooling margin reduction, i.e., the degree of increase in the fuel and the coolant temperatures. The stabilization of power associated with reactivity feedback is also an important aspect of the accident. The analysis is performed with the SSC-K code, which was developed on the basis of the SSC-L code for the

analysis of the transient system response. Actually, the possibility of sodium loss by pipe break is very low and the large thermal capacity of the pool makes system transients slower.

The core design and the heat transfer system of KALIMER are summarized in the following section. In addition, the safety philosophy of KALIMER is introduced. Next, main features of SSC-K code modeling are described. The analysis method, results of the pipe break and conclusions follow.

2. KALIMER DESIGN

KALIMER is a pool-type liquid metal-cooled reactor that has four intermediate heat exchangers (IHXs), four electromagnetic-type primary coolant pumps. In the KALIMER conceptual design [3], focus has been on the nuclear steam supply system (NSSS) and essential BOP (Balance of Plant) systems. The ultimate objectives for the KALIMER conceptual design are to make it safer, more economical, more resistant to nuclear proliferation, and yield less impact on the environment. Figure 1 represents the schematic of the KALIMER NSSS.

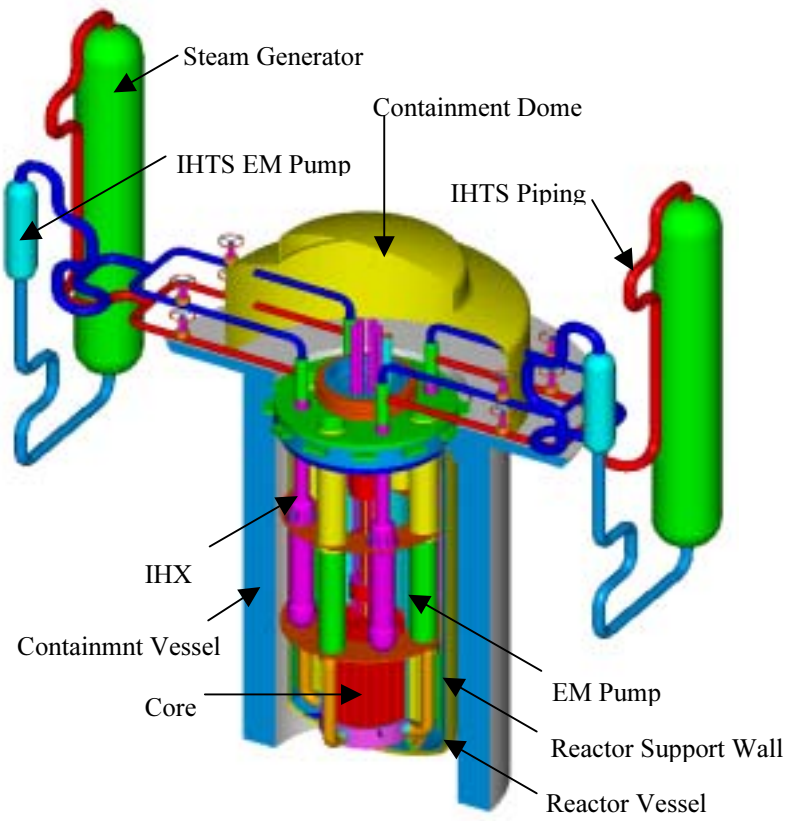

FIG. 1. Schematic of KALIMER system.

KALIMER has a net electrical rating of 150 MWe and the required core thermal output is 392 MWth. The plant system design parameters are based on the electrical rating and core thermal power.

2.1. KALIMER core design

The core adopts a heterogeneous configuration in the radial direction as shown in Fig. 2.

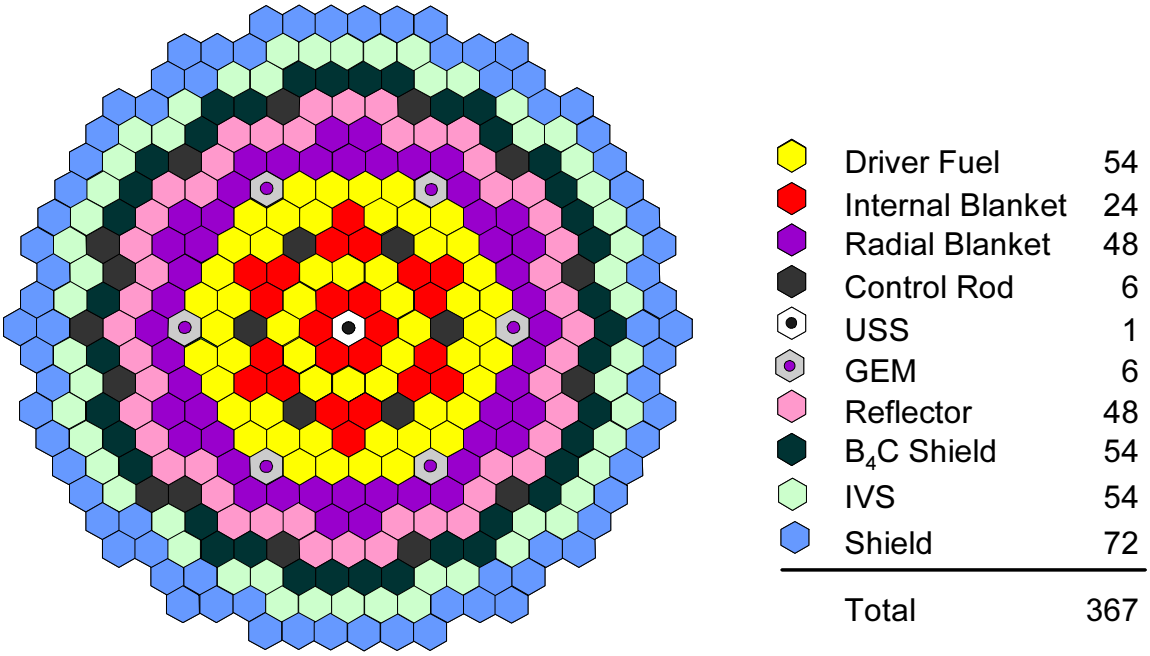

FIG. 2. Breakeven core configuration.

The core consists of driver fuel assemblies, internal blanket assemblies, radial blanket assemblies, control rods, ultimate shutdown system (USS) assembly, gas expansion modules (GEMs), reflector assemblies, B_4C shield assemblies, shield assemblies, and in-vessel storages (IVSs). There are no upper or lower axial blankets surrounding the core. A fission gas plenum is located above the fuel slug and sodium bond. The bottom of each fuel pin is a solid rod end plug for axial shielding. The reflector assemblies contain solid Inconel-600 rods. The control assemblies use a sliding bundle and a dashpot assembly within the same outer assembly structure as the other assembly types.

The reactivity and power control rod system consists of two identical clusters. Each control rod unit consists of an array of tubes containing B_4C to provide a gravity-driven rod drop and a powered drive-in. Gas expansion modules (GEMs) located at the periphery of the active core are passive reactivity feedback assemblies that insert negative reactivity into the core during the loss of flow events.

The ultimate shutdown system (USS) located at the center of the core is a self-actuated shutdown system. The USS is actuated passively when the temperature of the primary sodium reaches the Curie point. The USS drops neutron absorbers by gravity as a means to bring the reactor to cold critical conditions in the event of a complete failure of the normal scram system and after the inherent reactivity feedbacks have brought the core to a safe, but critical state at an elevated temperature.

2.2. Heat transport systems

The primary heat transport system (PHTS) mainly delivers the core heat to the intermediate heat transport system (IHTS) and IHTS works as the intermediate system between PHTS and the steam generator system (SGS) where the heat is converted to steam. The steam generator is a once-through type with helical tube generating superheated steam. The reactor core, the primary coolant pumps and the intermediate heat exchangers (IHXs) are immersed in a large volume of sodium in the primary pool as shown in Fig. 3.

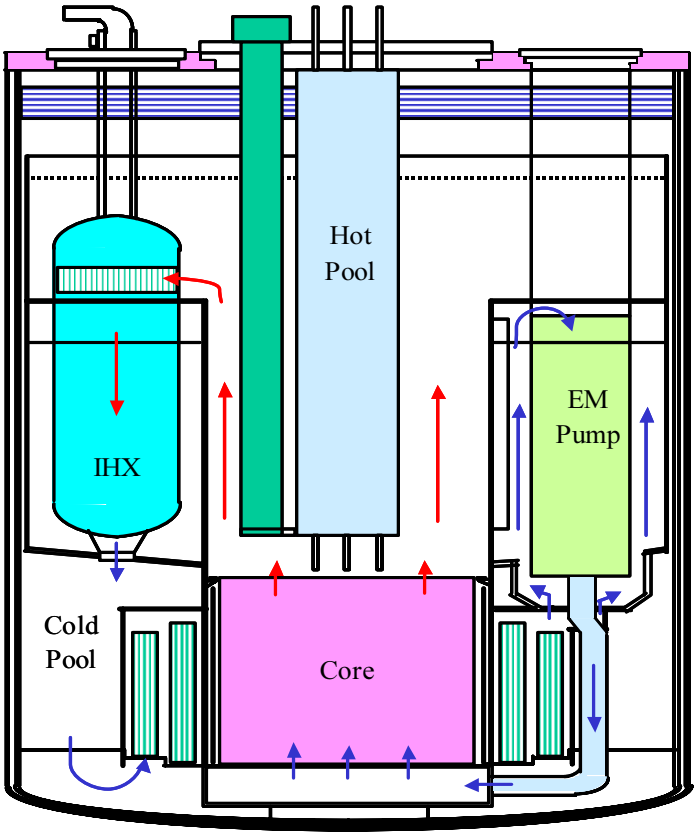

FIG. 3. Schematic of primary heat transport system.

A vertical wall, called reactor baffle, divides the primary pool into hot and cold pools. The large thermal inertia provided by the large pool enhances the plant safety. The IHTS consists of two loops and each loop has its own steam generator and related systems.

The reactor structures, consisting mainly of the reactor vessel, containment vessel, reactor head, reactor internal structures, and reactor support structure, comprise a reactor coolant system and connected systems. The reactor vessel is the container and the support for the reactor core, primary sodium, and reactor internal structures. The containment vessel assures that the reactor core will not be uncovered and core cooling can be accomplished even if the reactor vessel leaks.

The system reliability is improved by using electro-magnetic (EM) pumps that have no moving parts for both of the primary and intermediate coolant pumping. The flow inertia

device compensates for the low momentum inertia of the EM pump. The device stores rotating kinetic energy when the EM pump runs normally, but supplies electricity to the EM pump by converting the stored rotating kinetic energy as to electricity at a pump power supply failure. The primary EM pumps transfer the cold sodium in the cold pool into the core through the inlet plenum. Elevation differences feed the hot sodium in the hot pool into the inlet of the IHXs, past the tube bundle and into the cold pool. The only primary piping is from the discharge side of the pump to the core inlet plenum.

3. KALIMER SAFETY PHILOSOPY

KALIMER is designed in accordance with a defense-in-depth safety philosophy that utilizes multiple fission product barriers to prevent the release of radioactivity to the environment, and multiple levels of safety to protect these barriers and reduce the consequences of their failure. The fuel pin cladding, the primary vessel boundary, and the containment provides the multiple barriers of KALIMER. Multiple levels of safety are provided by the basic plant design that guarantees the reliability of the normal operation, high resistance to external challenges, protection against anticipated transients, mitigation of accidents, and prevention of core damage and large radioactivity release.

To achieve the design objective of safety, efforts are devoted to the simplicity in all aspects of design, construction, operation and maintenance. It is also emphasized to utilize highly reliable reactor protection systems and built-in safety features like the GEMs. Maintaining the core power reactivity coefficient negative during all modes of plant status is crucial for plant safety. The negative temperature and power reactivity coefficients limit the power increase during the transients.

The use of passive mechanism has, in general, superior reliability in mitigating an accident. In addition, long grace time during an accident provides improved reliability of the plant safety function and more flexibility in coping with an accident. The safety systems of KALIMER are based on the enhanced safety features, such as using metallic fuel, USS, GEM, and PSDRS, which improve the reliability of KALIMER safety functions. The large thermal capacity of the pool provides more time to cope with abnormal events and higher probability to terminate the abnormal events before their entering into accidents. KALIMER accommodates unprotected anticipated transients without scram (ATWS) events without operator action, and without the support of active shutdown, shutdown heat removal, or any automatic system, without damage to the plant and without jeopardizing public safety. Neither operator action, nor offsite support is required for at least three days without violating core protection limits during an accident.

The KALIMER design highly emphasizes inherent safety, which maintains the core power reactivity coefficient negative during all modes of plant status and under accidental conditions as well. The reactivity feedback mechanisms consist of Doppler, thermal expansion of the fuel and coolant, thermal bowing of the core, thermal expansion of the core structure and core support structure, and thermal expansion of the control rod driveline. These effects result from either the physics laws, or both the physics laws and core design.

Sufficient margins needs to be imposed in the fuel and core design for investment protection and for reducing the core damage probability. Emphasis should be given not only to safety grade decay heat removal, but also to non-safety grade decay heat removal. The negative power reactivity coefficient is also crucial in preventing core damage. The CDF of KALIMER is aimed to be lower than that of currently planned LWR. For prevention of large radioactivity releases the containment is the last barrier. The KALIMER containment is

designed to assure that the release rate targets considering the fuel source characteristics. The large dose release rate limit is less than 10^{-7} per reactor year.

The ultimate mechanism to ensure public protection from the consequences of postulated ATWS are the inherent negative reactivity feedback when the reactor system temperature increases, and the heat removal function of PSDRS. The analyses of the selected ATWS are conducted to assure the effectiveness of inherent safety features in the KALIMER design. The events considered are: Unprotected control rod withdrawal (UTOP), Unprotected loss of heat sink (ULOHS), Unprotected loss of primary flow (ULOF), and combinations of those events.

4. THE SSC-K CODE AND MODELS

The SSC-K code [4] has been developed by KAERI for the analysis of system behaviour during transients. The SSC-K code features a multiple-channel core representation coupled with a point kinetics model with reactivity feedback. It provides a detailed, one-dimensional thermal-hydraulic simulation of the primary and secondary sodium coolant circuits, as well as the balance-of-plant steam/water circuit.

The SSC-K code was used for assessment of the inherent safety features in the KALIMER conceptual design. The SSC-K aims not only at extensive analysis capability and flexibility, but also at sufficiently fast running to simulate long transients in a reasonable amount of computer time. The code is capable of handling a wide range of transients, including normal operational transients, shutdown heat removal transients, and hypothetical ATWS events. The SSC-K code is currently used as the main tool for system transient analysis in the KALIMER development.

The SSC-K is based on the methods and models of SSC-L [5], which was originally developed to analyze loop-type liquid metal reactor transients. Because of the inherent difference between the pool and loop designs, major modification to the SSC-L has been made for the analysis of the thermal hydraulic behaviour within a pool-type reactor. Now, the SSC-K code has the capability to analyze both, loop and pool type liquid metal cooled reactors.

Additional developments in the SSC-K code include models for reactivity feedback effects for the metallic fuel, and the PSDRS. Also a two dimensional hot pool model has been build into SSC-K for analyzing the thermal stratification phenomenon in the hot pool. The control system model in SSC-K is flexible enough to handle any control system. For code maintenance and readability, SSC-K was converted to FORTRAN 90 free form and the use of standard FORTRAN 90 has enhanced code portability.

The SSC-K code simulates multiple heat transport system modules and associated controllers. A full plant model for SSC-K is used to represent KALIMER as shown in Fig. 4, in which several major components are represented. The PHTS is represented by the flow passage in the pool, the primary pump, and the shell side of the IHX. The IHTS consists of the tube side of the IHX, the connecting pipes, the shell side of the steam generator (SG), and the intermediate pump.

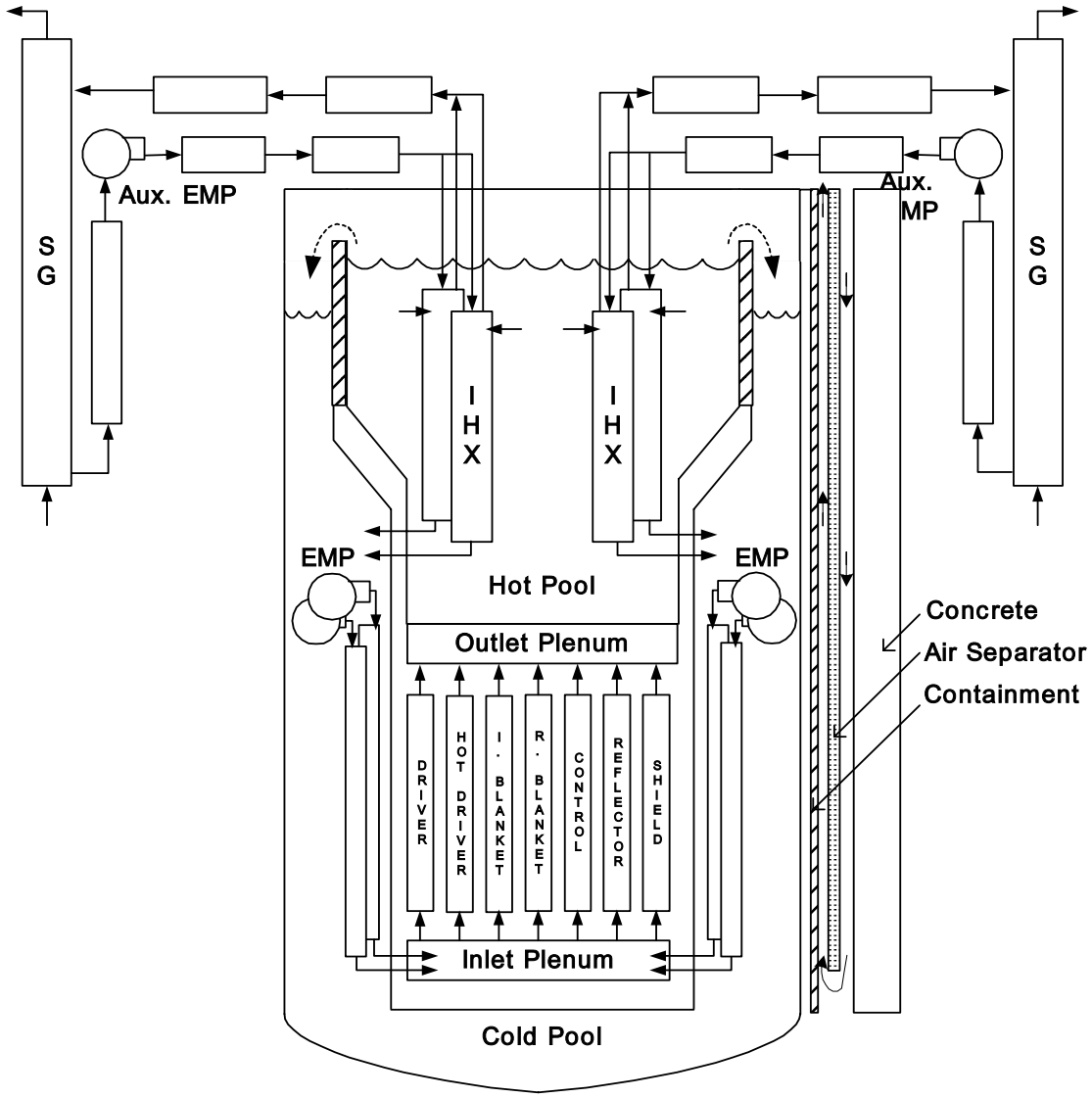

FIG. 4. SSC-K modeling for KALIMER plant.

4.1. Pool thermal-hydraulic model

A major modification of SSC-K has been made in order to analyze the thermal hydraulic behaviour within the pool. In KALIMER, both the hot and cold pools have free surfaces and there is direct mixing of the coolant with these open pools prior to entering the next component. Therefore, at least two different flows will have to be modeled to characterize the coolant dynamics of the primary system. The first flow from the pump to the hot pool through the core is determined by the pump head and losses in the flow passages.

The second flow from IHX to the cold pool is determined by the level difference between the two pools as well as the gravity gain in the IHX, which could be significant for low-flow conditions.

For the pump flow we have:

$$\frac{dW_p(k)}{dt}\sum_p \frac{L(k)}{A(k)} = P_{Po}(k) - P_{Rin} - \sum_p \Delta P_{f,g}(k), \qquad k = 1,\cdots,N_{path} \tag{1}$$

In above equation, the pump exit pressure, P_{Po}, is obtained from

$$P_{Po} = P_{Pin} + \rho_{Pin} g\, H \tag{2}$$

where H is the pump head, obtained from the pump characteristics. The pump inlet pressure can be obtained by calculating the elevation head for the cold pool sodium level.

For the IHX flow we have:

$$\frac{dW_{1X}(k)}{dt}\sum_X \frac{L(k)}{A(k)} = P_{Xin} - P_{Xo} - \sum_X \Delta P_{f,g}(k), \qquad k = 1,\cdots,N_{path} \tag{3}$$

The IHX inlet and exit pressures, P_{Xin} and P_{Xo}, are obtained from static balance as

$$P_{Xin} = P_{gas} + \rho_h g(Z_{HP} - Z_{Xin}) \tag{4}$$

$$P_{Xo} = P_{gas} + \rho_c g(Z_{CP} - Z_{Xo}) \tag{5}$$

Equations (1) and (3) are solved as coupled differential equations with the equations derived for the mass and momentum conservation at the core inlet plenum.

When reactor scram occurs, the heat generation is reduced almost instantaneously, while the coolant flow rate follows the pump coastdown. This can result in a situation where the core flow is colder than the bulk hot pool sodium. This temperature difference leads to stratification, when the flow momentum is not large enough to overcome the negative buoyancy force. The two-zone model employed in the original SSC-L code has been modified. The hot pool is divided into two perfectly mixing zones determined by the maximum penetration distance of the core flow. The time rate change of energy in the pool is added to the energy balance equations in the SSC-K code to make for conservation. In addition, the two-dimensional pool model has been developed to calculate the coolant temperature and velocity profiles in the hot pool. The governing equations for conservation of mass, momentum, energy, and both turbulent kinetic energy and the rate of turbulent kinetic energy dissipation for the κ-ε turbulence model are set in a generalized coordinate system. The SIMPLEC algorithm is used for pressure-velocity coupling. After validation of the stand-alone version of the two-dimensional pool model [6] against the sample problem, it is coupled into the SSC-K code.

4.2. Reactivity models for a metallic fueled core

To facilitate modeling of the metal fuel used in KALIMER, several reactivity models are modified in SSC-K code. For neutronic calculations, SSC-K uses point kinetic equations with detailed reactivity feedback from each channel. Reactivity effects are required both for transient safety analysis and for control requirements during normal operation. Reactivity changes are calculated for control rod scram, the Doppler effect in the fuel, sodium voiding or density changes, fuel thermal expansion, core radial expansion, thermal expansion of control rod drives, and vessel wall thermal expansion. Figure 5 shows the components of reactivity feedback considered in the KALIMER core. The effect of fuel expansion becomes more significant when metallic fuel is used.

In addition to the reactivity model, a GEM model has been developed for SSC-K. The GEM assemblies are added to the KALIMER core in order to supplement the negative reactivity feedback once the pump is tripped. For an increased safety margin in the event of loss of the primary coolant flow, GEMs are included at the periphery of the active core. A GEM has the same external size and configuration as the ducts of the other core assemblies. The GEMs are hollow assembly ducts, that are open (to flow) at the bottom, but are closed (to flow) at the top. The GEMs are filled with vessel cover gas before insertion into the core, and this gas is compressed as the GEMs are filled with sodium.

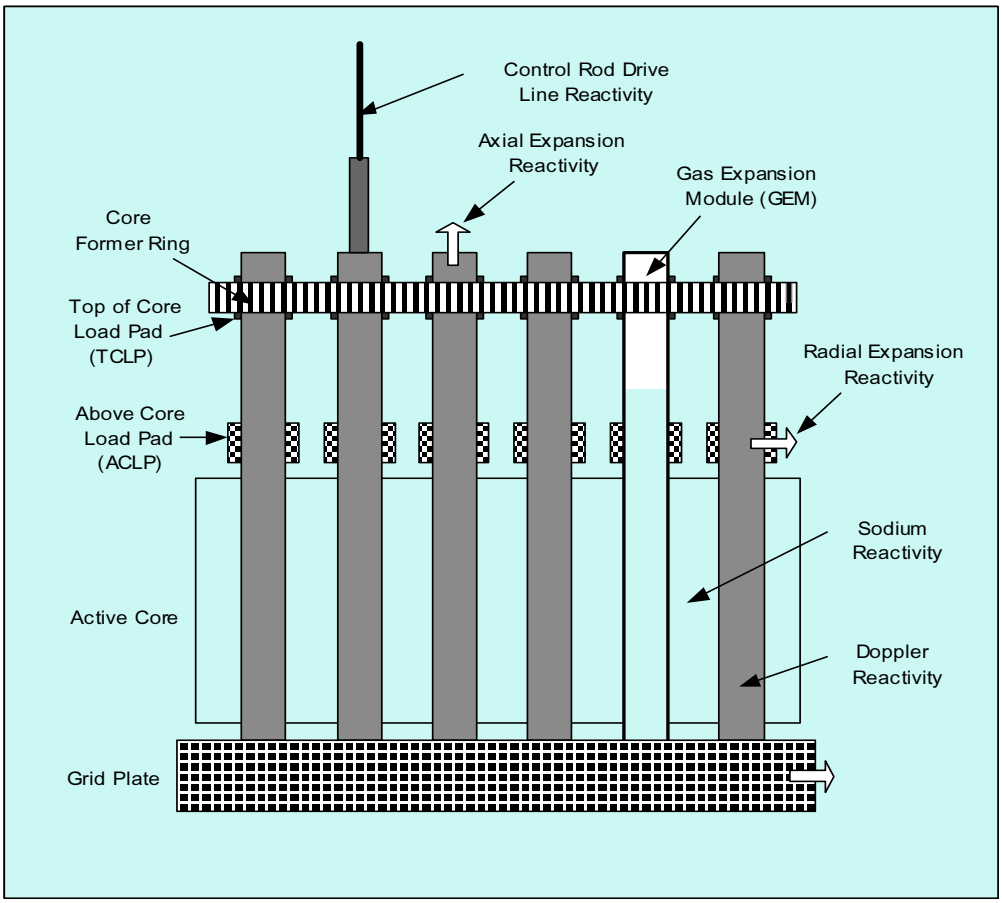

FIG. 5. Reactivity components in a metallic fueled core.

With the primary pumps on, the high pressure in the inlet plenum compresses the gas captured in the GEMs and raises the sodium level in the GEMs to a region above the active core. When pumping power is lost in the primary system and the pressure drops, the gas expands, which results in a displacement of the sodium in the GEMs to a level below the active core.

The resultant void near the core periphery increases neutron leakage and introduces significant negative reactivity, which limits the peak temperatures attained during the loss of flow events. Currently, the sodium density inside the GEM is assumed to be the axial average of the neighboring channels. A sensitivity study is needed to investigate the effect of sodium density on the sodium level. The temperature of the GEM gas is assumed to be the average of the structural temperature of neighboring channels.

4.3. Passive decay heat removal system model

PSDRS is a heat removal feature in the KALIMER designed to cool the containment outer vessel with atmospheric air in a passive manner. The gap between the reactor vessel and the containment vessel is filled with argon gas and thus heat transfer by radiation prevails due to the high temperature of these walls. Atmospheric air comes in from the inlets located at the top of the containment, and flows down through the annular gap between the air separator and the concrete silo. It then turns back upwards passing through the other annular gap between the containment outer surface and the air separator, and finally flows out through the stack at a temperature raised by the energy gained from cooling the containment vessel. The flow rate of air is determined from various parameters, such as the air temperature difference between the two annular channels, flow path or pressure drop of an orifice placed for flow control, and friction exerted on the surfaces.

The significance of PSDRS in the KALIMER design is that it is the only heat removal system in the case of a total-loss-of-heat-sink accident. For this reason, its function is crucial to prevent core damage, so that performance analysis as well as realistic modeling of the system will be a key issue to provide essential knowledge for a safety evaluation of the KALIMER design.

The PSDRS model was developed to predict the heat removal rate by this system. The model calculates not only energy balances by heat transfer between the walls, but also the air flow rate driven by gravitational force between the air flow channels to estimate the heat removal rate. Non-linear differential equations are solved using the Runge-Kutta method, while the air temperature profile is obtained from theoretical considerations. The PSDRS model is included in to SSC-K code, and the heat removal calculation based on the PSDRS model is coupled with the SSC-K calculation.

5. PIPE BREAK ANALYSIS

5.1. Analysis method

In the KALIMER design, the postulated pipe rupture can only happen in the pump discharge line to reactor core. This accident reduces the core mass flow and thus may increase the fuel temperature as well as the coolant temperature.

The main concern of the accident is associated with reduction of the subcooling margin and power stabilization resulting from reactivity feedback. In the present analysis it is assumed that one of the four pipes connecting the pump discharge to core inlet plenum is ruptured. The break is located at 3.7 m below the pump outlet and the diameter of the crack is 0.4 m, which means that the rupture area is about 0.1257 m^2. It is also assumed that the reactor is not

scrammed after the initiation of the break. Therefore, the pumps keep on running during the accident. The break is assumed to occur at 5 s after the transient.

To describe the flow after the rupture has occurred, Eq. (1) has to be modified to:

$$\frac{dW_p}{dt}\sum_{uob}\frac{L}{A} = P_{Po} - P_{bin} - \sum_{uob}\Delta P_{f,g} \tag{6}$$

When a pipe break occurs, an additional equation is needed to describe the flow downsteam of the break:

$$\frac{dW_{dob}}{dt}\sum_{dob}\frac{L}{A} = P_{bo} - P_{Rin} - \sum_{dob}\Delta P_{f,g} \tag{7}$$

The inlet and outlet pressures at break location, P_{bin} and P_{bo}, respectively, are calculated by the break model. The external pressure for the break, which is needed to compute these pressures, is obtained from static balance as:

$$P_{ext} = P_{gas} + \rho_C g(Z_{CP} - Z_b) \tag{8}$$

The external pressure for the break corresponds to the static head of the cold pool. This pressure acts as the opposing pressure against the flow out of the break. The value of this pressure is much larger than that for loop-type designs, where it is generally equal to atmospheric pressure until the sodium in guard vessel covers the break location. This will make the pipe break in pool-type designs less sever relative to loop-type designs described above.

The present version of the SSC-K code only allows the modelling of primary systems with one loop. In other words, the flow paths constituted by the four discharge line and four inlet pipe are simplified into one imaginary flow path. Therefore, there is the possiblity that the break flow from one inlet pipe is not modelled accurately and the flow from the intact sides to the broken side is not described physically. To take into account this deficiency in break modelling, a sensitivity study is performed in the present study to adjust the resultant core flow.

The base case with a break area equivalent to one pipe diameter results in the reduction of core flow to about 65% full flow. The break flow is artificially increased to reduce the core flow below 50% full flow, which compensates conservatively the deficiency in primary system modelling. The summary of reactivity worths for KALIMER breakeven core is provided in Table 1.

TABLE 1. REACTIVITY WORTH FOR KALIMER BREAKEVEN CORE

Reactivity parameter	BOEC	EOEC
Fuel temperature (doppler) coefficient (Δρ/ dT)		
Sodium flooded	$-0.08692T^{-1.44}$	$-0.08191T^{-1.42}$
Sodium voided	$-0.08787T^{-1.47}$	$-0.08657T^{-1.46}$
Uniform raidal expansion coefficient		
(dk/k) /(R/dR)(pcm/%)	-143	-141
dk/dT (10^{-4}/K)	-8.6899	-8.3742
Sodium void effect (pcm)		
Driver fuel (DF)	560.63	760.40
Internal blanket (IB)	606.71	664.46
Radial blanket (RB)	-186.66	-159.50
DF + IB	1205.75	1462.89
DF + IB + RB	1012.74	1298.46
DF + IB + RB + GEM	-302.48	130.54
Control rods (pcm)		
1 rod	970.13	1021.63
3 rods (cluster)	3632.25	3793.89
6 rods (total)	7688.38	8051.33
Interaction factor		
Adjacent rods	0.925	0.931
Clusters	1.058	1.061
GEM (pcm)	1228.55	1086.66
USS (pcm)	1441.87	1847.07

5.2. Analysis results and discussion

The analysis is performed using the SSC-K code. As soon as the break occurs, all flow rates are changed abruptly as shown in Fig. 6. In the base case, the core flow decreases drastically to less than 65% full flow within 5 s after the break. The core flow is reduced because the pressure at the break after the initiation of the transient is changed rapidly from a steady state value in the pipe to a hydraulic head established by the sodium in the cold pool. The pump discharge flow increases to about 146% of the initial steady value. All coolant passing through the pumps does not enter the core, and part of it, amounting to 56% of the total pump flow, discharges through the break into the cold pool.

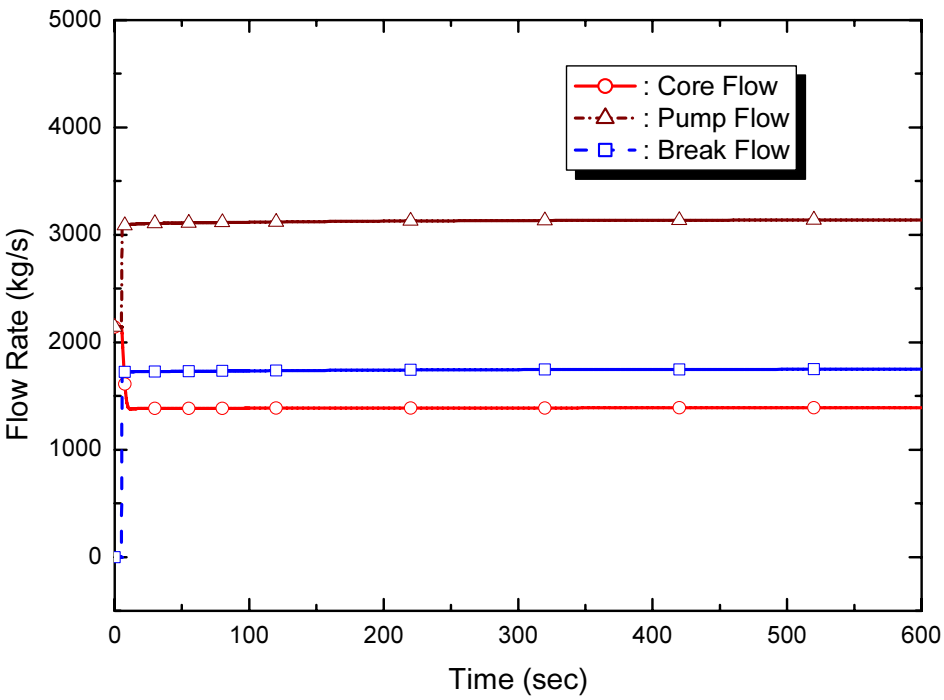

FIG. 6. The core, pump and break flows in a pipe break event (base case).

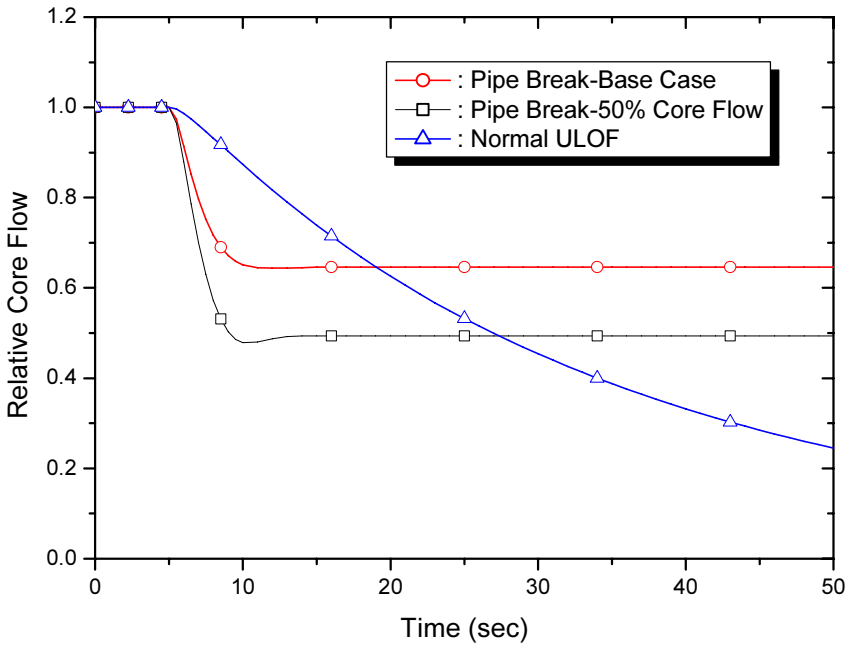

FIG. 7. The core flow rate in the pipe rupture events and the normal LOF.

In Fig. 7, the core flow rates in cases where a pipe breaks are compared with the flow rate in normal LOF case. The core flow in the pipe break case drops more rapidly than that of the normal LOF case, thus, a more severe mismatch between the power and the flow can be expected.

The relative power and flow during the transients are shown in Fig. 8 for the base case and for the 50% core flow case, respectively.

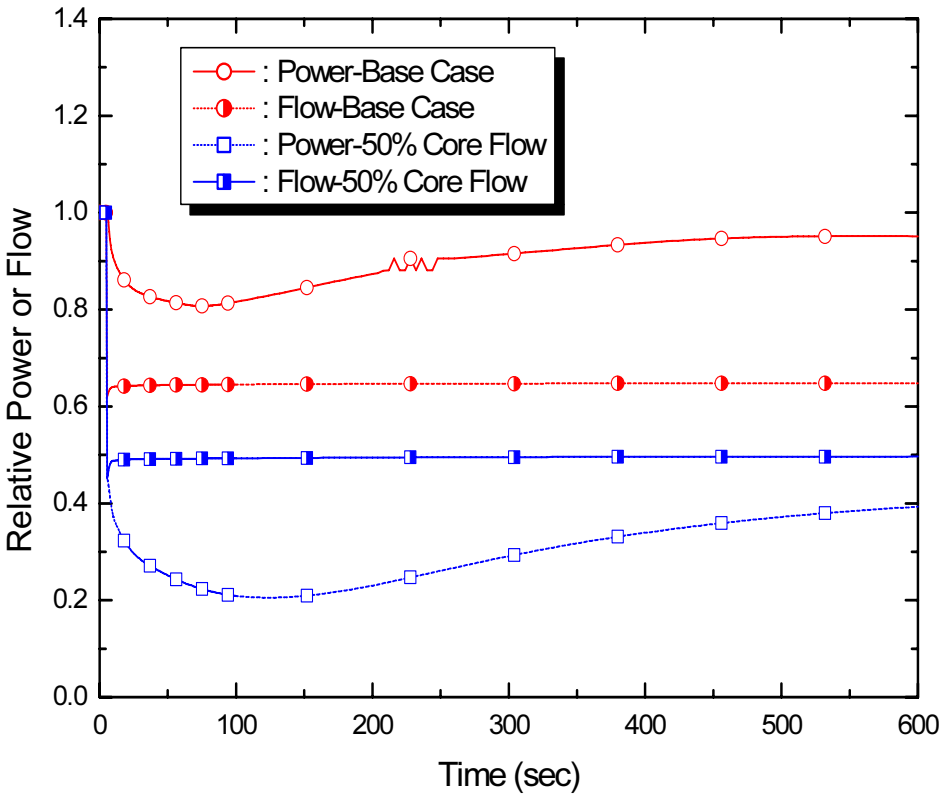

FIG. 8. Trends of relative power and flow in pipe rupture events.

For the base case, the reduction in core flow is much larger than the reduction in power. Therefore, the transient is expected to accompany higher coolant and fuel temperatures.

On the other hand, the power generation rate is reduced much more than the core flow rate in the 50% core flow case. The reason of these power trends can be found in the reactivity feedback effects as shown in Figs 9 and 10.

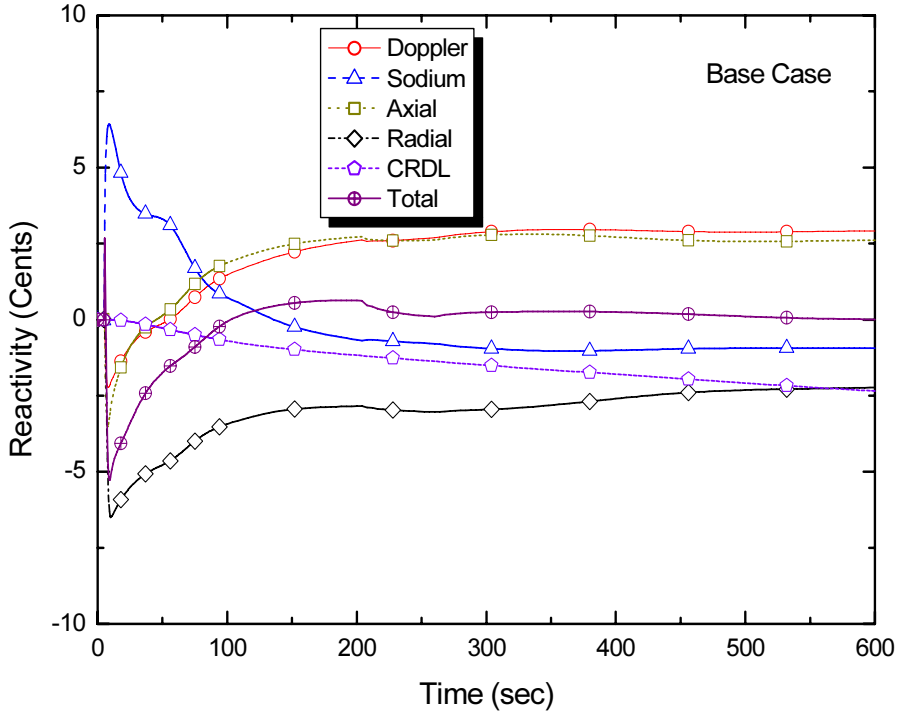

FIG. 9. The reactivity feedback in a pipe rupture event (base case).

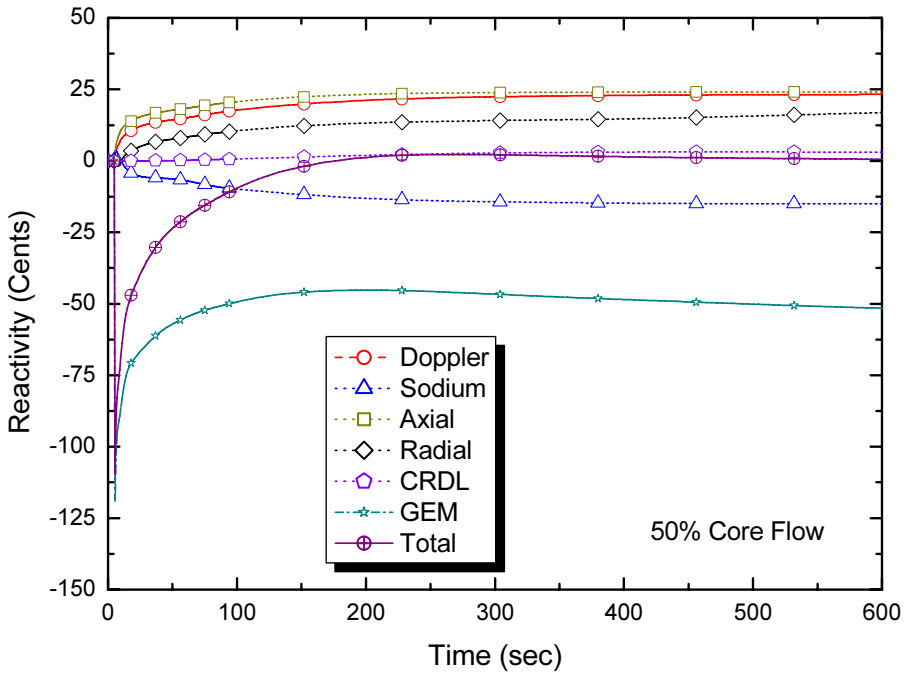

FIG. 10. The reactivity feedback in a pipe rupture event (adjusted 50% core flow).

The most remarkable difference is the effect of GEM. KALIMER is equipped with the advanced safety feature of GEM to provide additional negative reactivity in response to loss-of-flow events. When the pumps are operating at normal condition, sodium is pumped into the GEM, and the trapped helium gas is compressed into the region above the active core. However, when the pumps are off or the flow to core is reduced, the helium gas region expands into the active core region, displacing the sodium in the GEM below the active core top. The resultant void near the core periphery increases neutron leakage and introduces significant negative reactivity.

For the adjusted 50% core flow case, the effect of GEM is dominant and all the feedback effects except the sodium reactivity and the GEM reactivity go positive. The GEM level for the base case remaines above the active core top as shown in Fig. 11, and negative reactivity is not provided by GEM. In contrast, the GEM level for the 50% core flow case is maintained below the active core top and negative reactivity is introduced by the effect of the GEM.

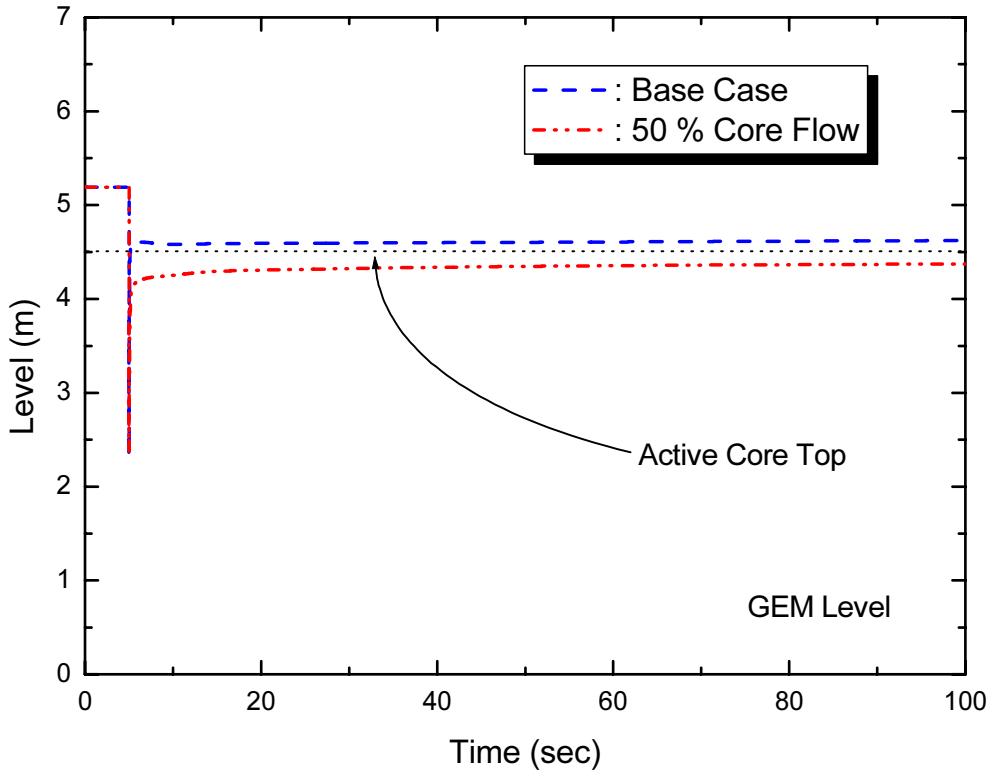

FIG. 11. Prediction of GEM levels in pipe rupture events.

The GEM level is influenced by the pump inertia force exerted to the inlet plenum and the level difference between the hot pool and the cold pool. The hot and cold pool levels are predicted for the base case and the 50% core flow case in Fig. 12. The pressure at the break rapidly drops from the initial value to that corresponding to sodium head in the cold pool, so that the cold pool level soars instantaneously by more than 3 m for base the case and 4 m for the 50% core flow case. This leads to a decrease of the pressure drop between the core inlet and the core outlet, thus resulting in the core flow reduction.

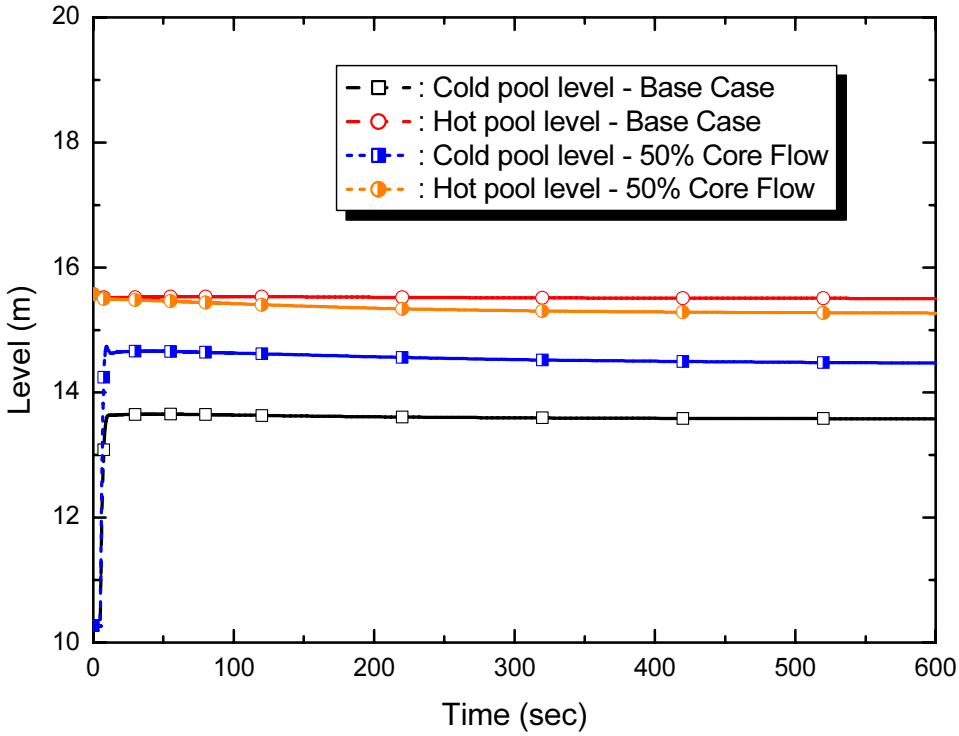

FIG. 12. Hot and cold pool levels in pipe rupture events.

The cold pool level, either remains nearly constant under the new conditions established. The hot pool level also keeps almost the initial level except negligible reduction at the very beginning.

The cold pool temperature begins to decrease due to the addition of the cold coolant flowing in from the pump outlet and finally reaches an equilibrium temperature at about 400 s for the base case of pipe break. The hot pool temperature increases until 100 s due to the reduction of core flow and the power-to-flow mismatch, and then an equilibrium temperature is maintained after that. Its change rate is rather slow and small due to the large heat capacity of the pool.

The pool temperatures for the 50% core flow case show quite different behaviours from those of base case. Because the rate of power reduction is larger than the rate of flow reduction as shown in Fig. 8, both the hot and cold pool temperatures decrease continuously after the initiation of the break. The pool temperature behaviours can be seen in Fig. 13.

The fuel, cladding, and coolant temperatures for base case are represented in Fig. 14. The temperature in the core channels increase drastically due to the rapid drop of the core flow, which leads to the large power-to-flow mismatch. The fuel centreline temperature shows the same trend with the power variation governed by the reactivity feedbacks. The cladding and sodium temperatures show similar early peaks, however, they stabilize much earlier than the fuel centreline temperature. The peak fuel temperature is about 1109 K and the peak sodium temperature is about 865 K, which guarantees the subcooling margin of more than 400 K. The fuel and coolant temperatures in the core for the 50% core flow case are not detailed because it is presumed that there will be no significant temperature increase in this case.

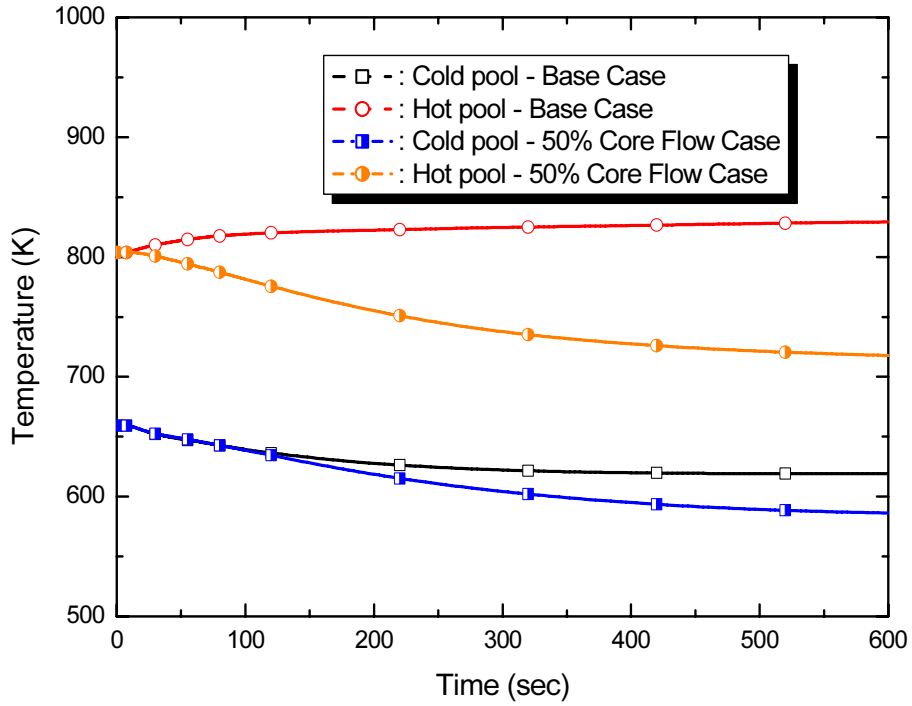

FIG. 13. Hot and cold pool temperatures in pipe rupture events.

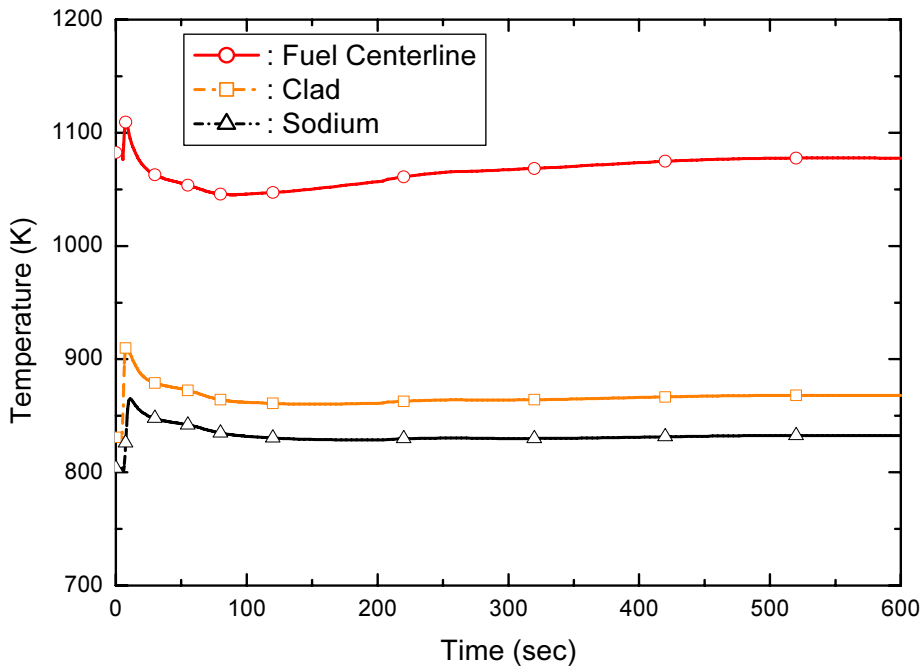

FIG. 14. Fuel and coolant temperatures in a pipe rupture (base case).

6. SUMMARY AND CONCLUSIONS

The break of one of the four core inlet pipes of KALIMER is analyzed and the inherent safety of KALIMER against a pipe break is evaluated in the present study. The reactivity feedbacks, the power trend and other parameters are predicted to show quite different behaviors depending on whether the GEM becomes effective or not. In the base case, in which the break area is equivalent to the diameter of inlet pipe, the core flow is reduced to about 65% full flow and the GEM level remains above the active core top. In this case, the power is governed by the combined effect of the reactivity feedbacks induced by the Doppler, sodium, radial, axial and control rod driveline behaviors. To overcome the deficiencies in modelling the pipe break with the SSC-K code, the core flow is artificially reduced to about 50% full flow, which results in the operation of GEM.

Even though the fuel and sodium temperatures increase after the initiation of the breaks, more than 400 K of subcooling margin is always guaranteed for the pipe break accident in KALIMER. In addition, the power stabilizes by the reactivity feedbacks even though the GEM is not effective when there is a smaller reduction of core flow. If the core flow is reduced sufficiently to lower the GEM level below the active core top, the negative reactivity of GEM results in a rapid drop of reactor power and guarantees enough subcooling margin and stabilization of the reactor dynamics.

The present study confirmes the superior resistance and inherent safety of KALIMER against a pipe break accident. The slow response of the hot pool temperature, which is another advantage of pool type liquid metal reactor, is also demonstrated. The GEM is found to be very helpful to provide sufficient negative reactivity for the passive shutdown mechanism and to mitigate the consequences of some spectrum of pipe breaks.

REFERENCES

[1] HAHN, D., KWON, Y.M., CHANG, W.P., SUK, S.D., LEE, Y.B., JEONG, K.S., “Safety Analysis for Key Design Features of KALIMER with Breakeven Core”, KAE RI/TR-2152/2002, KAERI (2002).

[2] VAN TUYLE, G.J., SLOVIK, G.C., KENNETT, R.J., CHAN, B.C., ARONSON, A., “ Analyses of unscrammed events postulated for the PRISM design”, Nucl. Technol., 91 (1990) pp. 165-184.

[3] HAHN, D., et al., KALIMER Conceptual Design Report, KAERI/TR-2204/2002, KAERI (2002).

[4] KWON, Y.M., LEE, Y.B., CHANG, W.P., HAHN, D., SSC-K Code User’s Manual (Rev.1), KAERI/TR-2014/2002, KAERI (2002).

[5] AGRAWAL, A.K., et al., “Super System Code (SSC, Rev.0) An Advanced Thermohydraulic Simulation Code for Transients in LMFBRs”, NUREG/CR-3169, U.S. NRC (1983).

[6] LEE, Y.-B., CHANG, W.P., KWON, Y.M., JEONG, K.S., HAHN, D., Development of a two-dimensional model for the thermohydraulic analysis of the hot pool in liquid metal reactors, Ann. Nucl. Energy, 29 (2002) pp. 21-40.

ANALYSIS OF EMERGENCY SITUATIONS CAUSED BY BN-800 PRIMARY CIRCUIT PRESSURE PIPE DEPRESSURIZATION

V.S. GORBUNOV, V.A. ZAMIATIN, Yu.L. KAMANIN, N.G. KUZAVKOV, V.A. SOBOLEV
Experimental Designing Bureau of Machine Building (OKBM), Nizhny Novgorod, Russia

Abstract

The results of the analysis of emergency situations caused by BN-800 pressure pipe depressurization are presented in this paper. The Russian fast reactor BN-600 and BN-800 designs have characteristic features that influence the processes during the primary circuit pressure pipes depressurization:

- Individual suction of primary circuit main circulation pump (MCP);
- Safeguard housings at the diagrid and pressure pipes;
- Pressure pipes leak detection system;
- Safeguard devices in the support belt.

The results of the analysis of emergency situations and their consequences from the viewpoint of their effect upon the core and support belt are presented. The following initial events are assumed:

- A leak of 0.5 mm equivalent diameter (DN) in the pressure pipe, as a result of an initial defect in the pipeline weld penetration through the whole wall thickness;
- Postulated ruptures of pressure pipes of 55 mm equivalent diameter (DN 55), DN 120, DN 200;
- Instantaneous guillotine rupture of one of the six pressure pipes DN 600 with moving apart of the pipeline ends (outflow from two DN 600 sections).

The analysis of all the aforementioned events shows that reactor safety is secured in all situations, including the instantaneous guillotine rupture of one DN 600 pipeline (sodium boiling and fuel melting do not occur).

1. INTRODUCTION

The philosophy, principles, criteria and limitations of the Russian concepts for fast reactors during their development and the evaluation of plant safety in situations with primary pipelines depressurization are considered in this paper. The BN-800 is an integral fast reactor cooled with sodium. The BN-800 design, developed on the basis of design decisions achieved in BN-350 and BN-600, has improved safety. Information on the BN-800 design and its characteristics are available elsewhere [1, 2].

The following components are located in the BN-800 reactor tank with its integral lay-out of the primary circuit:

- Core;
- Above-core structures;
- Three main centrifugal pumps of the primary circuit;
- Six intermediate heat exchanger (IHX) (Fig. 1).

Pumps and heat exchangers are located on the support belt. The support belt is a box-shaped structure, consisting of three horizontal plates and two vertical shells. The space between the shells is divided into three compartments by vertical ribs. Each compartment has a primary pump suction plenum and the sodium outlet from two IHXs of the heat exchange loop (concept with individual suctions of MCP-1). The DN 1125 pressure pipes (of 1.125 mm diameter) of the pump in the upper part have a T-joint that splits DN 1125 pressure pipes into two DN 600 pressure pipes (Figs. 2 - 4). The diagrid and six pressure pipes have safeguard housings (Figs. 4 and 6). The diagrid, pressure pipes and their housings are made of stainless steel X18H10T, which is highly ductile.

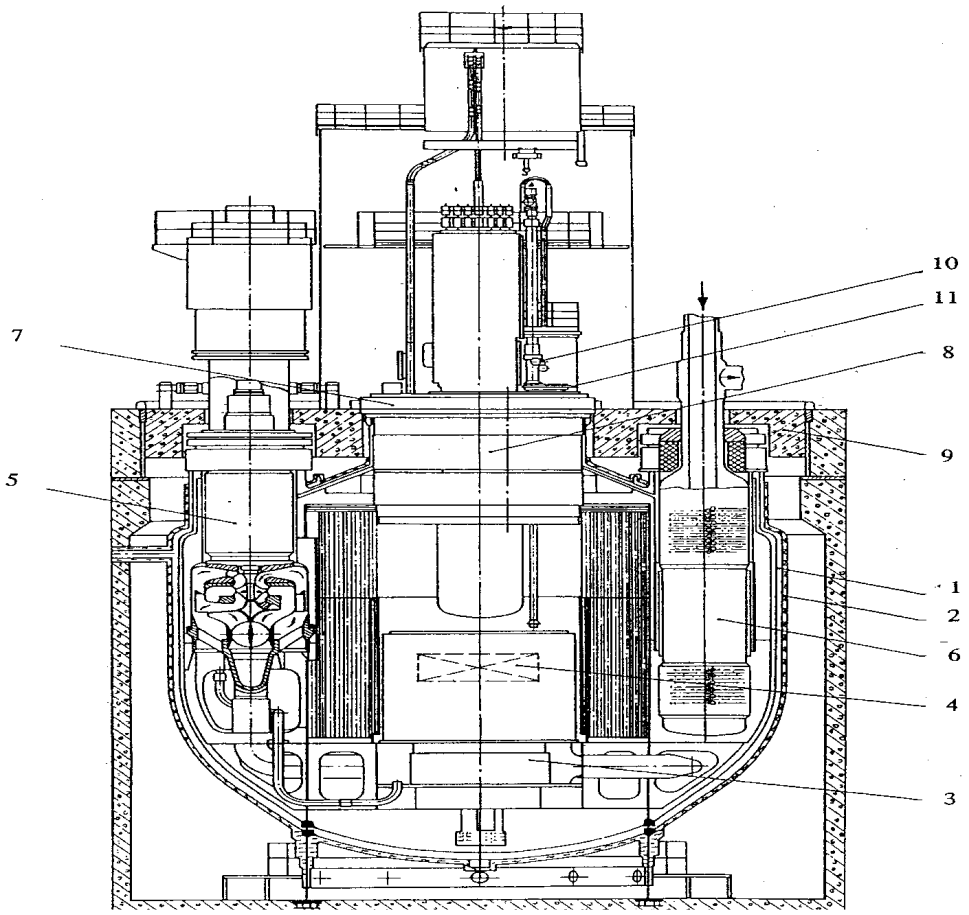

1 – main reactor vessel
2 – guard vessel
3 – core diagrid
4 – reactor core
5 – reactor coolant pump
6 – intermediate heat exchanger (IHX)
7 – large rotating plug
8 – above core structure
9 – upper stationary shield
10 – refuelling mechanism
11 – small rotating plug

FIG. 1. BN-800 Unit cross-sections (through main equipment).

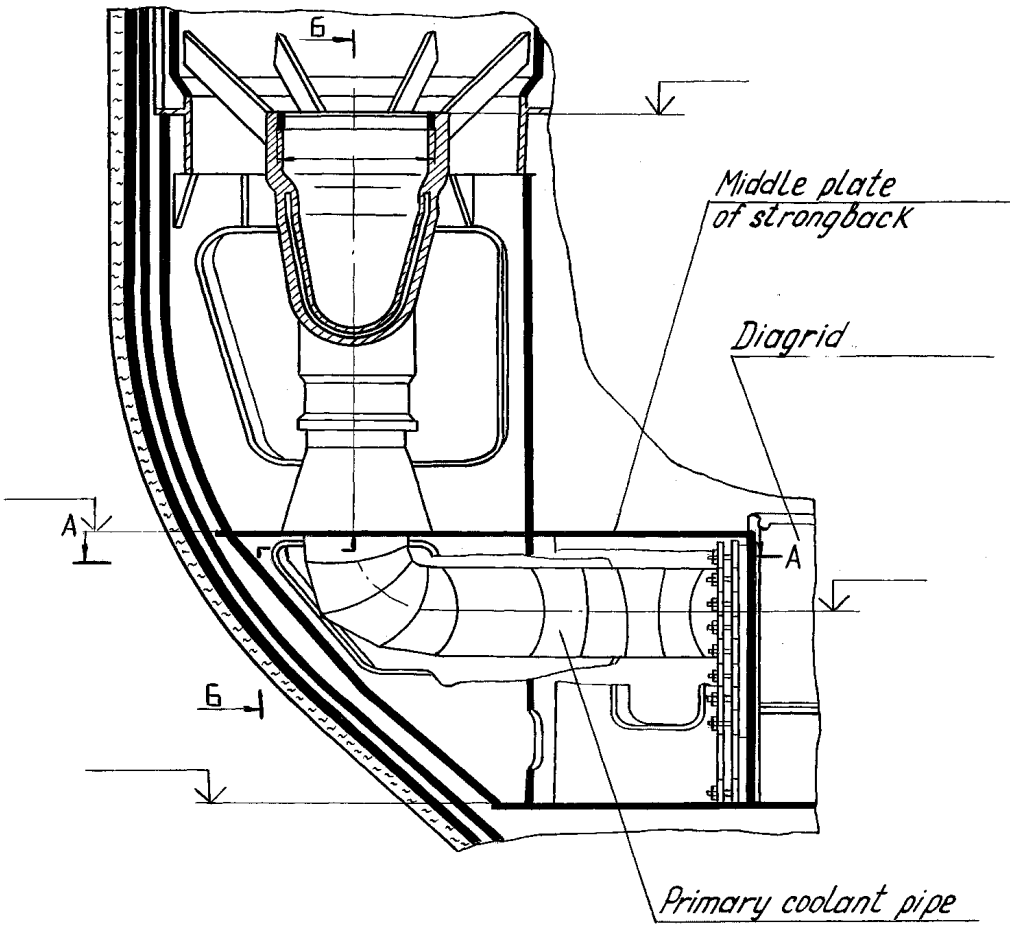

FIG. 2. BN-800 primary pipe.

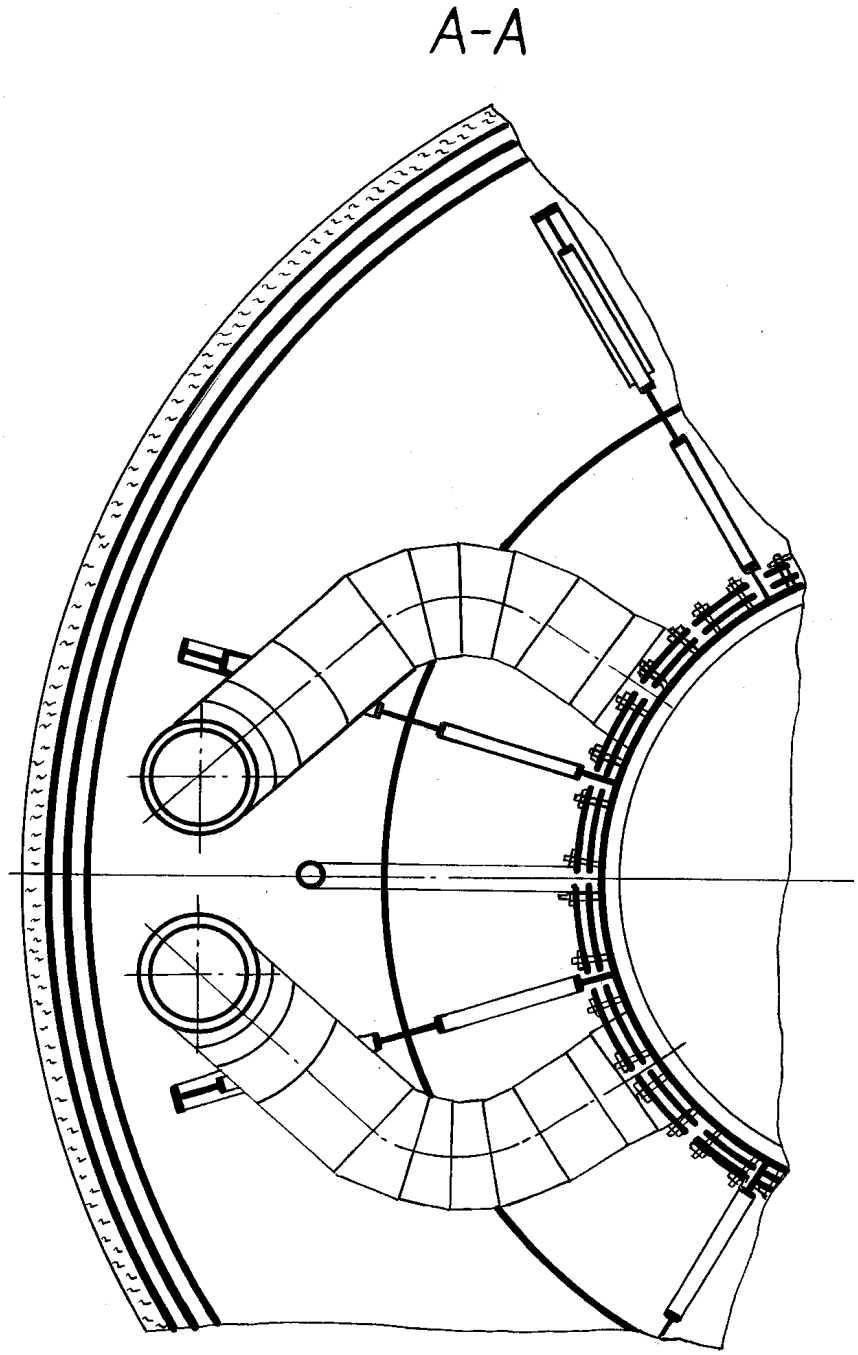

FIG. 3. BN-800 primary pipe (Section A-A in FIG. 2).

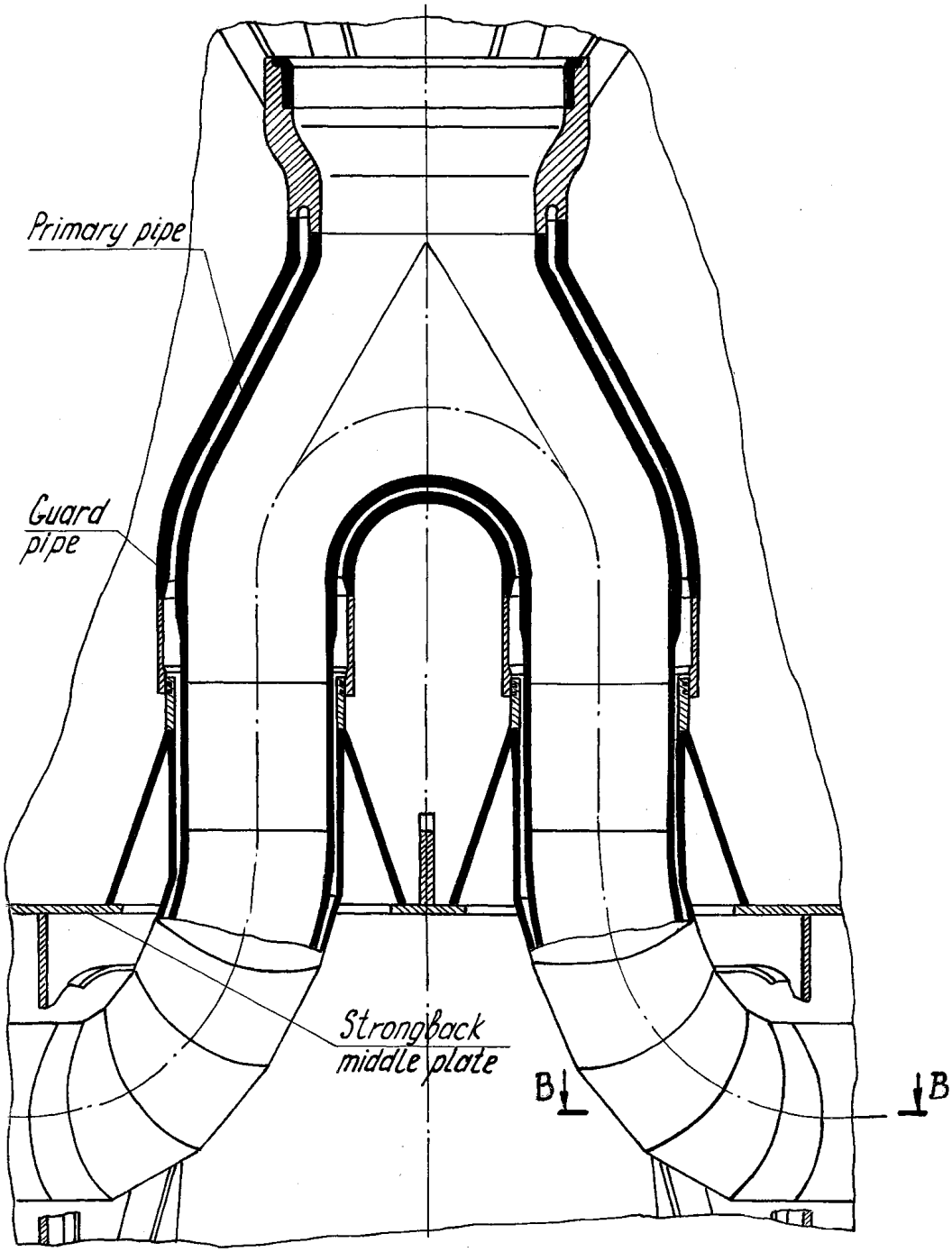

FIG. 4. Section B-B in FIG. 1.

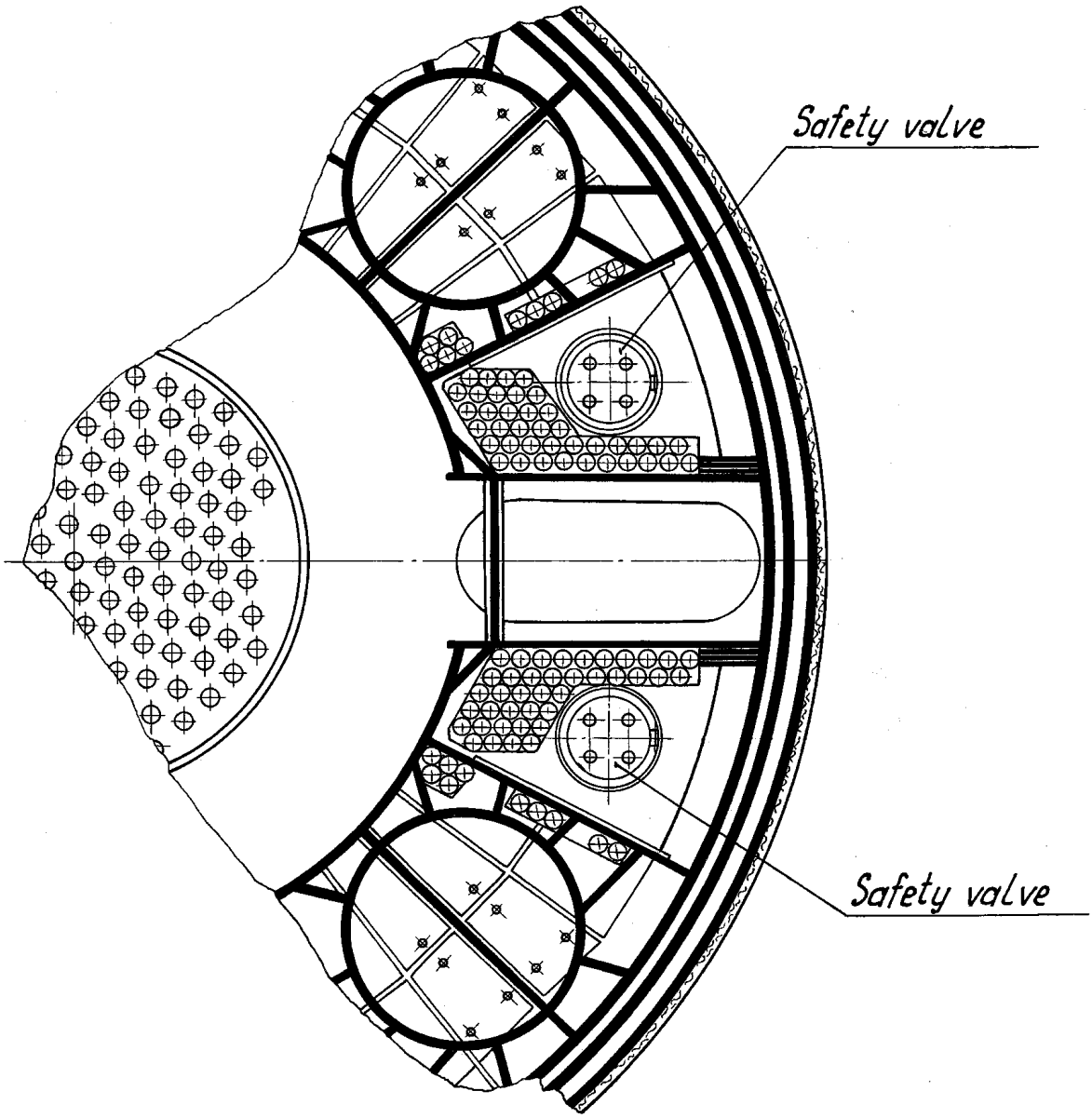

FIG. 5. Safety valves on the strongback.

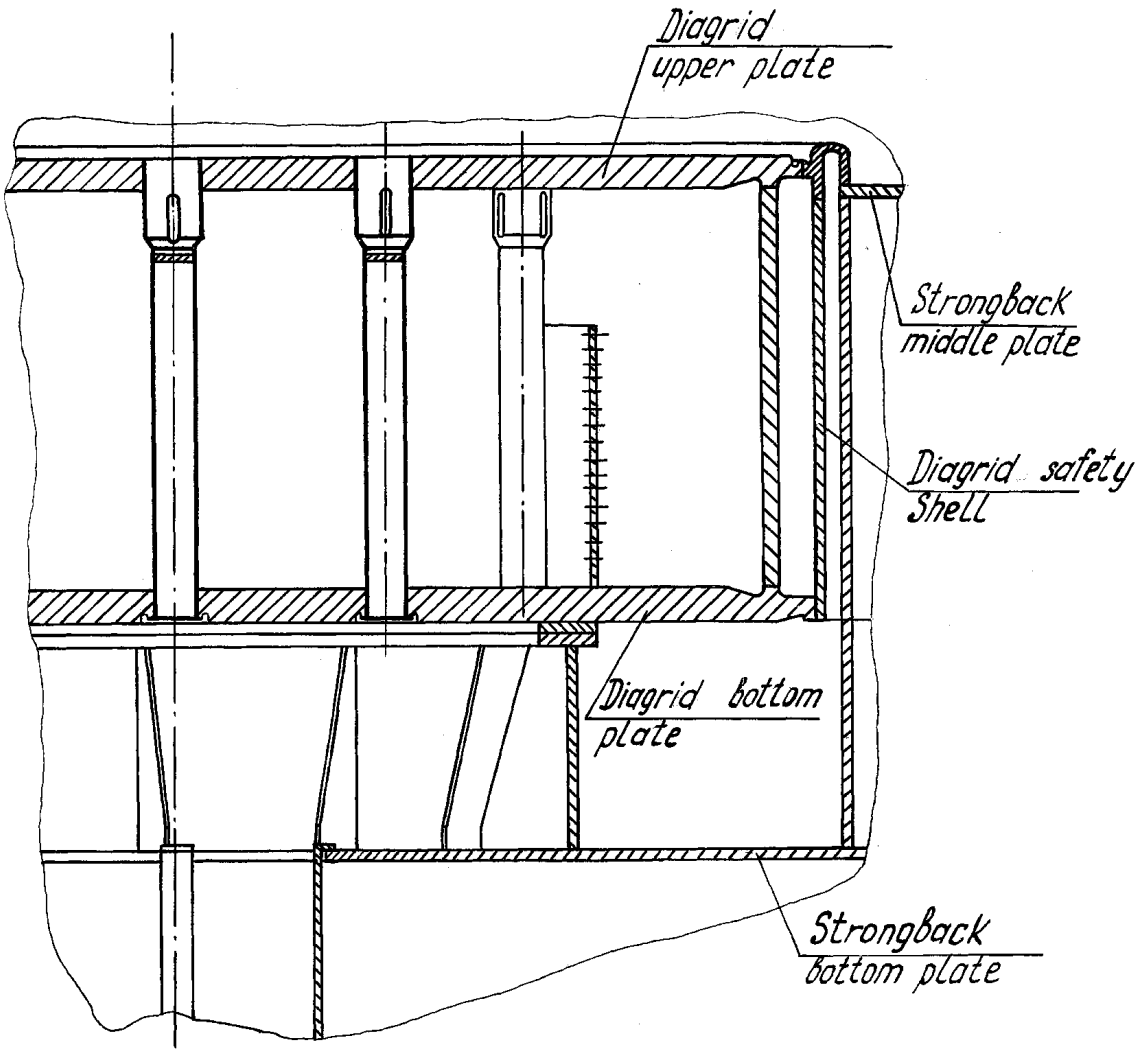

FIG. 6. BN-800 diagrid.

The safeguard housings have three functions:

- They allow to implement the pipeline leak detection system;
- They decrease considerably the sodium leakage from pressure pipes to the pump suction;
- They limit the displacement of broken pipeline ends in case of a continuous annular crack.

2. EVALUATION OF THE SAFETY CONCEPT FOR A SITUATION WITH PRESSURE PIPE DEPRESSURIZATION

Structural materials, calculation methods and necessary margins were selected to provide serviceability of the diagrid-pressure pipes system during the whole reactor life.

In order to implement consistently the leak before break (LBB) concept and prevent dangerous depressurization, safeguard housings and a pipeline leak tightness control system (PLC) are installed at the diagrid and pressure pipes.

In the case of a well-designed leak, that is larger than the system's detection threshold, the system will detect it, and the reactor is safely cooled down, awaiting an appropriate decision about the repair or about the plant's removal from operation, if repair is impossible.

If the leak detection system is not actuated and the leak, smaller than the detection threshold, is instantaneously built up into a larger one as a result of an annular closed crack formation, the tube ends may move apart, but the safeguard housing prevents the separation of the ends of broken pipeline. The leak detection system detects the leak as soon as the detection threshold is reached, and the reactor is safely shut down and cooled down.

The safeguard vessel is designed in such a way that it may work under the total head of the primary pumps during the reactor lifetime (30 - 40 years).

An analysis of the subsequent ruptures of the main pressure pipe and the safeguard vessel was also performed. This analysis has shown that such an event results in an increase of the pressure in the compartment below the middle plate of the support belt of the emergency loop. The analysis showed that the pressure increase could lead to fuel assemblies (FAs) and/or support belt being pushed to the coolant surface. To avoid the risk of FAs or support belt being pushed to the surface, the compartments of the support belt at the middle plate have two safety valves that provide a by-pass and flow supply to the suction area of the main circulation pump (see Fig. 5). Even with only one open valve, there are no FAs being pushed to the surface.

Therefore, in the BN-800 design, the following principles are implemented to prevent hazardous consequences in the case of primary circuit pipe depressurization:

- The industrial standards used in the nuclear industry are applicable to design, fabrication and control;
- The LBB criterion is fully realized;
- The multi-level protection approach is implemented to prevent dangerous consequences in the event of depressurization of the pressure pipes or diagrid.

3. SYSTEM FOR LEAKING PIPELINE DETECTION. CHARACTERISTICS OF SAFETY VALVES

The primary circuit pipelines tightness monitoring system measures the temperature difference between the sodium arriving at the heat exchanger from the hot chamber, and the sodium arriving through a tube at a thermocouple from the plenum between the pressure pipe and its housing:

- For a leak-tight pipe, the thermocouple, located in the tube coming from the plenum between the pressure pipe and its housing, shows an IXH inlet temperature of ~ 550°C;
- In a leaking pipe, the cold sodium flow rate increases;
- A considerable length of the tube is flooded by 550°C hot chamber sodium. If the sodium flow rate from the plenum between the pressure pipe and its housing is very low, the sodium in the tube is heated practically to 550°C;
- If the sodium flow through the tube exceeds some value Q_o, this sodium cannot be heated to 550°C, and there is a temperature difference (Δt) between the temperatures at the IHX inlet and at the thermocouple located at the outlet of the leak detection system tube;
- If $\Delta t > \Delta t$ (min) = 20°C, which is the system threshold sensitivity, the warning signal comes on;
- If $\Delta t > \Delta t_2 = 30$°C, the emergency signal comes on and the operator must stop the reactor with the protection button.

Each safety valve has a weight of 1 145 kg and the valve saddle has a diameter of 660 mm. The mass of the valve provides for its immobility and stability against support belt plate vibrations, in connection with mechanic vibrations of the primary circuit pumps.

The main characteristics of the safety valves are determined by the two pressure drops, ΔP_1 and ΔP_2, given by $\Delta P = (P_2 - P_1)$, where P_1 is a sodium pressure above the valve, and P_2 below the valve:

$\Delta P_1 = 0.032$ MPa, pressure drop at which the valve is opened;

$\Delta P_2 = 0.0445$ MPa, pressure drop at which the axis of valve hinge is released (it is the second threshold of valve actuation);

ΔP_1 and ΔP_2 are lower than the fuel assembly pressure drop ΔP, and also as the pressure required to push the support belt to the surface.

4. SMALL DESIGN LEAK OF PRESSURE PIPE

The analysis of possible crack dimensions in the pressure pipes was performed with the help of failure mechanics methods. In accordance with the calculations, the maximum stress in the pressure pipe at 100% power reactor operation is 459 MPa, taking into account residual welding stresses, thermal stresses, and self-compensation stresses from the displacement of supports and attachments.

It was assumed that in the weld there is an elliptic surface crack with a ratio of half length to depth (d/C) = 2/3, with C = 0.25, $S_o = 4$ mm (S_o is the thickness of the pipe wall, $S_o = 16$ mm), and the crack length 2d = 5.3 mm. The calculations have shown that the initial crack becomes a through crack for $d_o = 0.46$ mm after 2 100 cycles of reactor start-up and shutdown. As the expected number of such cycles for BN-800 is < 300, a depressurization of the pressure pipe is

not expected. Hence, if such crack occurred, the situation would not be dangerous: the sodium that leaks through the crack flows to the gap between the pressure pipe and its housing vessel. Then, the sodium flows to the support belt plenum through the gaps in the seals, and eventually through the vessel cooling system to the MCP-1 suction plenum.

Such a small leak in the pressure pipe cannot be detected by the existing pipe leak-tightness control (PLC) system, because the sodium temperature change at the IHX inlet is lower than the sensitivity threshold. In this case, the reactor continues its operation at nominal power.

5. RUPTURE OF THE PRESSURE PIPE OF 55 MM EQUIVALENT DIAMETER (DN55)

The PLC system is not actuated at depressurization areas smaller than those corresponding to 50 mm diameter. Hence, a rupture of the 55 mm equivalent diameter pipe (DN 50) must be postulated.

As the housing of the pressure pipe is a less stressed structure than the main pipeline, the probability of their simultaneous depressurization is low. In the case of a tight housing and an leaking main pipe with a DN 55 equivalent hole, the main reactor parameters (flow rate through the core, sodium temperature at the core outlet) remain practically unchanged, because after the rupture the hydraulic resistance of the seals between the main pipe and its housing, and the DN 25 (12.5 m) length tubes of the PLC system are added to the hydraulic resistance of the part between the pressure pipe and the MCP suction plenum.

6. POSTULATED SIMULTANEOUS DEPRESSURIZATION OF THE PRESSURE PIPE AND ITS SAFEGUARD HOUSING OF DN120 EQUIVALENT CROSS SECTION UNDER THE MIDDLE PLATE OF THE SUPPORT BELT

The consequences of such simultaneous depressurization include:

- Decrease of sodium flow rate through the core;
- Decrease of sodium pressure in the pressurizer;
- Possibly an increase of sodium pressure below the support belt of up to 0.0426 MPa;
- Opening of the safety valves, because $\Delta P > \Delta P_1$.

Such simultaneous depressurization is not detected by the PLC system, because ΔT is lower than the sensitivity threshold due to the housing tightness. Reactor parameter calculations at such depressurization showed the following change of parameters:

- The ratio of the reactor power to sodium flow rate (N/G) through the core increases from 1.00 to 1.03, protection by N/G is not actuated;
- The sodium temperature at the core outlet increases by only 6°C, protection at $T_{core\ outlet}$ increase by 30°C is not actuated;
- The unmeasured sodium flow rate through the vessel cooling system increases by approximately a factor of two;
- Neither fuel assemblies nor the support belt are pushed to the surface;
- The maximum temperature of the wrapper tubes of the fuel assemblies does not exceed 700°C.

7. POSTULATED SIMULTANEOUS DEPRESSURIZATION OF THE PRESSURE PIPE AND ITS SAFEGUARD HOUSING WITH DN 200 EQUIVALENT CROSS SECTION UNDER THE MIDDLE PLATE OF THE SUPPORT BELT

The DN 200 pipe rupture differs from the DN 120 pipe rupture by a larger decrease of the flow rate through the core ($\Delta G \sim 8\%$), by a higher temperature increase at the core outlet ($\Delta T \sim 15.4°C$), and a higher pressure increase in the reactor bottom part ($\Delta P = 0.157$ MPa).

Safety valves are actuated; the warning signalling is actuated by the core outlet temperature increase; signalling by N/G is not actuated. The operator must shut down the reactor with the protection button. Primary circuit pumps flow rates changes are so low that the pump head remains unchanged.

8. INSTANTANEOUS DEPRESSURIZATION OF THE PRESSURE PIPE WITH DN 600 FULL CROSS SECTION AND ITS HOUSING, OR OF THE DIAGRID

Diagrid depressurization in the welding area of braces, located between the upper and lower plates, seems more probable than simultaneous rupture of the DN600 full cross section pressure pipe and its housing. In the case of chain rupture of the welds connecting the braces and the lower plate of the pressure chamber, 91 annular gaps with a 12.3 mm slot depth may appear between the lower brace face and the inner surface of lower diagrid plate.

In the case of rupture of all braces from the lower plate of the diagrid, a ~ 0.278 m^2 flow rate area is formed, which is approximately equivalent to a DN 600 fuel cross section rupture. The pressure chamber plates stay intact.

In emergency situations with depressurization of the primary circuit pressure system of such a scale as DN 600 and higher, it is required to determine the pump characteristics taking into account possible cavitation. For the pumps of the primary circuit at 152 000 Pa nominal value of absolute argon pressure in the gas reactor cushion, the flow rate value at the break-down point is 15 800 m^3/hr.

The pump characteristic is described by the following equations:

Pump pressure, m of Na column	Sodium flow rate (Q), m^3/h
140	$Q = 0$
$H = 140 - 2.6\times10^{-3}\times Q$	$0 < Q < 10^4$
$H = 194 - 8.0\times10^{-3}\times Q$	$10^4 < Q < 1.5\times10^4$
$H = 3686.6 - 233.3\times10^{-3}\times Q$	$1.5\times10^4 < Q < 1.58\times10^4$
$H = 0.0$	For $Q > 1.58\times10^4$

A static calculation of the reactor hydraulics with a rupture under the middle plate of the support belt and two opened safety valves DN 660 has shown the following:

- Maximum sodium flow rate through the core is 17 000 m^3/hr – 48% G_{nom} (nominal flow rate);
- Additional pressure in the lower part of the vessel is equal to 0.235 MPa.

Dynamic calculations have shown that power to sodium flow rate N/G >1.2 is the first signal to trigger protection, since the change of flowmeters readings is less sluggish than the change of the reading of the thermocouples located above the fuel assemblies. The maximum increase of the fuel assembly cladding temperature stays below 70°C, and the absolute value of the fuel assembly cladding temperature in the hottest cell is < 800°C. The pumps regime is set to 250 rpm, and the reactor is safely cooled down.

Static calculations of the reactor hydraulics for the rupture under the middle plate of the support belt, considering the opening of only one safety valve yielded 18 800 m^3/hr sodium flow rate through the core. Dynamic behaviour and maximum temperatures are practically the same as those in the previous case.

In case of a rupture above the middle plate of the support belt, a static value of 15 830 m^3/hr sodium flow rate through the core was obtained. The critical temperature of fuel assembly claddings is not reached as a result of protection actuation by N/G = 1.2.

9. MOMENTARY GUILLOTINE–TYPE RUPTURE OF THE PRESSURE PIPE DN 600 AND ITS SAFEGUARD HOUSING WITH THE PIPE ENDS MOVING APART DUE TO THE ABSENCE OF THE FLOWS INTERACTION FROM BOTH ENDS OF THE PIPE

Though such a situation is rather unlikely for the BN-800 design, it was analyzed to understand if there is a difference between the scenarios with sodium outflow from one and two DN 600 cross sections.

The calculations performed have shown that in spite of some decrease of the static value of the flow rate through the core in the case of two DN 600 cross section outflows, the dynamic behaviour is the same as in the case with outflow from one DN 600 orifice:

- Protection is actuated when N/G reaches 1.2;
- Maximum temperature of fuel assembly claddings in the hottest cell is lower than 800°C, sodium does not boil, and fuel does not melt;
- Pumps regime is set to 250 rpm, and the reactor is safely cooled down (see Figs. 7 and 8).

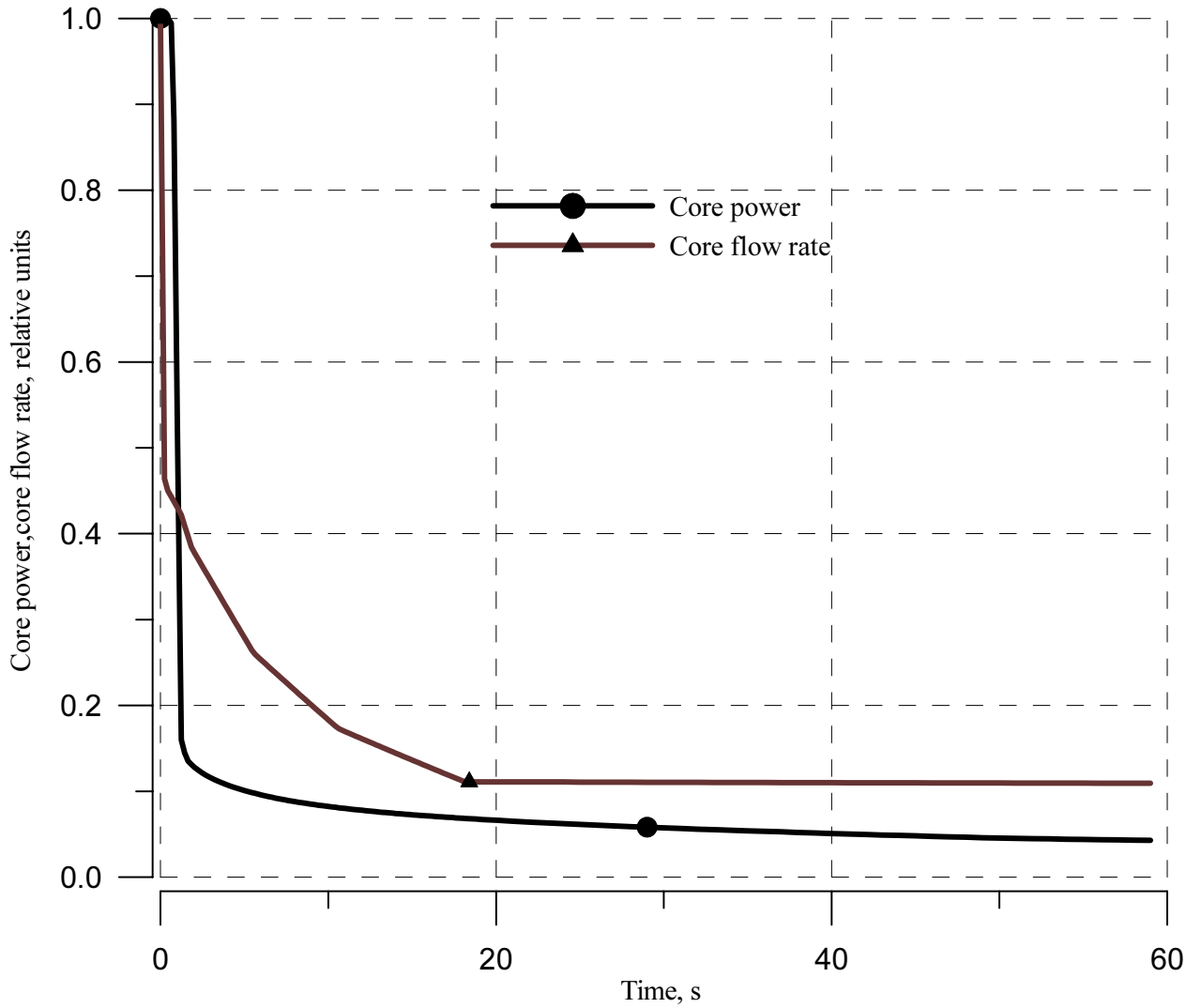

Fig. 7 - DN 600 mm pressure pipe rupture. Reactor shut down.
Pumps are transferred to 250 rpm.

FIG. 7. DN 600 m pressure pipe rupture. Reactor is shut down, and pumps are at 250 rpm.

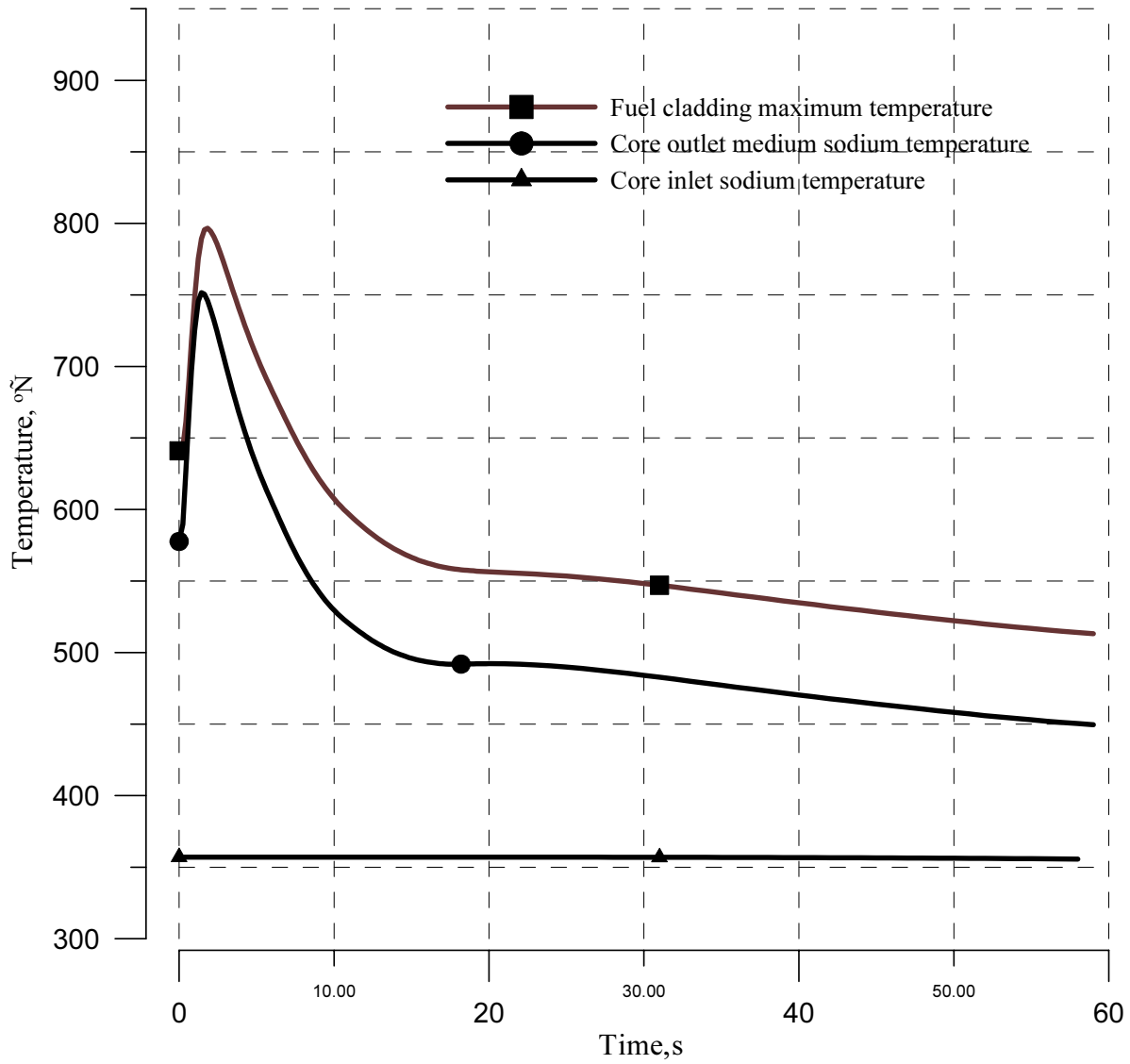

Fig. 8 - DN 600 mm pressure pipe rupture. Reactor shut down.
Pumps are transferred to 250 rpm.

FIG. 8. DN 600 mm pressure pipe rupture. Reactor is shut down, and pumps are at the 250 rpm.

10. CONCLUSIONS

This paper describes the BN-800 design of pressure pipes of the primary circuit and gives an analysis of a depressurization event. It was shown that the adopted pressure pipes leak-tightness control (PLC) system allows to determine pipe or pressure chamber leaks with holes of more than 50 mm diameter. Smaller leaks are not detected, but these leaks do not influence the plant parameters. Large pressure pipe and housing leaks corresponding to DN 120, 200 600, and 2×DN 600 with the pipe ends separated have also been investigated. In all cases, it was shown that the reactor protection is triggered by the core power to flow ratio (N/G), and that the reactor is safely shut down and cooled. The critical temperature of 800°C is not reached.

REFERENCES

[1] INTERNATIONAL ATOMIC ENERGY AGENCY, Fast Reactor Database, IAEA-TECDOC-866, Vienna (1996).

[2] INTERNATIONAL ATOMIC ENERGY AGENCY, Status of National Programmes on Fast Reactors (Proceedings of the International Working Group on Fast Reactors, Vienna, 4–7 May 1993) IAEA-TECDOC-741, Vienna (1994).

IMPROVED PRIMARY PIPE COOLANT DESIGN CONCEPTS FOR FUTURE FBRs

S.C. CHETAL, P. CHELLAPANDI
Indira Gandhi Centre for Atomic Research (IGCAR), Kalpakkam, India

Abstract

In this paper some design concepts are described that:
(i) Minimize the loss of coolant to core in case of pipe rupture;
(ii) Improve in-service inspection;
(iii) Eliminate double ended guillotine rupture (DEGR) from design basis event (DBE).

1. INTRODUCTION

The primary coolant pipes carry pressurized sodium (~ 0.8 MPa) from the pump header to the grid plate and thus, form a primary coolant pressure boundary. A rupture of the primary pipe is of great safety concern. Hence, structural reliability requirements are high for this component. In view of these considerations, a very ductile material, such as austenitic stainless steel type 316 LN, is selected and the pipe is designed as per Class 1 rules of RCC-MR [1].

High quality construction and very stringent pre-service inspection procedures are adopted. The layout, wall thickness, and junction profile are all optimized to achieve low stress field. Detailed structural mechanics analyses are carried out to comply with the RCC-MR, considering all possible loadings. Hence, failure of these pipes in the form of Double Ended Guillotine Rupture (DEGR) is a low probability event that can be considered a Beyond Design basis Event (BDBE). Accordingly, such an event does not need to be analyzed to predict the consequences.

However, to comply with the current safety philosophy that is followed in pressurized water reactors, the rupture of one of the pipes is considered, based on single failure criteria, and analyzed for its thermo-mechanical (temperature rise in fuel, cladding and coolant) and structural (mechanical interaction of failed pipe with adjacent pipes) consequences.

These analyses call for very complex 3-D modelling and solution techniques, since, in a simplified 1-D analysis, particularly in the design with a smaller number of pipes, it is difficult to demonstrate that temperature limits are respected with comfortable margins. Hence, it is worth considering alternative approaches, such as an increased number of smaller pipes, or provision for In Service Inspection (ISI), ensuring that even a small leak can be detected with confidence and that DEGR can be prevented. In this paper, some approaches are highlighted for the consideration of future FBR.

1.1. Concept 1: Increased number of smaller pipes

A greater number of pipes with reduced diameters have definite advantages. For the smaller diameter pipes, a lesser wall thickness can be chosen without increase of stress. As a result of this, the pipe become relatively flexible, which can accommodate higher thermal expansions.

Besides, in the case of DEGR of a pipe, the net loss of core flow is minimal. Consequently, the temperature rise in the fuel, cladding and coolant is reduced. It is also possible to consider seamless pipes with reduced thickness, by which the structural reliability can be improved significantly.

Figure 1 shows possible layouts with an increased number of pipes.

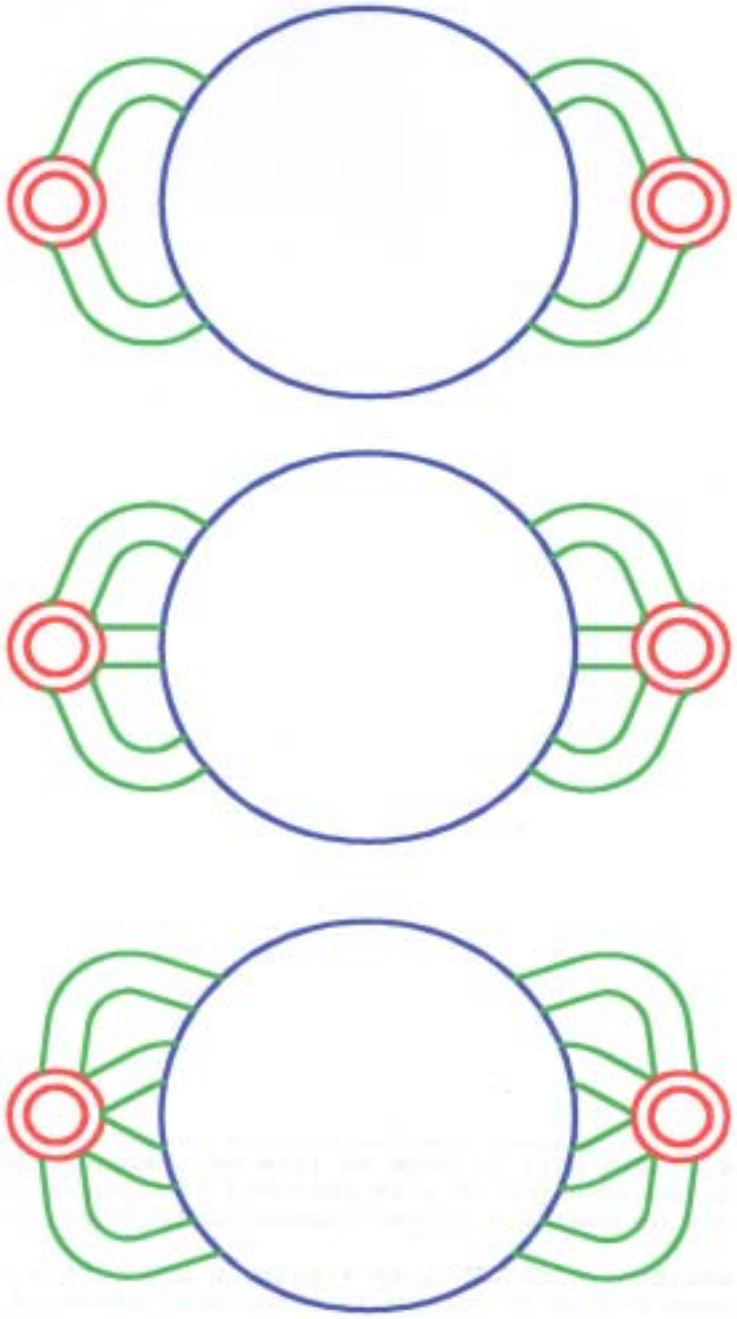

FIG. 1. Layout of primary pipes.

Table 1 provides an idea about the diameter and flow velocities with the increased number of pipes, for a typical 500 MWe FBR (PFBR) which has four pipes in the reference design with two primary pumps.

TABLE 1. PIPE DIAMETERS

No. of pipes	Velocity		
	7.5 m/s	10 m/s	15 m/s
4	600	520	420
6	480	420	340
8	420	360	300

However, there is a disadvantage in that an increased number of pipes may decrease the structural reliability due to an increase of pipe lengths.

1.2. Concept 2: Incorporation of a check valve

A check valve may be devised to be inserted into the grid plate end of the pipe, allowing free flow from pipe to the grid plate preventing coolant to flow from the grid plate to the pipe. This device could be a passive non-return valve that works on fluid drag principle. With such a device, the coolant bypass from the grid plate to the cold pool can be significantly reduced and thereby a flow increased of about 20 to 30% through core can be ensured. While designing such a device, its effectiveness during other design basis events, especially due to one primary pump trip should be investigated. Engineering development of this check valve needs to be carefully done. It should also be ensured that small parts of the flow diode device do not get separated and block the subassembly flow passage.

1.3. Concept 3: Demonstration of LBB by leak detection

A guard pipe filled with sodium can be provided that surrounds the primary pipe. The inter-space between the primary pipe and the guard pipe may be connected to a higher temperature location in the primary circuit, such as near the outer surface of the upper shell of the inner vessel in the PFBR by means of a small tube. When there is no leak in the primary pipe, the temperature of the sodium in this tube near its top end would be around 780 K, which is close to the hot pool sodium temperature. When the primary pipe starts leaking, cold sodium flows into this tube, and the temperature of the sodium near its top end reduces rapidly. Thus, the reduction in the temperature of sodium in this tube would give an indication of a leak in the primary pipe.

Alternatively, the approach followed in BN 600 can be adopted. In this concept, the outer wall is not leak tight and a tube is incorporated through which sodium can flow from the inter-space to the relatively hotter sodium in the space between inner vessel and the thermal baffle.

During no-leak condition, the temperature of the sodium in the tube is the same as its surrounding. Any sodium leak in the primary pipe can cause flow in the tube, the temperature of which will be reduced. Thereby a leak can be detected.

1.4. Concept 4: Demonstration of structural reliability

In order to eliminate DEGR, the structural integrity can be demonstrated by determining the structural reliability based on probabilistic methods in conjunction with studying the consequences for a maximum leak through a design basis crack opening area. The maximum leak area can be 1 cm^2, which is in fact the area considered for the secondary sodium pipe lines in estimating the design basis sodium leak event for the consideration of sodium fire. The approach followed by Japan is that the leakage area is equal to DT/4, i.e., $1/4^{th}$ of area for the rectangular slit having length equal to diameter and width equal to thickness.

1.5. Concept 5: Design with ISI

Low stress coupled with ISI could validate the rupture of pipe as BDBE. Accordingly, the present design of single wall piping could be retained with additional ISI features to ascertain the position and the size of the cracks in the pipes. In addition, the stress level could be kept low in the piping.

2. CONCLUSION

In this paper various design concepts, to minimize the loss of coolant to core in case of pipe rupture, to improve ISI and, to eliminate DEGR from DBE are highlighted. While the safety implications of incorporating more number of pipes require careful considerations of all aspects, the idea of improved ISI, particularly the concept used in BN 600, is worth considering for the future FBR design.

REFERENCE

[1] RCC-MR subsection NB for class 1 components, “Design and construction rules for Mechanical Components of FBR Nuclear Islands (RCC-MR)”, Association Française pour les règles de Conception et de Construction des matériels des chaudières Electro-Nucléaires (AFCEN), Paris, France (1993).

ABBREIVIATIONS

ANL	Argonne National Laboratory
ATWS	anticipated transients without scram
BDBA	beyond DBA
BC	begin of cycle
BOEC	begin of equilibrium cycle
BOP	balance of plant
CARR	Chinese advanced research reactor
CDA	core disruptive accident
CDF	core damage factor
CEFR	China experimental fast reactor
CFD	computational fluid dynamics
CHST	clad hot spot temperature
CIAE	China Institute of Atomic Energy
CRBRP	clinch river breeder reactor
CRIEPI	Central Research Institute of Electric Power Industry
CSA	core subassemblies
CSR	control and safety rod
CSRDM	control and safety rod drive mechanism
CSS	core support structure
DBA	design base accident
DBE	design basis event
DEGR	double ended guillotine rupture
DF	driver fuel
DN	equivalent diameter
DSL	design safety limits
DSR	diverse safety rod
DSRDM	diverse safety rod drive mechanism
EFD	European Fast Reactor
EFR	European Fast Reactor
EOEC	end of equilibrium cycle
FAs	fuel assemblies
FBR	fast breeder reactor
FBTR	fast breeder test reactor
FFTF	fast flux test facility
FSA	fuel sub-assembly
GEM	gas expansion module
GIF	Generation IV International Forum

GP	grid plate
HEFS	high energy fluid system
IB	internal blanket
IGCAR	Indira Gandhi Centre for Atomic Research
IHTS	intermediate heat transport system
IHX	intermediate heat exchangers
INPRO	International Project on Innovative Nuclear Reactors and Fuel Cycles
ISI	In Service Inspection
IVSs	in-vessel storages
JAERI	Japan Atomic Energy Research Institute
JIS	Japanese Industrial Standard
JNC	Japan Nuclear Cycle Development Institute
KAEC	Korea Atomic Energy Commission
KAERI	Korea Atomic Energy Research Institute
KALIMER	Korean Advanced Liquid Metal Reactor
LoD	lines of defence
LBB	leak before break
LIPOSO	LIaison POmpe SOmmier
LMFBR	liquid metal cooled fast breeder reactor
LOCA	loss of coolant accident
LOF	loss of flow
MCP	main circulation pump
MEFS	moderate energy fluid system
MV	main vessel
NPSH	net positive suction head
$NPSH_A$	available net positive suction head
$NPSH_R$	required net positive suction heas
NRC	Nuclear Regulatory Commission
NSSS	nuclear steam supply system
OKBM	Experimental Designing Bureau of Machine Building
PCP	primary coolant piping
PFBR	prototype fast breeder reactor
PHTS	primary heat transport system
PLC	pipe leak-tightness control
PSAR	preliminary safety analysis report
PSDRS	passive safety decay heat removal system
PSP	primary sodium pumps
RA	reactor assembly
RB	radial blanket

RCB	reactor containment building
RCC-MR	règles de conception et de construction des matériels mécaniques des îlots nucléaires
SA	sub-assembly
SASHST	sub-assembly sodium hot spot temperature
SFR	sodium-cooled fast reactor
SG	steam generators
SGS	steam generator system
SSE	single stress event
T_{Cl}	cladding hotspot temperature
T_{Na}	sodium hotspot temperature
TS	top shield
ULOF	unprotected loss of flow
ULOHS	unprotected loss of heat sink
USS	ultimate shutdown system
UTOP	unprotected transient over power
VHTR	very high temperature reactor

LIST OF PARTICIPANTS

Balasubramanian, V.	Indira Gandhi Centre for Atomic Research Reactor Assembly & Sodium Circuits Division Kalpakkam-603 102 India
Baldev, R.	Indira Gandhi Centre for Atomic Research Metallurgy & Materials Group Kalpakkam-603102 India
Bhanu Sankara Rao, K.	Indira Gandhi Centre for Atomic Research Mechanical Metallurgy Division Kalpakkam-603102 India
Bhoje, S.B.	Indira Gandhi Centre for Atomic Research Kalpakkam-603 102 India
Chauhan, B.S.	SO/G, NPSD Atomic Energy Regulatory Board Niyamak Bhavan, Anushaktinagar Mumbai–400074 India
Chellapandi, P.	Indira Gandhi Centre for Atomic Research Mechanics & Hydraulics Division Kalpakkam-603102 India
Dufour, P.	CEA DEN Cadarache DER/SERI/LFEA bat 212 13108 St. Paul-lez-Durance France
Govindarajan, S.	Indira Gandhi Centre for Atomic Research Core Engineering & Component Handling Division Kalpakkam-603102 India
Hae-Yong, J.	Korea Atomic Energy Research Institute (KAERI) P.O. Box 105, Yusong Daejon, 305-600 Korea, Rep. Of
Hongy, Y.	China Institute of Atomic Energy P.O. Box 275(97) Beijing 102413 China

Jayakumar, T. — Indira Gandhi Centre for Atomic Research
Division for PIE & NDT Development
Kalpakkam-603102
India

Joseph, A. — Indira Gandhi Centre for Atomic Research
Division for PIE & NDT Development (DPEND)
Kalpakkam-603102
India

Kannan, S.E. — Indira Gandhi Centre for Atomic Research
Safety Engineering Division
Kalpakkam-603102
India

Kapoor, R.P. — Indira Gandhi Centre for Atomic Research
Reactor O&M Group
Kalpakkam-603102
India

Kasinathan, N. — Indira Gandhi Centre for Atomic Research
Mechanics & Hydraulics Division
Kalpakkam-603102
India

Lee, S.M. — Indira Gandhi Centre for Atomic Research (IGCAR)
SHINE Group
Kalpakkam 603 102
Tamil Nadu
India

Natesan, K. — Indira Gandhi Centre for Atomic Research
Mechanics & Hydraulics Division
Kalpakkam-603102
India

Ray, S.K. — Indira Gandhi Centre for Atomic Research
Materials Technology Division
Kalpakkam-603102
India

Srinivasan, G. — Indira Gandhi Centre for Atomic Research
Reactor Operations Division
Kalpakkam-603102
India

Sobolev, V. — OKBM
Burnakovsky Proezd 15
Nizhny Novgorod
Russian Federation

Stanculescu, A.	International Atomic Energy Agency (IAEA) Nuclear Power Division Wagramer Strasse 5 1400 Vienna, Austria
Vaidyanathan, G.	Indira Gandhi Centre for Atomic Research Engineering Development Group Kalpakkam-603102 India
Wakai, T.	Japan Nuclear Cycle Development Institute (JNC) Orai Engineering Center Advanced Technology Division 4002 Narita-cho, O-arai, Ibaraki 311-1393 Japan